

# Kinetic and modelling studies of the NAD<sup>+</sup>/NADH coenzyme with horse liver alcohol dehydrogenase

**Citation for published version (APA):**

Vanhommerig, S. A. M. (1995). *Kinetic and modelling studies of the NAD<sup>+</sup>/NADH coenzyme with horse liver alcohol dehydrogenase*. [Phd Thesis 1 (Research TU/e / Graduation TU/e), Chemical Engineering and Chemistry]. Technische Universiteit Eindhoven. <https://doi.org/10.6100/IR436533>

**DOI:**

[10.6100/IR436533](https://doi.org/10.6100/IR436533)

**Document status and date:**

Published: 01/01/1995

**Document Version:**

Publisher's PDF, also known as Version of Record (includes final page, issue and volume numbers)

**Please check the document version of this publication:**

- A submitted manuscript is the version of the article upon submission and before peer-review. There can be important differences between the submitted version and the official published version of record. People interested in the research are advised to contact the author for the final version of the publication, or visit the DOI to the publisher's website.
- The final author version and the galley proof are versions of the publication after peer review.
- The final published version features the final layout of the paper including the volume, issue and page numbers.

[Link to publication](#)

**General rights**

Copyright and moral rights for the publications made accessible in the public portal are retained by the authors and/or other copyright owners and it is a condition of accessing publications that users recognise and abide by the legal requirements associated with these rights.

- Users may download and print one copy of any publication from the public portal for the purpose of private study or research.
- You may not further distribute the material or use it for any profit-making activity or commercial gain
- You may freely distribute the URL identifying the publication in the public portal.

If the publication is distributed under the terms of Article 25fa of the Dutch Copyright Act, indicated by the "Taverne" license above, please follow below link for the End User Agreement:

[www.tue.nl/taverne](http://www.tue.nl/taverne)

**Take down policy**

If you believe that this document breaches copyright please contact us at:

[openaccess@tue.nl](mailto:openaccess@tue.nl)

providing details and we will investigate your claim.

---

---

Kinetic and modelling studies  
of the  $\text{NAD}^+/\text{NADH}$  coenzyme with  
horse liver alcohol dehydrogenase

---

---



Sylvia A.M. Vanhommerig

**KINETIC and MODELLING STUDIES**  
**of the NAD<sup>+</sup>/NADH COENZYME with**  
**horse liver alcohol dehydrogenase**

**Kinetic and modelling studies  
of the NAD<sup>+</sup>/NADH coenzyme with  
horse liver alcohol dehydrogenase**

**Proefschrift**

ter verkrijging van de graad van doctor aan de  
Technische Universiteit Eindhoven, op gezag van  
de Rector Magnificus, prof.dr. J.H. van Lint,  
voor een commissie aangewezen door het College  
van Dekanen in het openbaar te verdedigen op  
dinsdag 9 mei 1995 om 16.00 uur

door

**Sylvia Anna Maria Vanhommerig**

geboren te Heerlen

Dit proefschrift is goedgekeurd  
door de promotoren:

prof.dr. E.M. Meijer  
prof.dr. E.W. Meijer

Copromotor: dr. R.J. Meier

CIP-DATA KONINKLIJKE BIBLIOTHEEK, DEN HAAG

Vanhommerig, Sylvia Anna Maria

Kinetic and modelling studies of the  $\text{NAD}^+$ / $\text{NADH}$  coenzyme  
with horse liver alcohol dehydrogenase / Sylvia Anna  
Maria Vanhommerig. - Eindhoven : Eindhoven University of  
Technology

Thesis Technische Universiteit Eindhoven. - With ref. -  
With summary in Dutch.

ISBN 90-386-0026-7

Subject headings: enzymes ; modelling studies /  $\text{NADH}$  / dehydrogenases.

Aan mijn ouders

Voor John en Rebecca

# Contents

Abbreviations	vii
<b>Chapter 1</b>	
<b>Introduction</b>	<b>9</b>
1.1 Nicotinamide Adenine Dinucleotide (NAD <sup>+</sup> /NADH)	9
1.2 Coenzyme dependent enzymes in industrial reactions	11
1.3 The NAD-dependent HLADH	12
1.4 The rate stereospecificity of hydride-transfer	14
1.5 Computational chemistry of enzymes	15
1.6 Synthetic NADH models	16
1.7 Outline of this thesis	16
References	17
<b>Chapter 2</b>	
<b>Semiempirical AM1 and PM3 studies on active site models of HLADH</b>	<b>21</b>
2.1 Introduction	21
2.2 Methods	23
2.3 Results and discussion	24
2.3.1 The influence of the total charge of the model complexes	24
2.3.2 Mechanism and rate of hydrogen-transfer in HLADH	27
2.3.3 Hydrogen tunnelling effects	29
2.3.4 Effects of the presence of H-bonding groups and side-chain modifications in NAD	30
2.3.5 Water in the active site	32
2.3.6 Substitution of the zinc ion by other metal ions	33
2.4 Conclusions	34
References	34
<b>Chapter 3</b>	
<b>Checking the AMBER 4.0 force field with leucine, alanine and <i>N</i>-methylacetamide</b>	<b>37</b>
3.1 Introduction	37
3.2 Methods	37
3.3 Results and discussion	40
3.3.1 The leucine crystal	40
3.3.2 The alanine crystal	44
3.3.3 The <i>N</i> -methylacetamide crystal	46
3.4 Conclusions	47
References	48

<b>Chapter 4</b>	
<b>Rotational barriers of NAD<sup>+</sup>/NADH, its analogues and derivatives</b>	<b>49</b>
4.1 Introduction	49
4.2 Computational methods	49
4.3 Results	51
4.3.1 Force field results	51
4.3.2 Semiempirical methods	51
4.3.3 <i>Ab initio</i> calculations	53
4.4 Discussion	54
4.5 Determination of $V_H/2$ for NAD <sup>+</sup> /NADH and analogues	56
4.6 Conclusions	57
References	57
<b>Chapter 5</b>	
<b>Kinetic and modelling studies of polyethylene glycol bound NAD<sup>+</sup> versus native NAD<sup>+</sup></b>	<b>59</b>
5.1 Introduction	59
5.2 Experimental	60
5.2.1 Materials	60
5.2.2 Kinetic measurements	60
5.2.3 Formation of adducts	60
5.2.4 Determination of the number of tryptophans	61
5.3 Computational methods	61
5.4 Results and Discussion	63
5.4.1 Kinetic results	63
5.4.2 Measurements of intrinsic reactivities	65
5.4.3 Binding studies	66
5.4.4 Check of the HLADH monomer-dimer equilibrium	68
5.5 Modelling studies	70
5.5.1 Course of the simulations	71
5.5.2 Overall structure	71
5.5.3 Change in the coenzyme position	73
5.5.4 Changes in the coenzyme conformation	75
5.5.5 Changes of the polypeptide chain	78
5.5.6 Changes in the interactions between enzyme and coenzyme	78
5.5.7 The proton relay system	83
5.5.8 The hydride-transfer	84
5.6 Conclusions	86
References	87



<b>Chapter 6</b>	
<b>Kinetic and modelling studies of NAD<sup>+</sup> analogues</b>	<b>89</b>
6.1 Introduction	89
6.2 Experimental	90
6.2.1 Materials	90
6.2.2 Kinetic measurements	90
6.3 Modelling calculations	90
6.4 Results	91
6.4.1 Kinetic experiments	91
6.4.2 Modelling studies	93
6.5 Discussion	96
6.6 Conclusion	100
References	100
<b>Chapter 7</b>	
<b>The synthetic NADH model N,N,1,2,4-pentamethyl-1,4-dihydronicotinamide</b>	<b>103</b>
7.1 Introduction	103
7.2 Experimental	104
7.3 Reactivity of C=O compounds towards NADH model 1	105
7.4 Stereoselectivity and mechanism of the hydride-transfer	108
7.5 Concluding remarks	109
References	109
<b>Chapter 8</b>	
<b>The out-of-plane concept <i>discussion</i></b>	<b>111</b>
Appendix 1	115
Appendix 2	117
Appendix 3	121
Appendix 4	122
Summary	124
Samenvatting	126
Curriculum vitae	127
Acknowledgments/Dankwoord	129

## Abbreviations

vii

acPdAD <sup>+</sup> /acPdAD	3-acetylpyridine adenine dinucleotide
acPdADH	reduced form of acPdAD <sup>+</sup>
Ade	adenine
AMBER	assisted model building with energy refinement
BSA	bovine serum albumin
cnPdAD <sup>+</sup>	3-cyanopyridine adenine dinucleotide
DMSO	dimethyl sulphoxide
EDTA	ethylenediaminetetraacetic acid
EtOH	ethanol
EtO <sup>-</sup> /EtO	ethoxide
fPdAD <sup>+</sup> /fPdAD	3-formylpyridine adenine dinucleotide
fPdADH	reduced form of fPdAD <sup>+</sup>
GAPDH	glyceraldehyde-3-phosphate dehydrogenase
HLADH	horse liver alcohol dehydrogenase
IPA/iPrOH	isopropanol
iPrO <sup>-</sup> /iPrO	isopropoxide
k <sub>cat</sub>	turn over number
k <sub>H</sub>	rate of hydrogen-transfer
K <sub>m</sub>	Michaelis-Menten constant
LADH	liver alcohol dehydrogenase
MM	molecular mechanics
MD	molecular dynamics
NAD <sup>+</sup> /NAD	nicotinamide adenine dinucleotide
NADH	reduced form of NAD <sup>+</sup>
ND	not determined
NMN <sup>+</sup>	nicotinamide mononucleotide
NMR	nuclear magnetic resonance
PEG-NAD <sup>+</sup>	polyethylene glycol bound NAD <sup>+</sup>
PEG-NADH	reduced form of PEG-NAD <sup>+</sup>
Rib	ribose
RMS	root mean square
sNAD <sup>+</sup> /sNAD	thionicotinamide adenine dinucleotide
sNADH	reduced form of sNAD <sup>+</sup>
TMS	tetramethyl silane
TS	transition state
UV	ultraviolet

Abbreviations for amino acids are in accordance with recommendations of the IUPAC-IUB Commission on Biochemical Nomenclature (*Eur. J. Biochem.* **136**, 9-37 (1984)).



# 1 Introduction

## 1.1 Nicotinamide Adenine Dinucleotide ( $\text{NAD}^+/\text{NADH}$ )

The coenzyme **Nicotinamide Adenine Dinucleotide** (see Figure 1.1) is involved in many cellular processes like electron transport and oxidative phosphorylation<sup>[1-4]</sup>.

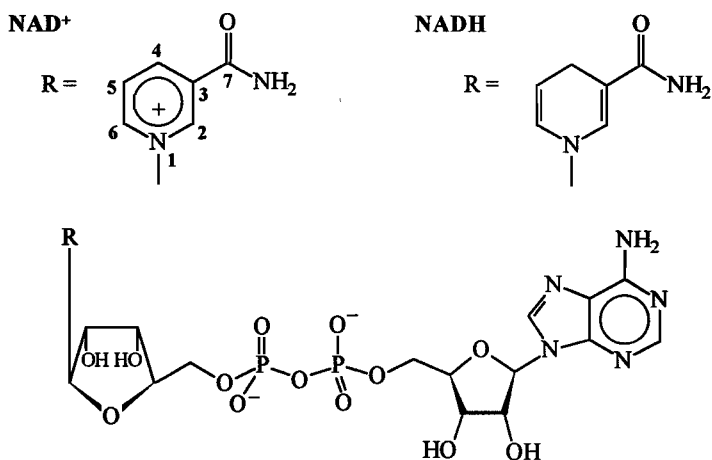
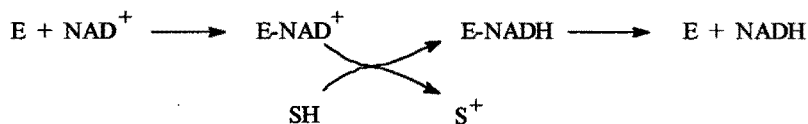


**Figure 1.1** Schematic representation of  $\text{NAD}^+$  and  $\text{NADH}$ .

The reduction/oxidation of  $\text{NAD}^+/\text{NADH}$  in the biological cell is achieved by enzymes requiring this redox couple as a cofactor (see Scheme 1.1). These enzymes (called dehydrogenases) position both the coenzyme  $\text{NAD}^+/\text{NADH}$  and the substrate in their active sites in such a way that a very efficient and fast reaction can take place. The reaction is generally considered as a concerted process, i.e. a formal transfer of a hydride ion.

All dehydrogenases show high stereoselectivity for the hydrogen transferred from the



*Scheme 1.1 Schematic representation of the enzymatic (E) reduction of  $\text{NAD}^+$  to  $\text{NADH}$  with a substrate (SH).*

C4 atom of  $\text{NADH}$ . With deuterium labelled substrates it was demonstrated<sup>[5]</sup> that, depending on the type of enzyme (A- or B-type), one of the two available hydrogen atoms at C4 of  $\text{NADH}$  is transferred, as illustrated in Figure 1.2. The  $\text{H}_\text{A}$  or  $\text{H}_\text{B}$  specificity originates from electrostatic and steric interactions of the substrate and the coenzyme with the enzyme (see paragraph 1.4). Dehydrogenases also show a high degree of stereo- and regiospecificity with respect to the substrate.

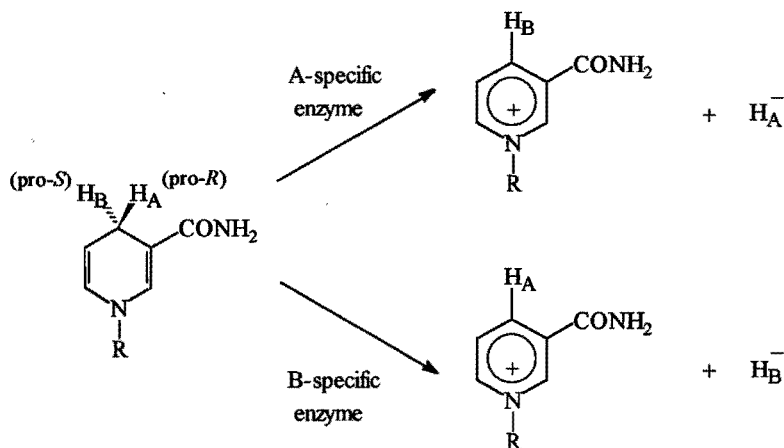


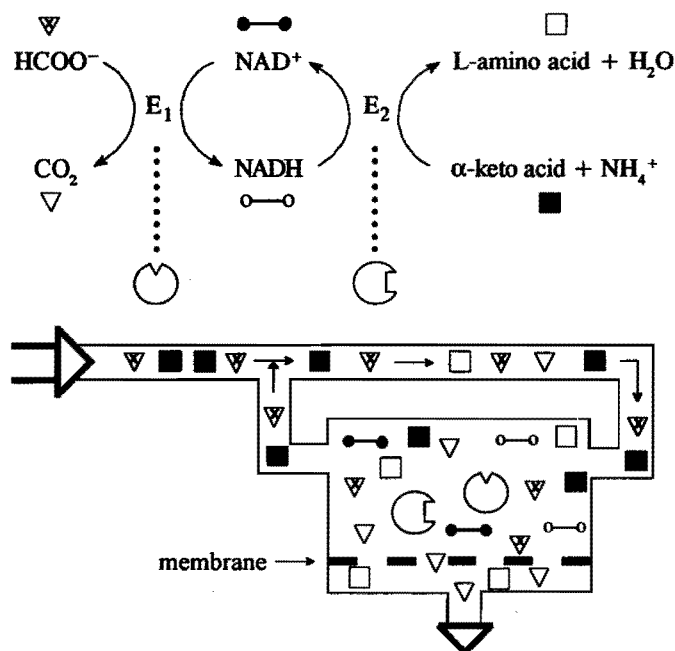
*Figure 1.2 Stereospecific hydride-transfer by A- and B-specific dehydrogenases.*

The remarkable catalytic power and the high stereo- and regiospecificity of dehydrogenases under mild physiological conditions, make them excellent candidates to be used in the synthesis of optically pure compounds. For many applications, e.g. building blocks in the preparation of medicines, it is essential to obtain chiral synthons in enantiomer pure form. However, the use of enzymes in organic synthesis is still limited, mainly due to the often difficult preparation and purification of the enzymes, the necessity of expensive

cofactors for many enzymatic reactions, the limited number of accepted substrates and the restricted operational conditions in organic media.

## 1.2 Coenzyme dependent enzymes in industrial reactions

A commercially attractive example of a dehydrogenase-dependent synthesis of optically pure compounds is the production of L-amino acids from their corresponding  $\alpha$ -keto acids. Normally, in the enzymatic production of L-amino acids, NADH would be used as a stoichiometric reagent. However, nicotinamide cofactors are very expensive (\$1000/g) and in order to employ NAD-dependent enzymes commercially, cofactor recycling is a must. This was, amongst others, nicely accomplished by Wandrey and coworkers<sup>[6-8]</sup> using a so-called continuous enzyme membrane reactor in which the coenzyme NAD<sup>+</sup>/NADH is simultaneously regenerated by adding a second enzyme and a second substrate (see Scheme 1.2). The second substrate should be cheap and it is essential that its oxidation product can be easily removed from the reaction mixture<sup>[9]</sup>. The HCOO<sup>-</sup>/formate dehydrogenase system



**Scheme 1.2** Enzyme membrane reactor concept for continuous enzymatic synthesis with coenzyme regeneration. E<sub>1</sub> = formate dehydrogenase; E<sub>2</sub> = amino acid dehydrogenase.

meets these requirements.

The retention of the  $\text{NAD}^+$  coenzyme is more difficult to achieve. Due to its relatively small size,  $\text{NAD}^+$  can easily pass through the membrane. One way to overcome this problem is to increase the molecular size of the coenzyme to such an extent that it will be too large to cross the membrane, just like the enzymes. An elegant method to enlarge  $\text{NAD}^+$  is covalently linking of the coenzyme to polyethylene glycol (PEG- $\text{NAD}^+$ ). The kinetic behaviour of PEG- $\text{NAD}^+$  is subject of the investigations reported in Chapter 5.

### 1.3 The NAD-dependent horse liver alcohol dehydrogenase (HLADH)

Horse liver alcohol dehydrogenase, HLADH, is one of the best documented NAD-dependent enzymes (see for example references 10-12). It catalyses the interconversions of alcohols to their corresponding aldehydes/ketones and vice versa. Many kinetic data and several three-dimensional structures of HLADH are available<sup>[13-19]</sup>, including an X-ray structure of the ternary complex of this enzyme, with NADH and the dummy substrate DMSO bound to the apo-enzyme<sup>[20-21]</sup>, making this enzyme one of the best characterized dehydrogenases.

HLADH is only active as a dimer (see Figure 1.3) and the monomeric units (subunits) can be classified as the ethanol type (E) or steroid type (S) referring to their substrate specificities. Only the EE-dimer will be discussed here, in the context of this thesis. Each

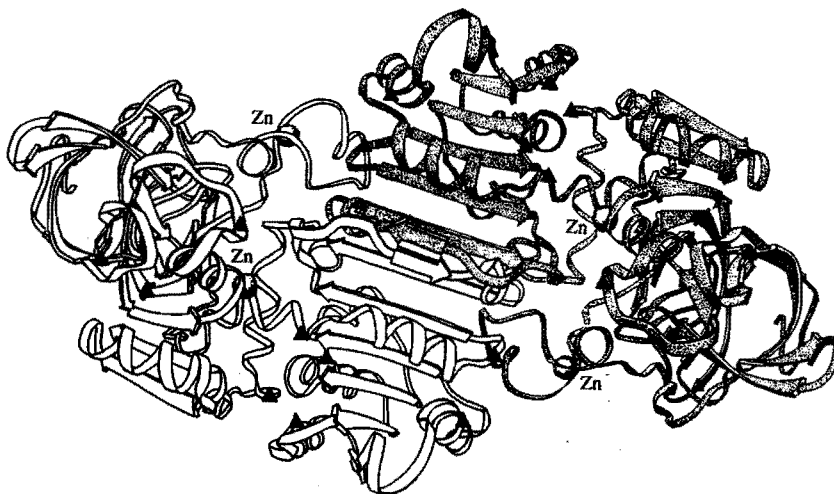
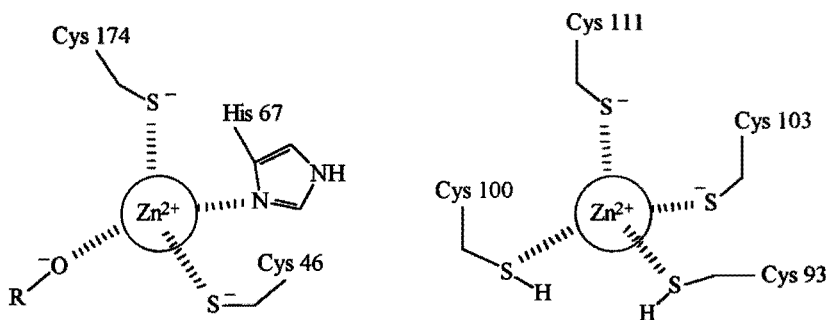


Figure 1.3 Schematic representation of the horse liver alcohol dehydrogenase dimer [22].

(E) subunit of the HLADH-dimer consists of a catalytic and a coenzyme domain<sup>[23]</sup>. The coenzyme binding domain is regularly built from six  $\alpha$ - $\beta$  units and contains the residues 175-318<sup>[13,24]</sup>. Similar binding sites for  $\text{NAD}^+$  have been found with other dehydrogenases<sup>[25,26]</sup>. The catalytic domain comprises two regions of the polypeptide chain: residues 1-174 and 319-374. It is known from X-ray analysis that the active form of HLADH is represented by a 'closed' structure. When the  $\text{NAD}^+$  coenzyme enters its binding site in the open form of the apo-enzyme, it subsequently induces conformational changes resulting in efficient binding interactions between apo-enzyme and coenzyme<sup>[11,12,17,27,28]</sup>.

The two zinc atoms of each subunit are complexed to residues from the catalytic domain as shown in Figure 1.4. The catalytic zinc is tetracoordinated by Cys 46, His 67, Cys 174 and a water or substrate molecule. The second zinc atom is believed to have a structural role<sup>[29,30]</sup>, liganded by four sulphur atoms from cysteine residues 97, 100, 103 and 111.



**Figure 1.4** Schematic drawing showing the ligands of the catalytic zinc atom (left) and the structural zinc atom (right).  $R=H$  or alkyl/aryl.

The catalytic zinc ion in the active site of HLADH positions the substrate relative to the coenzyme (see Figure 1.5) and activates the substrate by coordinating the relevant oxygen atom (see Figure 1.4, left drawing). During alcohol oxidation,  $\text{Zn}^{2+}$  stabilizes the alcoholate ion in order to make the hydride-transfer step feasible<sup>[31]</sup>. In the reverse reaction, zinc plays the role of electron attractor, which gives rise to an increased electrophilic character of the aldehyde/ketone, consequently facilitating the hydride-transfer towards the aldehyde/ketone.



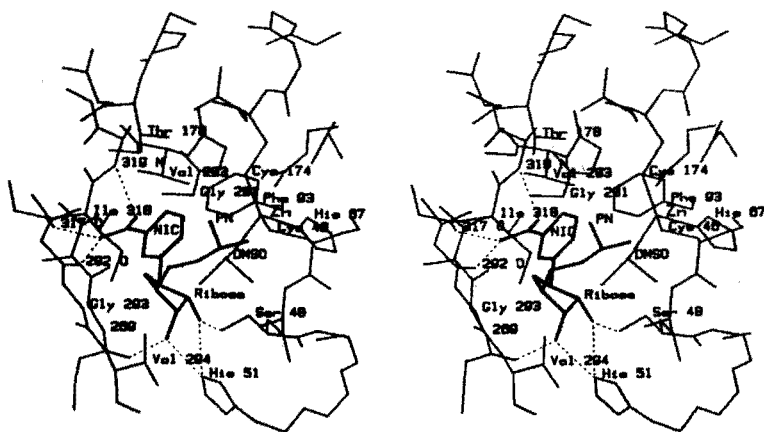


Figure 1.5 Stereo-plot of the active site of HLADH [20]. The NMN half of the coenzyme is shown in thick lines, and the protein residues, Zn and DMSO are displayed with thin lines. Hydrogen-bonds are plotted with dotted line.

#### 1.4 The rate and stereospecificity of hydride-transfer

Levy and Vennesland<sup>[32]</sup> convincingly demonstrated with deuterium labelled substrates the A-stereospecific nature of HLADH. The A-specificity of HLADH originates from the fact that the B-side of the nicotinamide moiety of the coenzyme is shielded by a hydrophobic wall of the residues Thr 178, Val 203 and Val 294 of the enzyme, whereas the A-side is directed toward the substrate. Since the enzyme positions both the nicotinamide ring and the substrate in a narrow pocket, there is no space left to accommodate the nicotinamide ring if it is rotated 180° around the glycosidic bond ( $\chi_N$ ), turning the B-side toward the substrate (see Figure 1.5 and 1.6).

The relevance of the positioning of the carboxamide group for the dynamics of the enzyme-catalyzed hydride-transfer was first suggested by Dutler<sup>[33]</sup> for HLADH. Donkersloot and Buck<sup>[34]</sup> using quantum mechanical calculations on a model complex, found evidence that the enthalpy of the transition state of hydride-transfer is at a minimum in case the C=O dipole and the direction of hydride-transfer are *syn* oriented. This implies that the amide carbonyl dipole is directed towards the substrate (see Chapter 8 for further discussions).

The so-called "*syn*-out-of-plane" concept is supported by röntgen crystallographic data. In the X-ray structure of the ternary complex of HLADH (1.8 Å resolution,

crystallographic  $R$  factor of 0.17)<sup>[21]</sup> the carboxamide side-chain shows an out-of-plane rotation ( $\theta$ ) of  $23^\circ$  towards the A side of the nicotinamide moiety (see also Figure 1.5). In the active site of HLADH, the amide side-chain is involved in the formation of hydrogen-bonds with the amino acids Val 292, Ala 317 and Phe 319 (see Figure 1.6)<sup>[16,17]</sup>. In the ternary complex of HLADH/NAD<sup>+</sup>/substituted benzyl alcohol (2.1 Å resolution, crystallographic  $R$  factor of 0.183)<sup>[19]</sup> a similar out-of-plane value could be determined. In the B-specific glyceraldehyde-3-phosphate dehydrogenase (GAPDH) from *Bacillus stearothermophilus* (1.8 Å resolution, crystallographic  $R$  factor of 0.177)<sup>[35]</sup> an out-of-plane rotation of  $22^\circ$  is found, this time on the B side of the ring, again directed towards the substrate.

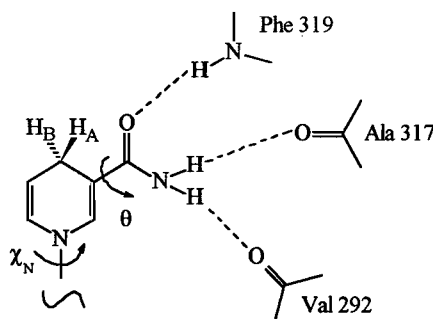


**Figure 1.6** Schematic drawing showing the hydrogen-bonds (in dotted lines) between amino acids of HLADH and the carboxamide side-chain.

## 1.5 Computational chemistry on enzymes

Computational chemistry is a branch of chemistry, which is attracting more and more interest among experimental chemists. Complex (bio)chemical problems can be approached with the use of computational methods in combination with experimental verification.

Computer simulations of complex biological molecules are possible nowadays, but there are still some fundamental problems. The first one is the global minimum problem. Due to the large degree of conformational freedom in proteins, it is difficult and almost impossible to correctly evaluate and rank the relative energies of all conformations. Secondly, large molecules (such as proteins) can only be studied using simplified potential energy equations.

Commonly used programs in the field of simulations on biological molecules are the

so-called force field programs like GROMOS<sup>[36,37]</sup>, INSIGHT<sup>[38]</sup>, CHARMM<sup>[39,40]</sup> and AMBER<sup>[41,42]</sup>. The least time consuming are the molecular mechanics calculations, which seek the closest local minimum at the potential energy curve. Molecular dynamics, i.e. integration of Newton's equation of motion, gives more information about the dynamic aspects of a system at a certain temperature and pressure, and allows the molecule studied to cross certain barriers so that small conformational changes can occur, and lower minima can be found.

A combination of molecular mechanics/dynamics and quantum mechanical methods is preferred if one attempts to model processes such as chemical reactions or enzyme catalysis. In order to study molecular solvation, ligand binding and enzyme catalysis, free energy perturbation methods are useful. The free energies of molecular systems describe their tendencies to associate and react. Combined with experimental data such as activities and free energies of binding, the fitting of new substrates or coenzymes can be studied.

In our group, molecular mechanics calculations have been performed on ternary complexes of HLADH/DMSO/NAD<sup>+</sup> (analogues)<sup>[43-46]</sup>.

## 1.6 Synthetic NADH models

Another way of gaining insight into the enzymatic mechanism is with the aid of model systems. The reversible and stereoselective hydride-transfer from NADH to prochiral substrates under the influence of dehydrogenases has inspired many chemists to design NADH models useful as efficient enantioselective reducing agents<sup>[47-50]</sup>. These NADH models have been developed not only to elucidate the mechanism of these enzymes, but also their use as efficient stereoselective catalysts to produce optically active products has been investigated.

For example the concept of the out-of-plane rotation of the amide carbonyl of NAD<sup>+</sup>/NADH has been verified experimentally (*in vitro*) with the NADH model N,N,1,2,4-pentamethyl-1,4-dihydronicotinamide<sup>[50-52]</sup>.

## 1.7 Outline of this thesis

The research reported in this thesis is focussed on various aspects of the mechanism of NAD-dependent dehydrogenases.

In order to obtain better insight in the mechanism of hydride-transfer, semiempirical calculations on active site models of HLADH were carried out (Chapter 2).

The AMBER 4.0 force field optimization, using well defined crystal structures of amino acids as starting structure, is discussed in Chapter 3.

Because small and medium sized molecules are not always correctly described in force field programs, a study was made of the rotational barrier around the C3-C7 bond of the pyridinium ring (Chapter 4).

With an adapted AMBER 4.0 force field, the ternary complex of HLADH was investigated. Both molecular mechanics and dynamics calculations were performed in order to study the interaction of PEG-NAD<sup>+</sup> with HLADH (Chapter 5).

Modelling studies on other NAD<sup>+</sup> analogues are reported in Chapter 6, in an attempt to rationalize the kinetic data for these coenzymes.

Chapter 7 deals with the synthetic NADH model N,N,1,2,4-pentamethyl-1,4-dihydronicotinamide and its reactivity towards several carbonyl substrates. The existence of a ternary complex during this reaction and the *syn*-out-of-plane concept are discussed.

An historical overview of the ideas and concepts of the rate and stereospecificity of the hydride-transfer is given in Chapter 8 and discussed.

## References

1. S.P. Colowick, J. van Eys and J.M. Park, *Comp. Biochem.* (Florkin and Stolz, eds.) **14**, 1-98 (1966).
2. H. Sund and H. Theorell in *"The Enzymes"* (P.D. Boyer, H. Lardy and K. Myrbäach, eds.) 2nd ed., Academic Press, New York and London, **7**, 25-85 (1962).
3. H. Sund in *"Pyridine Nucleotide-dependent dehydrogenases"* (H. Sund, ed.) de Gruyter, Berlin, Germany (1977).
4. K.S. You, *CRC. Crit. Rev. Biochem.* **17**, 313-451 (1984).
5. B. Vennesland and F.H. Westheimer in *"The Mechanism of enzyme action"* (W.D. McElroy and B. Glass, eds.) John Hopkins Press, Baltimore (1954).
6. R. Wichmann, C. Wandrey, A.F. Bückmann and M.R. Kula, *Biotechn. and Bioeng.* **23**, 2789-2802 (1981).
7. C. Wandrey and R. Wichmann, *Biotechn. Series 5*, 177-208 (1985).
8. C. Wandrey in *"Proceeding 4th European Congress on Biotechnology"* (O.M. Neijssel, R.R. van der Meer and K.Ch.A.M. Luyben, eds.) **14**, 1-98 (1966).
9. H.K. Chenault and G.M. Whitesides, *Appl. Biochem. Biotechn.* **14**, 147-197 (1987).
10. J.-F. Biellmann, *Acc. Chem. Res.* **19**, 321-328 (1986).
11. H. Eklund and C.-I. Brändén in *"Coenzymes and Cofactors, Pyridine Nucleotide coenzymes"* (D. Dolphin, O. Avramovic and R. Poulson, eds.) John Wiley and Sons, New York, **2A**, 51-98 (1987).
12. H. Eklund and C.-I. Brändén, *Biological Macromolecules and Assemblies*, 73-142 (1987).
13. H. Eklund, B. Nordström, E. Zeppezauer, G. Söderland, I. Ohlsson, T. Boiwe, B.-O. Söderberg, O. Tapia and C.-I. Brändén, *J. Mol. Biol.* **102**, 27-59 (1976).

14. H. Eklund, J.-P. Samama and L. Wallén, *Biochemistry* **21**, 4858-4866 (1982).
15. E. Cedergren-Zeppezauer, J.-P. Samama and H. Eklund, *Biochemistry* **21**, 4895-4908 (1982).
16. B.V. Plapp, H. Eklund, T.A. Jones and C.-I. Brändén, *J. Biol. Chem.* **258**, 5537-5547 (1983).
17. H. Eklund, J.-P. Samama and T.A. Jones, *Biochemistry* **23**, 5982-5996 (1984).
18. E. Cedergren-Zeppezauer, *Biochemistry* **22**, 5761-5772 (1983).
19. S. Ramaswamy, H. Eklund and B.V. Plapp, *Biochemistry* **33**, 5230-5237 (1994).
20. H. Eklund, J.-P. Samama, L. Wallén, C.I. Brändén, Å. Åkeson and T.A. Jones, *J. Mol. Biol.* **146**, 561-587 (1981).
21. S. Al-Karadaghi, E.S. Cedergren-Zeppezauer and S. Hövmoller, *Acta Cryst.* **D50**, 793-807 (1994).
22. H. Eklund in *"Coenzymes and Cofactors, Pyridine Nucleotide coenzymes"* (D. Dolphin, O. Avramovic and R. Poulson, eds.) John Wiley and Sons, New York, **2A**, p. 84 (1987).
23. M.G. Rossmann in *"Struct. Conform. Nucleic Acids Protein-Nucleic Acid Interactions, Proc. Annu. Harry Steenbock Symposium"* 4th, 353-374 (1974, Publ.1975).
24. M. Levitt and Chothia, *Nature* **261**, 552-558 (1976).
25. J. Ohlsson, B. Nordström and C.-I. Brändén, *J. Mol. Biol.* **89**, 339-354 (1974).
26. M.G. Rossmann, D. Moras and K.W. Olsen, *Nature* **250**, 194-199 (1974).
27. H. Eklund and C.-I. Brändén, *J. Biol. Chem.* **254**, 3458-3461 (1979).
28. F. Colonna-Cesari, O. Perahia, M. Karplus, H. Eklund, C.-I. Brändén and O. Tapia, *J. Biol. Chem.* **261**, 15273-15280 (1986).
29. D.E. Drum, T.-K. Li and B.L. Vallee, *Biochemistry* **8**, 3783-3791 (1969).
30. D.E. Drum, T.-K. Li and B.L. Vallee, *Biochemistry* **8**, 3792-3797 (1969).
31. J. Kvassman, A. Larsson and G. Pettersson, *Eur. J. Biochem.* **114**, 555-563 (1981).
32. B. Vennesland and F.H. Westheimer in *"The Mechanism of Enzyme Action"* (W.D. McElroy, B. Glass, eds.) John Hopkins Press, Baltimore, USA (1957).
33. H. Dutler in *"Pyridine Nucleotide-dependent Dehydrogenases"* (H. Sund, ed.) W. de Gruyter, Berlin, Germany, 339-350 (1977).
34. M.C.A. Donkersloot and H.M. Buck, *J. Am. Chem. Soc.* **103**, 6554-6558 (1981).
35. T. Skarzynski, P.C.E. Moody and A.J. Wonacott, *J. Mol. Biol.* **193**, 171-187 (1987).
36. GROMOS, W.F. van Gunsteren and H.J.C. Berendsen: *Groningen Molecular Simulation, Library Manual*, Biomos, Groningen (1987).
37. J. Hermans, H.J.C. Berendsen, W.F. van Gunsteren and J.P.M. Postma, *Biopolymers* **23**, 1513-1518 (1984).
38. INSIGHT/DISCOVER, Biosym Inc., San Diego, California, USA.
39. QUANTA/CHARMM, Molecular Simulations Inc., Waltham, Massachusetts, USA.
40. B.R. Brooks, R.E. Bruccoleri, B.D. Olafson, D.J. States, S. Swaminathan and M. Karplus, *J. Comput. Chem.* **4**, 187-217 (1983).
41. P.K. Weiner and P.A. Kollman, *J. Comput. Chem.* **2**, 287-303 (1981).
42. S.J. Weiner, P.A. Kollman, D.T. Nguyen and D.A. Case, *J. Comput. Chem.* **7**, 230-252 (1986).
43. P.M.T. De Kok, N.A. Beijer, H.M. Buck, L.A.Æ. Sluyterman and E.M. Meijer, *Recl. Trav. Chim. Pays-Bas* **107**, 355-361 (1988).
44. P.M.T. De Kok, N.A. Beijer, H.M. Buck, L.A.Æ. Sluyterman and E.M. Meijer, *Eur. J. Biochem.*

- 175, 581-585 (1988).
45. N.A. Beijer, H.M. Buck, L.A.Æ. Sluyterman and E.M. Meijer, *Biochim. Biophys. Acta* **1039**, 227-233 (1990).
  46. N.A. Beijer, H.M. Buck, L.A.Æ. Sluyterman and E.M. Meijer, *Ann. N. Y. Ac. Sc.* **613**, 494-500 (1990).
  47. A. Ohno, M. Ikeguchi, T. Kimura and S. Oka, *J. Am. Chem. Soc.* **101**, 7036 (1979).
  48. A. Ohno, M. Kashiwagi, Y. Ishihara, S. Ushida and S. Oka, *Tetrahedron* **42**, 961 (1986).
  49. A.I. Meyers and T.J. Oppenlaender, *J. Am. Chem. Soc.* **108**, 1989-1996 (1986).
  50. P.M.T. de Kok, L.A.M. Bastiaansen, P.M. van Lier, J.A.J.M. Vekemans and H.M. Buck, *J. Org. Chem.* **54**, 1313-1320 (1989).
  51. P.M.T. de Kok, M.C.A. Donkersloot, P.M. van Lier, G.H.W.M. Meulendijks, L.A.M. van Hooff, H.J.G. Kanters and H.M. Buck, *Tetrahedron* **42**, 941-959 (1986).
  52. J.P.G. Versleijen, M.S.T.H. Sanders-Hovens, S.A.M. Vanhommerig, J.A.J.M. Vekemans and E.M. Meijer, *Tetrahedron*, **49**, 7793-7802 (1993).



# 2

## *Semiempirical AM1 and PM3 studies on active site models of HLADH*

### 2.1 Introduction

Horse liver alcohol dehydrogenase (HLADH) is a  $\text{NAD}^+/\text{NADH}$  dependent enzyme, stereoselectively catalyzing the interconversions of various alcohols into their corresponding aldehydes and ketones<sup>[1]</sup>. The kinetic behaviour of HLADH with both primary and secondary alcohols can be described with the mechanism in which the enzyme, coenzyme and substrate combine into a ternary complex<sup>[2-5]</sup>. In this complex the reaction takes place. If  $\text{NAD}^+$  is used as coenzyme and ethanol as substrate, the dissociation of the NADH from the enzyme is the rate-limiting step, whereas in the case of the poor substrate isopropanol the rate of hydride-transfer is limiting<sup>[5]</sup>.

Several 3-D structures of HLADH with NADH and DMSO have been determined by X-ray diffraction<sup>[6,7]</sup>. In this ternary complex of HLADH<sup>[6]</sup>, each subunit contains one catalytic Zn(II) ion (see Chapter 1), which participates in the enzymatic reaction. The alcohol is expected to coordinate to zinc and to react as an alkoxide ion. The zinc ion is furthermore coordinated to Cys 46, His 67 and Cys 174 (Figure 2.1). In the recently determined crystal structure of HLADH/NADH/DMSO (1.8 Å resolution)<sup>[7]</sup>, several water molecules could be located explicitly. Ramaswamy et al.<sup>[8]</sup> determined a ternary X-ray structure of HLADH with  $\text{NAD}^+$  and pentafluorobenzyl alcohol with a resolution of 2.1 Å. In this structure the alcohol is indeed ligated to the zinc ion and in addition 12 water molecules were found in each subunit. Zinc-bound water is absent in the above-mentioned structures.

In 1993, Ritter von Onciul and Clark reported a theoretical study of the catalytic oxidation of alcohols by LADH<sup>[9]</sup>. A model was used for the active site in which the catalytic zinc ion is surrounded by four ligands, i.e. a histidine, an alkoxide and two cysteine residues (see Figure 2.2). However, they did not use the exact coordinates of the X-ray structure to build their model and their optimized structures did not resemble the X-ray structure any more (*vide infra*). Furthermore the sulphur atoms of the cysteines contained hydrogen atoms, resulting in an overall charge of the model of +2. However, it is far more likely that these cysteine residues coordinated to a zinc dication, carry negative charges<sup>[6,10,11]</sup>. For example with papain, it was shown that zinc is capable of removing a



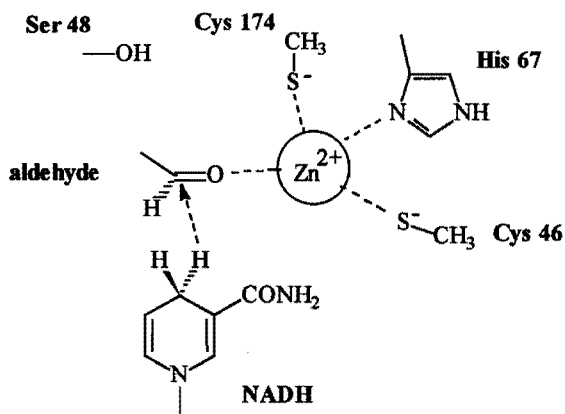


**Figure 2.1** Schematic representation of our active site model with ethanol as substrate (system 1), aldehyde state. The dotted arrow indicates the hydride-transfer path.

proton both from the thiol group of a cysteine and the imidazole group of a histidine in the active site<sup>[10]</sup>. Also in several papers dealing with HLADH it has been indicated that the cysteines surrounding the catalytic zinc ion are negatively charged<sup>[6,11]</sup>. Even more convincing is the fact that the pKa of the zinc-bound water is shifted from 15.7 to 7.6<sup>[11]</sup>, suggesting a similar pKa-shift for the cysteines (which normally have a pKa of approximately

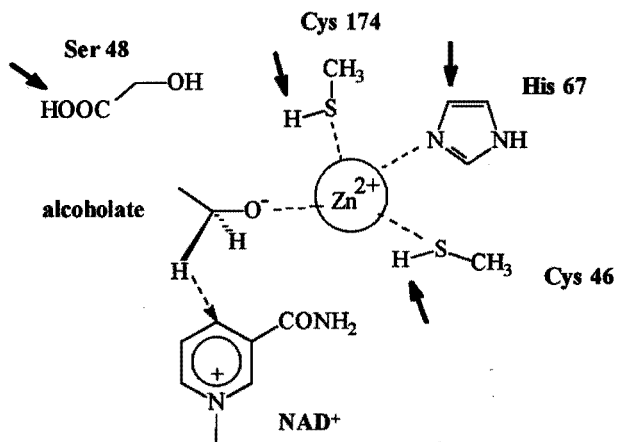


**Figure 2.2** Active site model of the TS state as used by Ritter von Onciul *et al.*<sup>[9]</sup>. Arrows indicate the differences with our active site model, system 1 (see Figure 2.1).

9), causing complete ionization of both cysteines at the near-neutral pH range of the enzyme activity. The conclusion seems therefore justified that the zinc-coordinated cysteine residues in HLADH are deprotonated and present as thiolate anions. This would result in an overall charge of zero rather than 2+ for model complexes as used by Ritter von Onciul and Clark<sup>[9]</sup>.

In this chapter semiempirical calculations (AM1 and PM3) are reported on active site models for the ternary complex of HLADH, using ethanol, 1-propanol and isopropanol as substrates. Our studies aim at improving the insight into the mechanism of hydrogen/hydride-transfer in HLADH. The influence of negatively charged cysteine residues on the geometric and electronic features of the model has been examined. The effect of the presence of water molecules has been included in the current investigation. Finally, some NAD analogues are being studied via semiempirical calculations, together with the effect of hydrogen-bonding interactions around the side-chain of the coenzyme.

## 2.2 Methods

AM1<sup>[12]</sup> and PM3<sup>[13]</sup> calculations were performed on an Alliant FX2816 computer using the semiempirical package MOPAC 6.0<sup>[14]</sup>. The crystallographic structure of the ternary complex of HLADH/NADH/DMSO (2.9 Å resolution, PDB file 6ADH)<sup>[6]</sup> was used to obtain

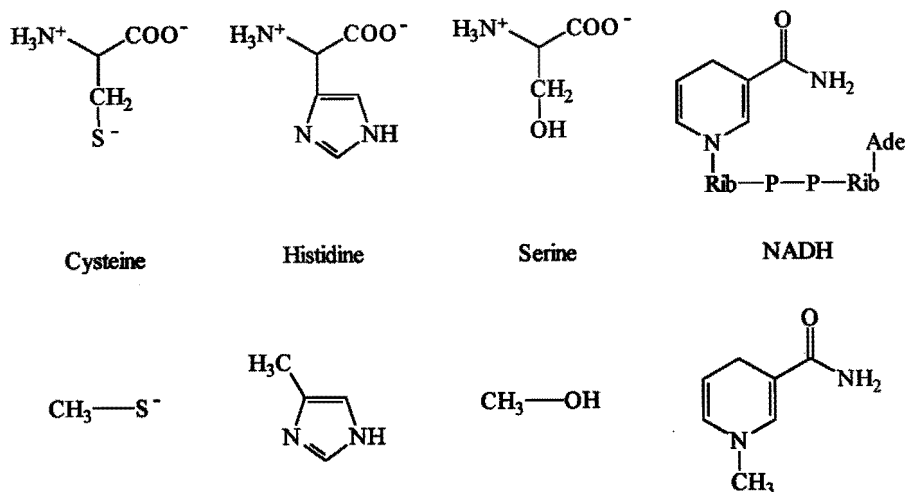


**Figure 2.3** Original compounds of the active site of HLADH (top row) and their derivatives as used in the calculations (bottom row). P denotes phosphate group.

a starting structure of the active site model. To limit the number of atoms involved in the calculations, derivatives of the amino acids and the coenzyme were used. Figure 2.3 shows the original residues in the active site of HLADH and their derivatives as used in these calculations.

The active site model consists of a zinc(II) ion, coordinated by the derivatives of Cys 46, His 67, Cys 174 and alkoxide/aldehyde/ketone (at the position of DMSO), and furthermore derivatives of Ser 48 and NAD<sup>+</sup>/NADH. All residues (see Figure 2.1) were separately optimized and these optimized structures were inserted in the active site model at the same position as in the X-ray structure, using the 'Molecular similarity → Match atoms' option from the QUANTA program<sup>[15]</sup> to obtain the best fit for each derivative with its original counterpart. When performing these kind of calculations, there are two choices one can make: 1) optimize all atoms 2) apply constraints to maintain good agreement with the crystal structure used as starting structure and stay close to the realistic situation as in natural systems. The last option was chosen in this thesis and resulted in fixating the carbon, sulphur and nitrogen atoms of the cysteines, serine, histidine and of the nicotinamide ring of NAD<sup>+</sup>/NADH at their X-ray positions. The carboxamide side-chain of NAD<sup>+</sup>/NADH, all hydrogen atoms, the alkoxide and, if present, the water molecule were allowed to move freely. A gradient norm (keyword GNORM) of 0.1 was applied unless stated otherwise. For each model system three states were calculated: the ground state with NAD<sup>+</sup> and alkoxide, the transition state and the ground state with NADH and aldehyde/ketone. They will be referred to as the alcohol state, the transition state (TS), and the aldehyde state, respectively. The ground states were determined using the EF algorithm. Transition states were located by applying the SADDLE keyword<sup>[16]</sup>; some structures obtained with SADDLE were further refined using the TS keyword<sup>[17]</sup> (EF algorithm for locating transition states).

The active site models with the NAD analogues were obtained starting from the optimized structure with the NAD<sup>+</sup>/NADH derivative. The positions for the new atoms in the side-chain were logically adjusted. In the case of the calculations including the H-bonding interactions around the carboxamide side-chain of NAD, the active site models also consist of NH<sub>3</sub> and two formaldehyde groups, which take the same positions as Phe 319, Ala 317 and Val 292, respectively, in the X-ray structure.

## 2.3 Results and discussion

### 2.3.1 The influence of the total charge of the model complexes

To allow a fair comparison between the results using geometrical constraints and a

total charge=0 and those published by Ritter von Onciul and Clark, who started from a transition state model of the active site (see Figure 2.2) without using geometrical constraints, we first followed their strategy. Within 1 kcal.mol<sup>-1</sup> differences we found the same energies for two of the three states (see Table 2.1). The results with the alcohol state could not be reproduced any better than within 8 kcal.mol<sup>-1</sup>, probably because the alcohol state had to be derived from their TS.

We then compared two active site models with ethanol as substrate (as described under methods), system 1, with S<sup>-</sup> groups and an overall charge of zero, and system 2 which contains SH groups and thus an overall charge of +2. Both active site models consist

**Table 2.1** AM1 and PM3 calculated heats of formation,  $E_{act}$  and  $\Delta H_f$  (in kcal.mol<sup>-1</sup>). The transition states are determined using the SADDLE keyword, unless stated otherwise.

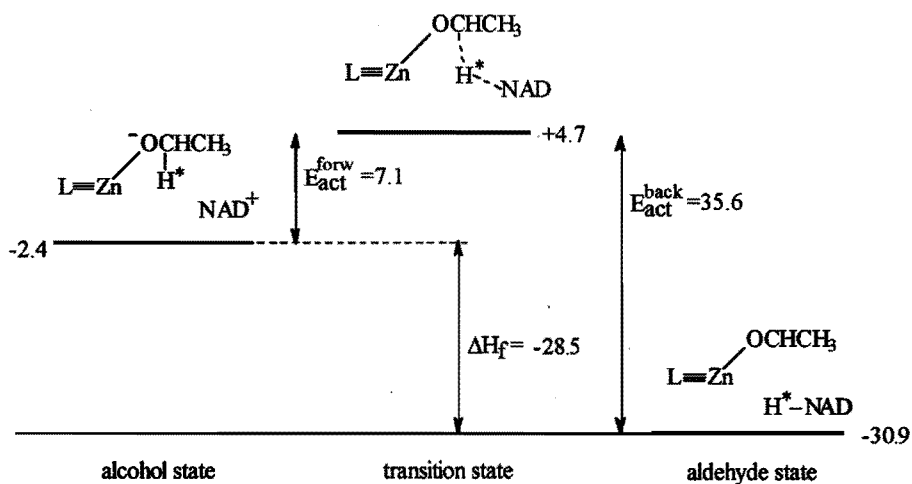
	total charge	$\Delta H_f^\circ$ alcohol state	$\Delta H_f^\circ$ transition state	$\Delta H_f^\circ$ aldehyde state	$E_{act}$ forward	$E_{act}$ backward	$\Delta H_f^a$
<b>Geometries based on X-ray structure<sup>[6]</sup></b>							
<b>PM3</b>							
system 1	0	-71.2	-37.8	-85.1	+33.4	+47.3	-13.9
system 2	2	+227.7	+269.0	+255.0	+41.3	+14.0	+27.3
<b>AM1</b>							
system 1	0	-2.4	+8.3	-30.9	+10.7	+39.2	-28.5
system 1 <sup>b</sup>	0	-2.4	+4.7	-30.9	+7.1	+35.6	-28.5
system 2	2	+292.1	+319.5	+312.6	+27.4	+6.9	+20.5
<b>Geometries according to Ritter von Onciul &amp; Clark<sup>[9]</sup></b>							
<b>AM1</b>							
present results	2	+114.9	+140.1	+113.3	+25.2	+26.8	-1.6
results Ritter et al. <sup>[9]</sup>	2	+106.8	+139.2 <sup>c</sup>	+113.3	+32.4	+25.9	+6.5

<sup>a</sup>  $\Delta H_f$  is defined as  $\Delta H_f^\circ(\text{aldehyde state}) - \Delta H_f^\circ(\text{alcohol state})$ .

<sup>b</sup> The transition state was refined using the TS keyword.

<sup>c</sup> Ritter et al. used the NS01A<sup>[18]</sup> or NLLSQ<sup>[19]</sup> method to locate the transition state.

of derivatives of  $\text{NAD}^+/\text{NADH}$ , Ser 48, Cys 46, His 67 and Cys 174 as shown in Figure 2.3. Furthermore they contain ethoxide/acetaldehyde and a tetracoordinated zinc ion. For our active site model with negative charges on the cysteines and an overall charge of zero (system 1), we find that the transition state of hydride-transfer is 10.7 and 33.4  $\text{kcal.mol}^{-1}$  higher in energy than the alcohol state and 39.2 and 47.3  $\text{kcal.mol}^{-1}$  higher in energy than the aldehyde state, as calculated with AM1 and PM3 respectively using the SADDLE keyword to find the transition state (see Scheme 2.1 and Table 2.1). The keyword TS resulted in a  $\Delta H_f^\circ = +4.7 \text{ kcal.mol}^{-1}$  for the transition state of system 1. With the FORCE keyword the gradients and number of imaginary frequencies of this calculated TS were checked.



**Scheme 2.1** The energy differences in hydride-transfer calculated with AM1; pathway of system 1: total charge=0 and some fixed atoms.

Although there are differences in the calculated activation energies with AM1 and PM3, the optimized geometries with AM1 and PM3 of the three states are almost identical. The energy differences found between the calculated AM1 and PM3 structures are only caused by the differences in the applied method. Only with the optimized geometry of the alcohol state both methods yield different results (the amide side-chain of NAD is oriented differently). Qualitatively the values we calculated for system 2 (containing SH groups) resemble the ones obtained for the geometries of Ritter von Onciul and Clark<sup>[9]</sup> (Table 2.1), i.e. the alcohol state being lower in energy than the aldehyde state with all these models.

If we now compare our active site model system 1 (with  $\text{S}^-$  groups) and system 2

(with SH groups), the most remarkable difference is the change in the sign of  $\Delta H_f$  both with AM1 and PM3 (Table 2.1).

Besides the differences in overall charge and in the side-chains of some amino acids (as illustrated with arrows in Figure 2.2), we used geometrical constraints on some of the atoms whereas Ritter von Onciul and Clark used none. These constraints were applied in order to maintain good agreement with the original X-ray structure. For example, the TS structure of Ritter et al.<sup>[9]</sup> shows for some atoms 5 Å deviation from the original crystal structure. The accuracy of the atom positions in this crystal structure 6ADH<sup>[6]</sup> is  $\leq 1$  Å. With our own model, using AM1 and no or very few constraints, the optimized geometry resulted in ring opening of the pyridinium moiety, due to the formation of a sigma bond between the ethoxide and the NAD<sup>+</sup> ring. When we attempted to use PM3 and no constraints at all, the optimized structures strongly deviate from the X-ray structure. Use of these optimized PM3 structures as starting structures for subsequent AM1 calculations, resulted in geometries with much lower energies, but very different from the original X-ray structures; far beyond one would expect taking into account the flexibility of the enzyme structure. Therefore geometrical constraints had to be included in our modelling studies (see Methods).

### 2.3.2 Mechanism and rate of hydrogen-transfer in HLADH

It is known that with the poor substrate isopropanol the hydride-transfer step is rate-limiting, in contrast with primary alcohols, where the dissociation of NADH from the binary enzyme complex is the rate-determining step<sup>[5,20]</sup> To obtain more information about the

**Table 2.2** AM1 calculated heats of formation,  $E_{act}$  and  $\Delta H_f$  (in kcal.mol<sup>-1</sup>) and the hydrogen transfer distance (in Å). NAD<sup>+</sup>/NADH is used as coenzyme with three different substrates.

Substrate	$\Delta H_f^o$ alcohol state	$\Delta H_f^o$ transition state	$\Delta H_f^o$ aldehyde state	$E_{act}$ forward	$E_{act}$ backward	$\Delta H_f$	hydrogen- transfer distance <sup>a</sup>
ethanol	-2.4	+4.7	-30.9	+7.1	+35.6	-28.5	0.60
1-propanol	-13.1	-1.7	-36.6	+11.4	+34.9	-23.5	0.61
isopropanol	-2.2	7.7	-36.2	+9.9	+43.9	-34.0	0.73

<sup>a</sup> The hydrogen-transfer distances are derived from the corresponding TS structures of model structures resembling Figure 2.1.

**Table 2.3** Relative turn over numbers of  $NAD^+$  in the enzymatic reduction by horse liver alcohol dehydrogenase with several alcohols as substrates.

	ethanol	1-propanol	isopropanol
$k_{cat}$ (our results)	100% [21]	98% <sup>a</sup>	13% [21]
$k_{cat}$ (Park and Plapp) <sup>[22]</sup>	100%	100%	
$k_{cat}$ (Dalziel and Dickinson) <sup>[5]</sup>	100%	119%	10%

<sup>a</sup> Unpublished results.

mechanism of hydride-transfer, the ground and transition states with three different substrates were calculated, using system 1 as starting structure. Besides ethanol, we also inserted 1-propanol and isopropanol in these active site models. The calculations show that with isopropanol the activation energy is a little higher than with ethanol (Table 2.2). This small increase in activation energy cannot explain the much lower  $k_{cat}$  found experimentally with isopropanol compared to ethanol (Table 2.3).

If hydrogen or hydride tunnelling is also involved in this mechanism, than the hydrogen-transfer distance (=the distance that the hydrogen  $H^*$  needs to cross from substrate to coenzyme) can affect the rate of tunnelling. The hydrogen-transfer distance of 0.73 Å in the case of isopropanol is significantly larger than the ones found with ethanol and 1-propanol. But also the height of the barrier plays an important role, and this barrier is lower with isopropanol compared to the one found with 1-propanol (see paragraph 2.3.3).

Some geometrical data are presented in Table 2.4. As is to be expected, the C4-C1 distances in the transition states are smaller than in the initial and final states. The angles N1-C4-C1 do not vary much from their mean values of 100° and 150°, respectively.

Taking a closer look at the van der Waals interactions, we find that with system 1

**Table 2.4** The N1-C4-C1 (coenzyme-coenzyme-substrate atoms) and C4-H\*-C1 angles (in degrees) and the C4-C1 distances (in Å) for the calculated geometries.

	NAD/ethanol			NAD/1-propanol			NAD/isopropanol		
	alc.	TS	ald.	alc.	TS	ald.	alc.	TS	ald.
C4-C1	3.43	2.86	3.52	3.40	2.88	3.53	3.40	2.98	3.57
N1-C4-C1	114	103	92	105	104	114	89	99	114
C4-H*-C1	158	164	129	142	167	158	136	161	164

(ethanol as substrate) in the aldehyde state the hydrogen H\* to be transferred from C4 of NADH to C1 of the acetaldehyde, is already close to C1 (see Figure 2.4a). The C4-H\* distance is extremely long (1.15 Å versus a C-H bond distance of 1.09 Å experimentally). In the transition state an increasing overlap occurs between H\* and C1; the distances between C4-H\* and H\*-C1 are 1.65 and 1.24 Å respectively. The charge on H\* in the TS state is -0.046 indicating a H<sup>-</sup> transfer reaction. In the alcohol state, there is no overlap between the C4 of NAD<sup>+</sup> and the H\* at C1 of the ethoxide (see Figure 2.4b). For the systems with 1-propanol and isopropanol as substrate similar hydrogen-transfer patterns can be derived (not shown).

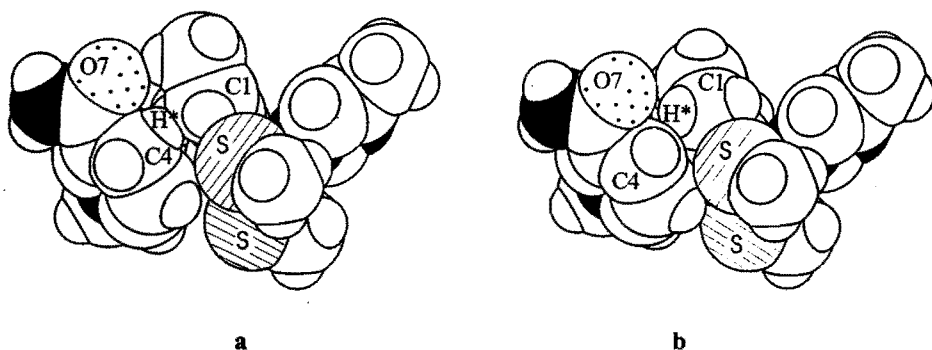


**Figure 2.4** a) The AM1 optimized geometries of the active site model with ethanol (the aldehyde state) by van der Waals representation, b) *Idem*, for the alcohol state.

### 2.3.3 Hydrogen tunnelling effects

So far we have neglected possible tunnelling effects and the influence of the protein environment, which all tend to reduce the (apparent) activation energies of hydride-transfer. Both the hydrogen tunnelling and the classical pathway depend on the height of the energy barrier. In addition the tunnelling rate is affected by the hydrogen distance to cross. Depending on which side of the reaction one starts (the alcohol or aldehyde state), the tunnelling rate is increased or decreased, depending on a negative or positive  $\Delta H_f$ , respectively<sup>[23]</sup>. In the case of ethanol the barrier for the forward reaction (7.1 kcal.mol<sup>-1</sup>) is lower than the expected vibration energy of the migrating hydrogen H\* (8.6 kcal.mol<sup>-1</sup>, equivalent with  $\nu_{\text{C-H}}=3000\text{ cm}^{-1}$ ) and the barrier can be taken the classical way. With 1-propanol and isopropanol the tunnelling probability can be calculated. Applying a barrier of 11.4 kcal.mol<sup>-1</sup> (see Table 2.2, forward reaction of 1-propanol), a C-H vibration energy

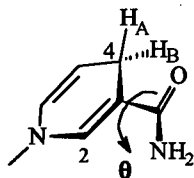


of  $8.6 \text{ kcal.mol}^{-1}$  and a hydride-transfer distance of  $0.61 \text{ \AA}$  (derived from the corresponding TS structure), a probability of  $5.10^{11} \text{ s}^{-1}$  can be calculated<sup>[24]</sup> for the tunnelling of a hydrogen. For isopropanol the probability for hydrogen tunnelling is  $8.10^{11} \text{ s}^{-1}$ , which is a factor 1.6 higher compared with the case for 1-propanol. Since for the classical pathway a probability of  $5.10^5 \text{ s}^{-1}$  and  $7.10^6 \text{ s}^{-1}$  results for 1-propanol and isopropanol respectively, it seems likely that tunnelling will occur in both systems. However, due to the flexible and dynamic nature of the enzyme, the transfer distance will heavily fluctuate, as will therefore the tunnelling probability. In reality, therefore, both the classical pathway and tunnelling are expected to occur. This might also explain the absence of measurable isotope effects in wild type HLADH<sup>[25]</sup>.

### 2.3.4 Effects of the presence of H-bonding groups and side-chain modifications in NAD

Many analogues of  $\text{NAD}^+$  are known and some of them are also active in HLADH. We studied the kinetics of three  $\text{NAD}^+$  analogues (see Chapter 6). They all differ only in the atoms of the pyridine side-chain compared to native  $\text{NAD}^+$ . Normally the carboxamide side-chain of  $\text{NAD}^+$  has hydrogen-bonding interactions with three neighbouring amino acids in the enzymatic complex. Changes in the pyridine side-chain thus results in changes in the H-bonding pattern with surrounding residues. But also the electronic features and therewith most likely the intrinsic reactivity of the pyridinium ring becomes different. The orientation of the side-chain relative to the pyridine plane (expressed in the dihedral angle  $\theta$ , Figure 2.5), is expected to play a role in the rate of the stereoselective hydride-transfer, as pointed out in paragraph 1.4. In Table 2.5 the results of the AM1 calculations are shown for NAD, the acetyl (acPdAD) and formyl analogue of NAD (fPdAD).

According to the data of Table 2.5,  $\theta$  is negative in the alcohol state of NAD/1-propanol and NAD/isopropanol. For X-ray structures with the substrates pentafluoro benzyl alcohol and DMSO positive values of about  $25^\circ$  could be derived. These out-of-plane orientations are stabilized by H-bonds to main chain peptide atoms. Therefore we also performed some calculations in which three additional groups (one  $\text{NH}_3$  and two  $\text{CH}_2\text{O}$



$$\theta = 0^\circ \pm 90^\circ \text{ if C=O is directed towards C4}$$

$$\theta = 180^\circ \pm 90^\circ \text{ if C=O is directed towards C2}$$

Figure 2.5 The out-of-plane dihedral angle  $\theta$ .

**Table 2.5** AM1 calculated heats of formation and  $\Delta H_f$  (in kcal.mol<sup>-1</sup>). acPdAD and fPdAD are NAD analogues with modified side-chains; NAD: CONH<sub>2</sub>, acPdAD: COCH<sub>3</sub>, fPdAD: COH.

	$\Delta H_f^\circ$ alcohol state	$\Delta H_f^\circ$ transition state	$\Delta H_f^\circ$ aldehyde state	$E_{act}$ forward	$E_{act}$ backward	$\Delta H_f$	$\theta$ alcohol state	$\theta$ TS state	$\theta$ aldehyde state
NAD/EtO	-2.4	+4.7	-30.9	7.1	35.6	-28.5	38°	36°	43°
NAD/1-prop.	-13.1	-1.7	-36.6	11.4	34.9	-23.5	-39°	32°	42°
NAD/IPA	-2.2	+7.7	-36.2	9.9	43.9	-34.0	-39°	36°	175°
acPdAD/EtO	-5.6	+2.0	-29.3	7.6	31.3	-23.7	-79°	-40°	23°
fPdAD/EtO	2.4	+8.2	-23.3	5.8	31.5	-25.7	-28°	-8°	14°

groups), positioned around the side-chain, mimic these hydrogen-bonding peptide groups. The results are shown in Table 2.6. The H-bonds do induce positive values of  $\theta$ , without changing  $\Delta H_f$ . Negative values of  $\theta$  are also obtained in the alcohol state and the TS of acPdAD and fPdAD with ethanol. On the contrary, the presence of hydrogen-bonding groups does not generate a positive value of  $\theta$  in the alcohol state (Table 2.6). No X-ray data are available in these cases, but also MD calculations show negative values of  $\theta$  with these analogues (see Chapter 6). In the TS, NAD exhibits a positive value of  $\theta$  of about 35° with the three substrates (Table 2.5). This seems to confirm the proposal of Donkersloot and

**Table 2.6** AM1 calculated heats of formation and  $\Delta H_f$  (in kcal.mol<sup>-1</sup>) of active site models with three hydrogen-bonding groups. Different coenzymes were used; NAD: CONH<sub>2</sub>, acPdAD: COCH<sub>3</sub>, fPdAD: COH.

	$\Delta H_f^\circ$ alcohol state	$\Delta H_f^\circ$ aldehyde state	$\Delta H_f$	$\theta$ alcohol state	$\theta$ aldehyde state
NAD and ethanol	-67.8	-91.8	-24.7	29	29
NAD and 1-propanol	-73.1	-97.6	-24.5	30	29
NAD and isopropanol	-59.0	-92.6	-33.6	29	25
acPdAD and ethanol	-66.0	-87.0	-21.9	-40	8
fPdAD and ethanol	ND	-84.4	ND	ND	24

Buck<sup>[26]</sup> concerning the cooperative effect of the carboxamide group in the hydrogen-transfer. No such effect apparently occurs in the analogues - and - as the values of  $\theta$  are negative, the carbonyl groups even point away from the substrates. It can be argued that the cooperative effect is not essential, as these analogues have by themselves already a higher intrinsic reactivity than NAD (see Chapter 6).

### 2.3.5 Water in the active site

From X-ray studies of the apo conformation of HLADH (binary complex of HLADH with only the coenzyme bound, PDB file 5ADH)<sup>[27]</sup>, it is known that there are many water molecules inside the enzyme and that one water is zinc-bound. Ritter von Onciul and Clark<sup>[9]</sup> found it likely that the substrate replaces the zinc-bound water in binding to the zinc ion. Recent studies on a refined structure of HLADH/NADH/DMSO<sup>[7]</sup> and on the ternary complex with pentafluorobenzyl alcohol as substrate<sup>[8]</sup>, indeed suggest that there is no water molecule present any more as a fifth ligand of zinc. However, it cannot be ruled out that the water molecule is too mobile to be recorded by X-ray crystallography.

In order to check if the water molecule in the apo-conformation remains zinc-bound during the calculations, we first performed a calculation of an active site model of the binary complex of HLADH<sup>[27]</sup> with one water molecule bound to zinc as a fourth ligand (thus before substrate binding has occurred). This active site model included Zn(II), Cys 46, His 67, Cys 174 and H<sub>2</sub>O. After the AM1 calculations, during which the water molecule was allowed to move freely, this water molecule remained coordinated to the zinc ion, resembling its original X-ray position. We then started from the optimized structures of system 1 (which contains ethanol and is based on the ternary complex<sup>[6]</sup>), adding one additional water molecule close to the zinc ion (system 3), as found in the X-ray structure of the apo conformation of HLADH<sup>[27]</sup>. The results of the calculations show that the water molecule moves away from the zinc ion and remains at a 4 Å distance of zinc, where it is neither involved in the formation of hydrogen-bonds nor functions as a fifth ligand of the zinc ion. This was also concluded from model-building experiments by Eklund et al.<sup>[28]</sup> and is in nice agreement with the X-ray studies on HLADH with NAD<sup>+</sup> and pentafluorobenzyl alcohol<sup>[8]</sup>.

It has been suggested<sup>[6,29]</sup> that the hydroxyl group of Ser 48 and the imidazole ring of His 51 are involved in a proton relay mechanism. It is unknown if also a water molecule is involved in the deprotonation of the substrate. We studied the possibility that, after the formation of the alkoxide ion, a water molecule is involved in the H-bonding range: alkoxide - - (H<sub>2</sub>O) - - Ser 48 - - His 51. In this model system (system 4), we again started from the optimized structure of system 1 and now the additional water molecule was placed in between

the alkoxide and Ser 48 (but not zinc-bound), serving as a potential hydrogen-bond acceptor and donor. AM1 calculations again show that the water molecule is moving away from the zinc ion. Minimizing the energy with a gradient norm of  $0.1 \text{ kcal.mol}^{-1}$ , we find that in the alcohol state the water molecule takes a position in which it could be involved in the proton relay mechanism, because it is at H-bonding distance from  $\text{EtO}^-$  and Ser 48 (Table 2.7). A gradient norm of  $1.0 \text{ kcal.mol}^{-1}$  however causes geometries in which the water molecule does not form hydrogen-bonds with the ethoxide and serine. (The energy differences between the states calculated with GNORM 1.0 and 0.1 are only  $0.5 \text{ kcal.mol}^{-1}$ ).

In conclusion the water molecule could well be involved in the proton relay mechanism but, based on the present results, definite evidence is lacking.

*Table 2.7 Calculated distances in Å.*

Distances in system 4	H1(WAT)–O(EtO <sup>−</sup> )	H1(WAT)–O(Ser 48)
GNORM 1.0		
alcohol state	3.10	4.10
aldehyde state	4.81	3.75
GNORM 0.1		
alcohol state	2.19	2.49
aldehyde state	4.71	3.98

### 2.3.6 Substitution of the zinc ion by other metal ions

The catalytic zinc ion plays an important role in the hydride-transfer process of HLADH. It acts as a Lewis acid, which activates and coordinates the substrate for its reaction with the NAD coenzyme. In the alcohol state, zinc stabilizes the alkoxide ion, which facilitates the hydride-transfer. In the reverse reaction (the aldehyde state), zinc plays the role of electron attractor, increasing the electrophilic character of the aldehyde.

Substitution of the zinc ion in HLADH with several metals has been studied. With secondary alcohols similar or even higher activities have been found with the Co substituted HLADH<sup>[30,31]</sup>. Drum et al.<sup>[32]</sup> found 30% and 70% loss of activity with the Co(II)- and Cd(II)-HLADH respectively. Nickel substitution appeared to result in only 12% of the activity found with Zn. Binding of  $\text{Mn}^{2+}$  to the catalytic sites of HLADH could not be detected and although  $\text{Cu}^{2+}$  was able to bind to the enzyme, its metal-binding site was quite

distorted, which explains the observed absence of enzymatic activity with Cu(II)-HLADH<sup>[30-35]</sup>. Crystallographic studies<sup>[32]</sup> of the Co(II)- and Cd(II)-substituted enzyme show that the coordination geometry is preserved. The rigidity of the protein structure is obviously responsible for the fact that tetrahedral coordination is observed in HLADH even with metals that tend to prefer planar coordination geometries, such as Cu(II) and Ni(II) ions<sup>[33]</sup>.

Unfortunately cobalt has not been parameterized for either AM1 or PM3. To check the effect of metal substitution we therefore inserted Cd (parameterized for PM3) in our active site model. A comparison with the kinetic data obtained with Cd(II)-HLADH could not be made however, since only the alcohol state of the model system could be determined and not the aldehyde and transition states.

## 2.4 Conclusion

It is likely that the zinc-coordinated cysteine residues in HLADH are present as thiolate anions. Therefore active site models of HLADH should incorporate negatively charged cysteines. AM1 and PM3 calculations show drastic differences in ground state energy levels for model systems incorporating negatively charged cysteine residues compared with active site models based on neutral cysteine residues.

The present calculations do not provide an explanation why isopropanol is a poorer substrate than ethanol. This suggests that in the enzyme there are factors not accounted for in the simplified model used in our research.

A negative charge on the hydrogen being transferred in the TS state can be calculated, pointing to a hydride-transfer mechanism. Probability calculations suggest that hydrogen tunneling may occur. However to draw definite conclusions one should take into account the dynamics of the enzyme system.

In the TS of NAD, the carboxamide group is rotated out of the pyridinium plane, the carbonyl dipole pointing in the direction of the substrate, supporting a previous proposal concerning the hydrogen-transfer rate. On the other hand, the carbonyl group points away from the substrate in the TS of acPdAD and fPdAD.

In the ternary model complex no water molecule is present as a fifth ligand of the zinc ion, in accordance with X-ray data.

## References

1. C.-I. Brändén, H. Jörnvall, H. Eklund and B. Furugren, *The Enzymes*, vol. 11, 3rd edition, P.D. Boyer (ed.), Academic Press, New York (1975) p. 103-190.
2. C.C. Wratten and W.W. Cleland, *Biochemistry* **2**, 935-941 (1963).
3. F.B. Rudolph and H.J. Fromm, *Biochemistry* **9**, 4660-4665 (1970).
4. H. Theorell and B. Chance, *Acta Chem. Scand.* **5**, 1127-1144 (1951).
5. K. Dalziel and F.M. Dickinson, *Biochem. J.* **100**, 34-46 (1966).
6. H. Eklund, J.-P. Samama and T.A. Jones, *Biochemistry* **23**, 5982-5996 (1984).
7. S. Al-Karadaghi, E.S. Cedergren-Zeppezauer and S. Hövmöller, *Acta Cryst.* **D50**, 793-807 (1994).
8. S. Ramaswamy, H. Eklund and B.V. Plapp, *Biochemistry* **33**, 5230-5237 (1994).
9. A. Ritter von Onciul and T. Clark, *J. Comput. Chem.* **14**, 392-400 (1993).
10. L.A.Æ. Shuyterman and J. Wijdenes, *Eur. J. Biochem.* **71**, 383-391 (1976).
11. J. Kvassman, A. Larsson and G. Pettersson, *Eur. J. Biochem.* **114**, 555-563 (1981).
12. M.J.S. Dewar, E.G. Zebisch, E.F. Healy and J.J.P. Stewart, *J. Am. Chem. Soc.* **107**, 3902-3909 (1985).
13. J.J.P. Stewart, *J. Comput. Chem.* **10**, 209-220 and 221-264 (1989).
14. MOPAC 6.0, QCPE Program No. 455, Quantum Chemistry Program Exchange, Indiana University, Bloomington, Indiana, USA (1991).
15. QUANTA/CHARMM, Molecular Simulations Inc., Waltham, Massachusetts, USA.
16. M.J.S. Dewar, E.F. Healy and J.J.P. Stewart, *J. Chem. Soc. Faraday Trans. II* **3**, 227-233 (1984).
17. J. Baker, *J. Comput. Chem.* **7**, 385-395 (1986).
18. M.J.D. Powell (ed.), *Non-Linear Optimization*, Academic Press, New York (1982).
19. R. Fletcher, *Practical Methods of Optimization*, Wiley, Chichester, UK (1982).
20. J. Kvassman and G. Pettersson, *Eur. J. Biochem.* **103**, 557-564 (1980).
21. S.A.M. Vanhommerig, L.A.Æ. Shuyterman and E.M. Meijer, *Biochim. Biophys. Acta*, in preparation.
22. D.-H. Park and B.V. Plapp, *J. Biol. Chem.* **267**, 5527-5533 (1992).
23. M.D. Harmony in *"Chemical Society Reviews"*, volume 1, 211-228 (1972).
24. P.W. Atkins in *"Physical Chemistry"*, 2nd edition, Oxford University Press, Oxford, p. 408-409 (1982).
25. B.J. Bahnson, D.-H. Park, K. Kim, B.V. Plapp and J.P. Klinman, *Biochemistry*, **32**, 5503-5507 (1993).
26. M.C.A. Donkersloot and H.M. Buck, *J. Am. Chem. Soc.* **103**, 6554-6558 (1981).
27. H. Eklund, J.-P. Samama, L. Wallén, C.-I. Brändén, Å. Åkeson and T.A. Jones, *J. Mol. Biol.* **146**, 561-587 (1981).
28. H. Eklund, J.-P. Samama and L. Wallén, *Biochemistry* **21**, 4858-4866 (1982).
29. V.C. Sekhar and B.V. Plapp, *Biochemistry*, **27**, 5082-5088 (1988).
30. I. Andersson, W. Maret, M. Zeppezauer, R.D. Brown III and S.H. Koenig, *Biochemistry*, **20**, 3433-3438 (1981).
34. H. Dietrich, W. Maret, H. Kozłowski and M. Zeppezauer, *J. Inorg. Biochem.* **14**, 297-311 (1981).

35. I. Andersson, W. Maret, M. Zeppezauer, R.D. Brown III and S.H. Koenig, *Biochemistry*, **20**, 3424-3432 (1981).

---

*This chapter is based on:*

S.A.M. Vanhommerig, R.J. Meier, L.A.Æ. Sluyterman and E.M. Meijer, *J. Mol. Struct. (Theochem)*, in preparation.

# 3

## *Checking the AMBER 4.0 force field with leucine, alanine and N-methylacetamide*

### 3.1 Introduction

Force fields have been used for over 15 years now and have been improved during this period of time. Still there are efforts made to improve the accuracy of molecular mechanics and dynamics simulations. In the past, several studies on hydrogen-bonded crystals have been carried out<sup>[1-6]</sup>.

We checked the AMBER 4.0 force field<sup>[7]</sup> for its application in describing the structure of proteins. Therefore, molecular mechanics (MM) and dynamics (MD) calculations on simple molecules were carried out for testing and evaluating this force field, by allowing one amino acid to move freely within the fixed cage of its crystal lattice, resembling the fitting of a substrate into its enzyme pocket. The small molecules used in these calculations have highly accurate X-ray crystal structures, which make them good starting structures for the simulations. Two amino acids were (leucine and alanine) and one peptide-like structure (*N*-methylacetamide) were studied.

### 3.2 Methods

We used the AMBER package<sup>[7,8,9]</sup>, with the following potential energy function:

$$\begin{aligned}
 V = & \sum_{\text{bonds}} k_r (r - r_e)^2 + \sum_{\text{angles}} k_\theta (\theta - \theta_e)^2 + \sum_{\text{dihedrals}} \frac{V_n}{2} (1 + \cos[n\varphi - \gamma]) \\
 & + \sum_{i < j} \left[ \frac{A}{r_{ij}^{12}} - \frac{B}{r_{ij}^6} + \frac{q_i q_j}{r_{ij} \epsilon} \right] + \sum_{H \text{ bonds}} \left[ \frac{C}{r_{ij}^{12}} - \frac{D}{r_{ij}^{10}} \right] \quad (3.1) \\
 & \text{nonbonded}
 \end{aligned}$$

consisting of five terms describing: bond-stretching, bond-bending, torsional, nonbonded van der Waals and electrostatic interactions and as fifth term the hydrogen-bonding interactions.



AMBER calculations require starting geometries of the structures to be calculated. Starting structures were obtained from the Crystal Structures Databank (leucine: CSD file name LEUCIN01, R-factor 0.058, spacegroup no. 4 ( $P2_1$ ); alanine: CSD file name LALNIN, R-factor 0.049, spacegroup no. 19 ( $P2_12_12_1$ )<sup>[10]</sup>; *N*-methylacetamide: CSD file name METACM, R-factor 0.169, spacegroup  $Pnma$ <sup>[11]</sup>). Using the option 'Crystal Builder' of the modelling package QUANTA 3.3.2<sup>[12]</sup> copies of the CSD structures were generated.

*Leucine.* For the leucine crystal a total of 264 residues were combined to surround the central residue in all directions by neighbour residues up to a distance of at least 20 Å distance. Two types of leucine residue files were used during the calculations, differing only in the atomic charges for each atom. In Table 3.1 the atomic charges used are listed.

**Table 3.1** The atomic charges for the leucine residues used in the calculations. For an explanation of the atom labels see Figure 3.1.

	LEU1 <sup>a</sup>	LEU2 <sup>b</sup>		LEU1	LEU2
backbone			side chain		
N	-0.259	-0.857	CB	-0.061	-0.061
H(NH <sub>3</sub> )	0.280	0.443	H(CB)	0.033	0.033
C	0.616	0.749	CG	-0.010	-0.010
O1	-0.706	-0.718	H(CG)	0.031	0.031
O2	-0.706	-0.718	CD1	-0.107	-0.107
CA	0.151	0.151	H(CD1)	0.034	0.034
H(CA)	0.048	0.048	CD2	-0.107	-0.107
			H(CD2)	0.034	0.034

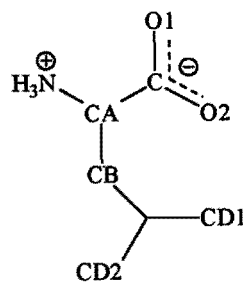


**Figure 3.1:** Leucine

<sup>a</sup> Standard AMBER 4.0 charges.

<sup>b</sup> Adapted charges for the NH<sub>3</sub><sup>+</sup> and COO<sup>-</sup> group, calculated with 6-31G.

*Minimization/Dynamics protocols.* All atoms were treated explicitly, including polar and non-polar hydrogens. A cutoff of 12 Å (or 18 Å when mentioned in the tables) for the electrostatic and van der Waals interactions was applied and the nonbonded parameters were updated every 25 steps. Minimizations were carried out using 750 steps of steepest descent and after that conjugate gradient algorithms, until the RMS gradient of the energy was less

than  $0.1 \text{ kcal.}\text{\AA}^{-1}$ . From the built crystal only the central residue was allowed to move freely during the simulations, after optimizing the positions of the hydrogen atoms of four  $\text{NH}_3^+$  groups near this central residue in order to get the optimal H-bond directions. In some cases, special constraints were used to maintain better agreement with the X-ray structure. These constraints are explained under results (paragraph 3.3.1). The minimized structure was used as starting structure for 75 ps MD simulations, which were carried out at room temperature with a time step of 2 fs. The Shake algorithm was used during MD calculations.

**Table 3.2** The atomic charges for the alanine residues used in the calculations. For an explanation of the atom labels see Figure 3.2.

	ALA1 <sup>a</sup>	ALA2 <sup>b</sup>	ALA3 <sup>c</sup>
N	-0.263	-0.857	-0.240
H(NH <sub>3</sub> )	0.312	0.443	0.220
C	0.524	0.749	-0.140
O1	-0.706	-0.718	-0.200
O2	-0.706	-0.718	-0.250
CA	0.151	0.151	-0.030
H(CA)	0.048	0.048	0.160
CB	-0.098	-0.098	-0.230
H(CB)	0.038	0.038	0.090

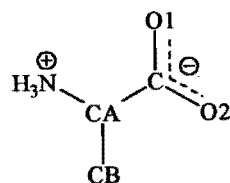


**Figure 3.2:** Alanine

<sup>a</sup> Standard AMBER 4.0 charges.

<sup>b</sup> Charges for the  $\text{NH}_3^+$  and  $\text{COO}^-$  groups from Table 3.1.

<sup>c</sup> Multipole charges<sup>[13]</sup>.

**Alanine.** With alanine 784 residues were used as starting structure. Again the central residue is surrounded by neighbouring residues till at least a distance of 20 Å. In Table 3.2 the three types of alanine charges used for the simulations are listed. The MM/MD protocol was similar to the one described under leucine. But instead of only optimizing the hydrogens of four  $\text{NH}_3^+$  groups, all hydrogen atoms of the  $\text{NH}_3^+$  groups were optimized before the minimization of the central residue was started.

**N-Methylacetamide.** For the N-methylacetamide crystal 549 copies were generated

(550 residues in total). The atomic charges used were obtained through 6-31G\*\*/6-31G *ab initio* calculation using the GAUSSIAN 90 [14] program (see Table 3.3). The MM/MD protocol was similar to the one mentioned above. Only in this case all hydrogens were first optimized before the minimization of the central residue was started.

**Table 3.3** *The atomic charges for the N-methylacetamide residues used in the calculations. For an explanation of the atom labels see Figure 3.3.*

	NMA		NMA
C1	-0.578	N	-0.789
H(C1)	0.164	H(N)	0.383
	0.203	C3	-0.267
	0.210	H(C3)	0.189
C2	0.740		0.190
O	-0.607		0.162

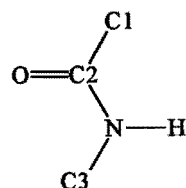


**Figure 3.3:**  
N-methylacetamide

### 3.3 Results and discussion

Normally periodic boundary conditions are applied when studying similar crystals as those studied here. However with the AMBER program, one has to surround the crystal unit cell either by a water layer, or use such a large crystal as starting structure, that no water need to be added. In the latter case the "box" is however too large to perform periodic boundary conditions.

#### 3.3.1 The leucine crystal

In the experimental leucine crystal (see Figure 3.4) each leucine residue has four hydrogen-bonds with neighbouring residues, resulting in a 3-D network. The two oxygens of the carboxylate group are involved in different hydrogen-bonds. O1 has interactions with a hydrogen of a residue positioned on its right or left side. The other oxygen atom O2 has one hydrogen-bonds with the NH<sub>3</sub> group of the residue above this O and with one belonging to a residue lying behind this oxygen atom.

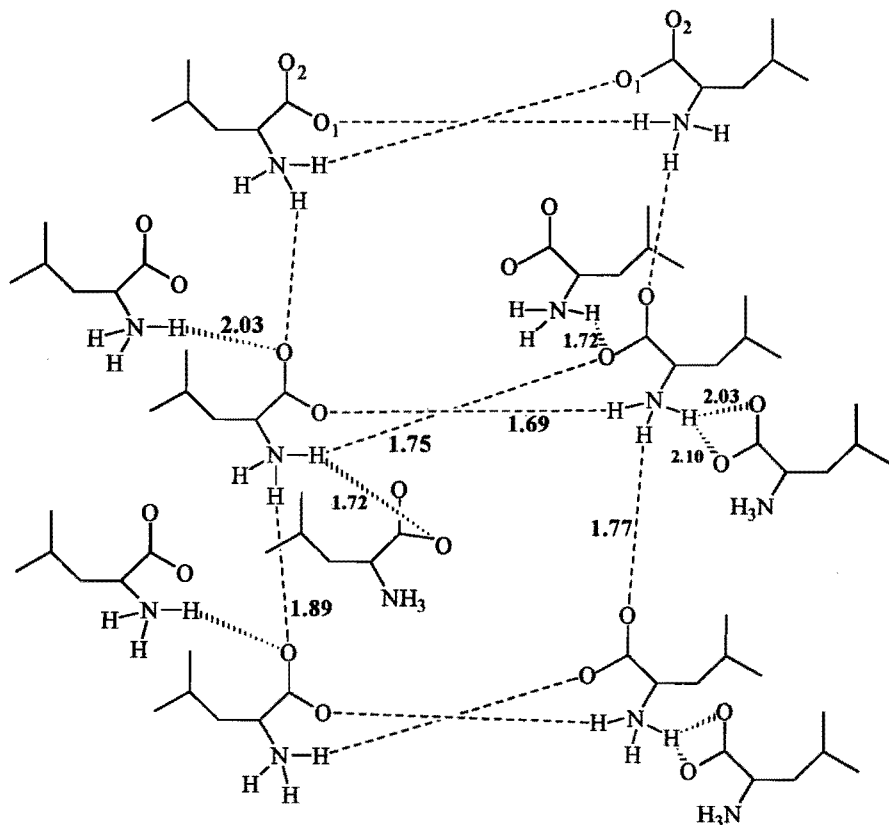


**Figure 3.4** The X-ray structure of the leucine crystal. The charges on the  $\text{NH}_3^+$  and  $\text{COO}^-$  groups are not indicated.

In the first set of calculations the four neighbouring  $\text{NH}_3^+$  groups were not optimized, but only (parts of) the central residue. The standard AMBER leucine residue resulted in large deviations especially for O2 and the side chain atoms CD1 and CD2 (Table 3.4). When the backbone atoms were fixed, the side-chain atoms showed significantly smaller deviations from the X-ray structure, suggesting that the hydrophobic interactions are fairly well calculated. In the opposite case the backbone atoms show almost similar deviations to those found when the total residue is allowed to move freely. The side-chain deviations appeared to be a secondary effect, caused by some inaccuracy in the calculation of the interactions of the charged atoms of the amino acid backbone. We therefore concentrated on the backbone interactions.

**Table 3.4** RMS deviations (in Å) of atomic positions of heavy atoms between X-ray structure and calculated structures of crystalline leucine, using constraints. The MD structure is a time-weighted average structure.

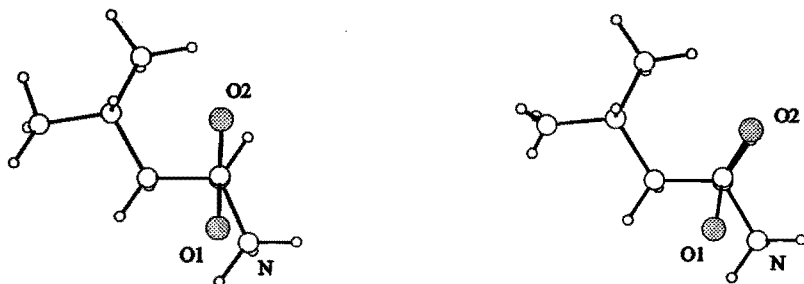
LEU1 <sup>a</sup> , free part	N	CA	C	O1	O2	CB	CG	CD1	CD2
Total residue, MD	0.151	0.101	0.166	0.176	0.407	0.123	0.311	0.246	0.413
Backbone, MD	0.151	0.046	0.104	0.134	0.442	-	-	-	-
Side-chain, MD	-	-	-	-	-	0.056	0.069	0.143	0.061

LEU1 <sup>b</sup> , total residue free	RMS	N	CA	C	O1	O2	angle
$\epsilon=1$ MM	0.190	0.055	0.083	0.115	0.095	0.384	18
$\epsilon=1$ MD	0.226	0.133	0.108	0.181	0.171	0.406	25
$\epsilon=3$ MM	0.148	0.070	0.119	0.156	0.177	0.288	ND

<sup>a</sup> O1 and O2 were defined as atom type O2 in AMBER.  $\epsilon=1$  was used.

<sup>b</sup> O1 and O2 were defined as atom type O in AMBER; only the central residue was optimized.



**Figure 3.5** The original lattice residue (right) and MD-averaged residue with  $\epsilon=1$ .

Although the O2 deviation is rather small, it is believed to be important, since larger changes are impossible due to the limited space available in the lattice. Especially remarkable is also the bending of the O2 atom out of the O1-C-CA-O2 plane (see Figure 3.5).

Because the standard AMBER set resulted in a strong bending of O2, constraints were added to the parm.in file to keep the O1-C-CA-O2 dihedral around the 180° (thus all four atoms in one plane). The constraints used are listed in Table 3.5.

On computing the MM results on LEU1 in the lower half of Table 3.4 with those

of Table 3.6, it is evident that the constraints have a positive effect. Further it was noticed that using a dielectric constant of 1 or 3 gave better agreement with the crystal structure than a distance dependent dielectric constant (not shown). With LEU1  $\epsilon=3$  was only slightly better than  $\epsilon=1$  (Table 3.6). With LEU1 also  $\epsilon=2, 4$  and  $6$  were used, but the results with the dielectric constant  $\epsilon=3$  gave the smallest RMS deviations.

A cutoff of 18 Å gave some improvement, but as this is rather artificial it was not used further.

The influence of different charges at the  $\text{NH}_3^+$  and  $\text{COO}^-$  groups was also checked (LEU2). The favourable effect of  $\epsilon=3$  rather than  $\epsilon=1$  suggested that the total charges of the  $\text{NH}_3^+$  and  $\text{COO}^-$  might be too high. Therefore the atomic charges on these atoms were changed into lower values with LEU2, in agreement with calculated charges for  $\text{NH}_3^+$  and  $\text{COO}^-$  with an *ab initio* 6-31G

**Table 3.5** Leucine carboxyl group constraints.

angle	degrees	kcal.mol <sup>-1</sup>
O1-C-O2	127.7°	1000
O1-C-CA	115.7°	1000
O2-C-CA	116.4°	1000
O1-C-CA-O2	179.4°	1000

**Table 3.6** RMS deviations (in Å) of atomic positions of heavy atoms between X-ray structure and calculated structures of crystalline leucine, using constraints. The MD structure is a time-weighted average structure.

		Total	RMS deviation					Bending
		RMS	N	CA	C	O1	O2	angle <sup>a</sup>
LEU1	$\epsilon=1$ MM	0.137	0.056	0.081	0.136	0.116	0.229	0.5
	$\epsilon=3$ MM	0.136	0.059	0.099	0.123	0.166	0.169	0.4
	$\epsilon=3$ MD	0.208	0.157	0.174	0.205	0.226	0.260	0.1
cutoff 18	$\epsilon=3$ MD	0.197	0.119	0.152	0.201	0.212	0.267	0.4
LEU2	$\epsilon=1$ MM	0.144	0.078	0.101	0.138	0.111	0.236	ND
	$\epsilon=1$ MD	0.167	0.112	0.131	0.162	0.110	0.266	0.3
	$\epsilon=3$ MM	0.101	0.037	0.095	0.095	0.110	0.141	0.5
	$\epsilon=3$ MD	0.150	0.061	0.165	0.158	0.170	0.168	0.3

<sup>a</sup> In the X-ray structure a bending angle of 0.6° is observed.

calculation on alanine<sup>[13]</sup>. The *ab initio* calculation at the 6-31G level resulted in a total charge of 0.479 for the  $\text{NH}_3^+$  group and  $-0.682$  for the  $\text{COO}^-$  group. Because AMBER 4.0 is parameterized for molecules with 6-31G atomic charges, the charges of LEU1 ( $\text{NH}_3^+$ : 0.580,  $\text{COO}^-$ :  $-0.796$ , standard AMBER charges) were accordingly adjusted towards  $\text{NH}_3^+$ : 0.472 and  $\text{COO}^-$ :  $-0.687$  as used in LEU2. At the same time some of the atomic charges were higher than in LEU1 (Table 3.1). Both the constraints, the lower charges at the  $\text{NH}_3^+$  and  $\text{COO}^-$  groups, and  $\epsilon=3$  gave the best agreement with the crystal structure.

The hydrogen-bonding parameters (see eqn. 3.1, fifth term) of AMBER 4.0 were also checked. The hydrogen-bonding term used by AMBER describes for each H-bonding couple a Lennard-Jones like potential, with a minimum of the curve at  $R_{\text{min}}$  and a corresponding energy  $E_{\text{min}}$ . By changing C and D in eqn. 3.1  $R_{\text{min}}$  and  $E_{\text{min}}$  can be adjusted. It turned out that a smaller  $R_{\text{min}}$  and increasing or decreasing values of  $E_{\text{min}}$  did not give better results than the standard AMBER 4.0 values.

In the final calculations (LEU2,  $\epsilon=3$ , MD) the N-O2 distance was 2.95 Å, reasonably close to the value of 2.84 Å in the X-ray structure.

### 3.3.2 The alanine crystal

The alanine crystal derived from the CSD, shows the hydrogen-bonding pattern as drawn in Figure 3.6. The ammonium ion of the L-alanine crystal forms three strong

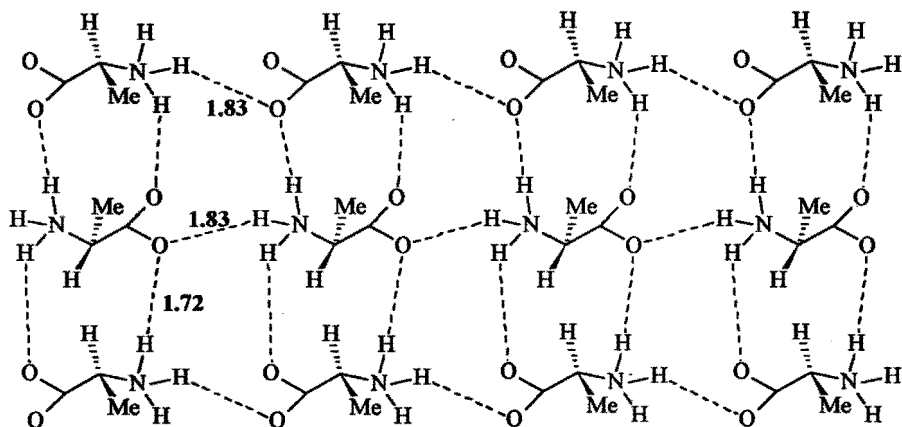


Figure 3.6 The X-ray structure of the alanine crystal. The charges of the  $\text{COO}^-$  and  $\text{NH}_3^+$  groups not indicated.

hydrogen-bonds with neighbouring  $\text{COO}^-$  groups, resulting in a 2-D network. With alanine the oxygens of the carboxylate group are involved in different hydrogen-bonding. O1 has only one H-bond, whereas O2 has two with hydrogen atoms of two different  $\text{NH}_3^+$  groups.

In Table 3.7 the results of the three alanine residues are listed. The charges of the  $\text{NH}_3^+/\text{COO}^-$  groups are: 0.673/-0.888 for ALA1, 0.472/-0.687 for ALA2 and 0.42/-0.59 for ALA3.

The larger cutoff of 18 Å does not show significant improvement compared with similar calculations using a cutoff of 12 Å.

**Table 3.7** RMS deviations (in Å) of the heavy atoms of alanine between X-ray structure and calculated structures of crystalline alanine.

		Total RMS	RMS deviation						Bending angle <sup>a</sup>
			N	CA	CB	C	O1	O2	
ALA1	$\epsilon=1$ MM	0.129	0.070	0.074	0.035	0.037	0.221	0.197	0.5
	$\epsilon=1$ MD	0.140	0.079	0.076	0.058	0.061	0.245	0.196	2.3
ALA1	$\epsilon=3$ MM	0.093	0.065	0.075	0.059	0.063	0.150	0.111	2.3
	$\epsilon=3$ MD	0.127	0.065	0.086	0.099	0.109	0.218	0.126	4.9
cutoff 18	$\epsilon=3$ MD	0.130	0.081	0.078	0.101	0.104	0.219	0.142	5.0
ALA2	$\epsilon=1$ MM	0.143	0.060	0.076	0.075	0.106	0.229	0.212	10.7
	$\epsilon=1$ MD	0.145	0.073	0.075	0.101	0.119	0.226	0.198	-9.5
ALA2	$\epsilon=3$ MM	0.104	0.058	0.077	0.074	0.089	0.149	0.139	7.5
	$\epsilon=3$ MD	0.132	0.063	0.085	0.107	0.124	0.216	0.139	-7.6
ALA3	$\epsilon=1$ MM	0.063	0.045	0.058	0.024	0.040	0.108	0.067	-0.5
	$\epsilon=1$ MD	0.142	0.078	0.072	0.049	0.062	0.250	0.201	2.3
ALA3	$\epsilon=3$ MM	0.064	0.059	0.069	0.059	0.066	0.107	0.102	-2.0
	$\epsilon=3$ MD	0.114	0.073	0.075	0.076	0.089	0.196	0.123	3.5

<sup>a</sup> In the crystal structure a bending angle of  $0.4^\circ$  is observed.

Contrary to leucine, the charges of ALA2 do not give better results than those of ALA1. The calculations with the multipole charges show the best results, especially when  $\epsilon=3$ . However, to apply these charges in enzymatic MM and MD calculations, all residues



used in those calculations should be defined with multipole charges, once they become available.

### 3.3.3 The *N*-methylacetamide crystal

In the *N*-methylacetamide crystal, the peptide bonds form hydrogen-bonds in layers (Figure 3.7). Only a linear network is spotted in this crystal.

In Table 3.8 the results of applying AMBER 4.0 are shown. Probably due to the very compact crystal structure, the central residue cannot move far away from its original X-ray position, which results in very small RMS deviations, unless a number of residues were liberated.

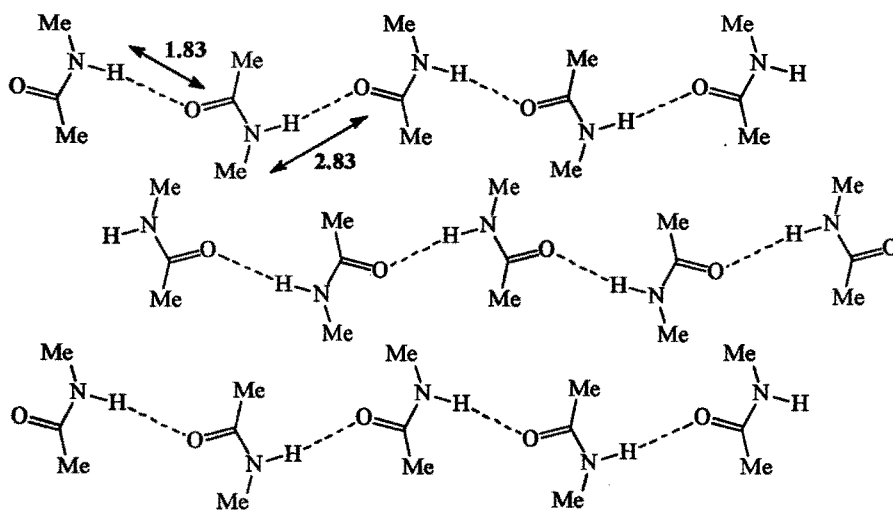


Figure 3.7 The X-ray structure of *N*-methylacetamide.

Allowing two or even ten residues (within 5 Å of the central residue) to move freely during the calculations, resulted in small RMS deviations in the case of  $\epsilon=1$ . With  $\epsilon=3$  and 10 free residues large deviations occur. With peptide bonds and no charged groups present  $\epsilon=1$  gives apparently the best results.

**Table 3.8** RMS deviations (in Å) of atomic positions of heavy atoms between X-ray structure and calculated structures of crystalline N-methylacetamide. The MD structure is a time-weighted average structure.

		number of free residues	Total RMS	RMS deviation				
				C1	C2	O	N	C3
NMA	$\epsilon=1$ MM	1	0.059	0.095	0.055	0.054	0.025	0.045
	$\epsilon=1$ MD	1	0.061	0.047	0.074	0.080	0.036	0.057
	$\epsilon=1$ MD <sup>a</sup>	2	0.055	0.065	0.062	0.054	0.033	0.052
	$\epsilon=1$ MD <sup>b</sup>	10	0.073	0.068	0.086	0.077	0.061	0.073
NMA	$\epsilon=3$ MM	1	0.082	0.096	0.057	0.070	0.079	0.100
	$\epsilon=3$ MD	1	0.091	0.105	0.065	0.067	0.100	0.107
	$\epsilon=3$ MD <sup>b</sup>	10	0.213	0.253	0.205	0.160	0.231	0.204

<sup>a</sup> Averaged RMS values of the two free structures.

<sup>b</sup> The RMS deviation of only the central residue is listed. The other nine residues which were allowed to move freely are positioned around this central residue.

### 3.4 Conclusions

According to the results obtained with leucine and alanine crystals,  $\epsilon=3$  is to be preferred when electrostatic interactions predominate. The peptide hydrogen-bond, however, requires  $\epsilon=1$ . As there are many more peptide bonds in the protein than charged groups, we decided to maintain the current value of  $\epsilon=1$  for modelling studies on HLADH. It might be worth trying to adapt the H-bond parameters (last term of eq. 3.1) of the peptide bond in such a way as to permit the use of  $\epsilon=3$  there too.

## References

1. A.T. Hagler and S. Lifson, *J. Am. Chem. Soc.* **96**, 5327-5335 (1974).
2. S. Lifson, A.T. Hagler and P. Dauber, *J. Am. Chem. Soc.* **101**, 5111-5121 (1979).
3. A.T. Hagler, S. Lifson and P. Dauber, *J. Am. Chem. Soc.* **101**, 5122-5130 (1979).
4. A.T. Hagler, P. Dauber and S. Lifson, *J. Am. Chem. Soc.* **101**, 5131-5141 (1979).
5. U. Dinur and A. T. Hagler in "Review of Computational Chemistry", volume 2, (K.B. Lipkowitz and D.B. Boyd, eds.), VCH, New York (1991).
6. S.J. Weiner, P.A. Kollman, D.A. Case, U.C. Singh, C. Ghio, G. Alagona, S. Profeta and P. Weiner, *J. Am. Chem. Soc.* **106**, 6243-6245 (1984).
7. D.A. Pearlman, D.A. Case, J.C. Caldwell, G.L. Seibel, U.C. Singh, P. Weiner and P.A. Kollman, AMBER 4.0, University of California San Francisco, California, USA (1991).
8. S.J. Weiner, P.A. Kollman, D.A. Case, U.C. Singh, C. Ghio, G. Alagona, S. Profeta and P.K. Weiner, *J. Am. Chem. Soc.* **106**, 765-784 (1984).
9. S.J. Weiner and P.A. Kollman, *J. Comput. Chem.* **7**, 230-252 (1986).
10. H.J. Simpson Jr. and R.E. Marsh, *Acta Crystallogr.* **20**, 550-555 (1966).
11. J.L. Katz and B. Post, *Acta Crystallogr.* **13**, 624-628 (1960).
12. QUANTA/CHARMM, Molecular Simulations Inc., Waltham, Massachusetts, USA.
13. R. Destro, R.E. Marsh and R. Bianchi, *J. Phys. Chem.* **92**, 966-973 (1988).
14. M.L. Frisch, M. Head-Gordon, G.W. Trucks, J.B. Foresman, H.B. Schlegel, K. Raghawachari, M.A. Robb, J.S. Binkley, C. Gonzalez, D.J. Defrees, D.J. Fox, R.A. Whiteside, R. Seeger, C.F. Melius, J. Baker, R.L. Martin, L.R. Kahn, J.J.P. Stewart, S. Topiol and J.A. Pople, GAUSSIAN 90, Gaussian Inc., Pittsburgh, Philadelphia, USA (1990).

## 4

# Rotational barriers of $NAD^+$ /NADH, its analogues and derivatives

## 4.1 Introduction

As mentioned in the preceding chapter, AMBER is designed for the modelling of nucleic acids and proteins. Molecules not belonging to these categories cannot be modelled with AMBER straight away. Missing parameters can often be obtained via extrapolation, but still one should be cautious when using force fields to examine the most stable conformations of small or medium-sized molecules. With respect to our aim of modelling the nicotinamide moiety in enzymatic systems, knowledge of the rotational barriers of the side-chain is important. In order to study these rotational barriers, simpler molecules, resembling the nicotinamide moiety of NAD, were chosen. The few known experimental barriers around the C3-C7 bond (Figure 4.1) of several derivatives of nicotinamide and related compounds were compared with the calculated ones. The calculations were performed using force field (AMBER 4.0, CVVF and CHARMM 21.3), semiempirical (AM1 and PM3) and *ab initio* methods. In Figure 4.2 the structures of all molecules studied are shown.

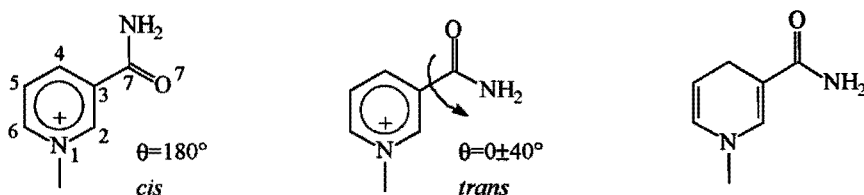
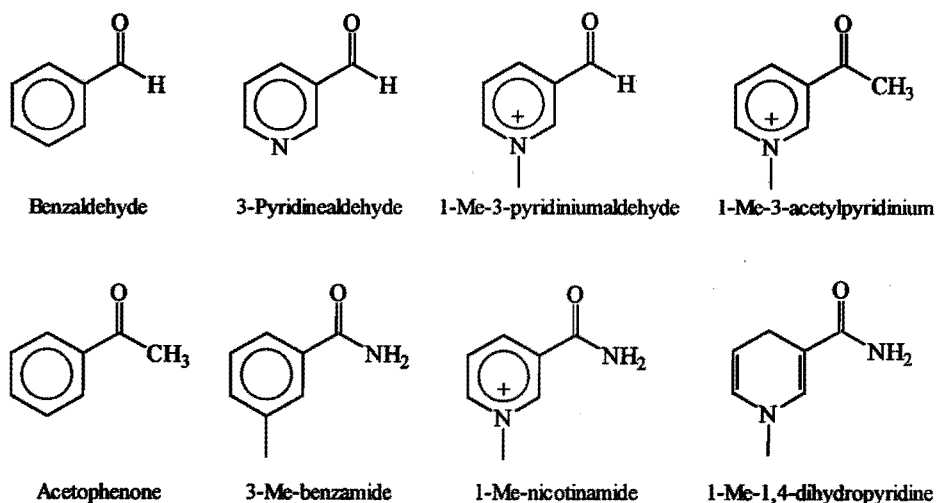


Figure 4.1 Cis and trans 1-methylnicotinamide and 1-Me-1,4-dihyronicotinamide (right).

## 4.2 Computational methods

The rotational barriers for 3-pyridinealdehyde and 1-Me-3-pyridiniumaldehyde were calculated using the GAUSSIAN 90 program<sup>[1]</sup> employing the 6-31G\* basis set. These *ab initio* calculations were performed on an Alliant FX2816 computer. The *cis* and *trans* conforma-

tions of these molecules were fully optimized. A perpendicular structure with the C2–C3–C7–O7 dihedral angle restricted at  $90^\circ$  was calculated in the same manner. In the case of benzaldehyde, 1-methylnicotinamide and 1-methyl-1,4-dihydropyridine data were obtained from literature<sup>[2-4]</sup>.



**Figure 4.2** The structures used in the calculations shown in the trans conformation.

Force field and semiempirical calculations were performed on the following molecules: benzaldehyde, 3-pyridinealdehyde, 1-Me-3-pyridiniumaldehyde, 1-Me-3-acetylpyridinium, acetophenone, 3-methylbenzamide, 1-methylnicotinamide and 1-Me-1,4-dihydropyridine. All force field and semiempirical calculations involve full geometry optimisation except for the relevant dihedral in the calculations of the rotational barrier height. Potential energies were obtained every  $15^\circ$  or  $30^\circ$  starting from  $\theta=0^\circ$ . The semiempirical calculations on the molecules from Figure 4.2, were performed using the MOPAC program version 6.0<sup>[5]</sup>, running on a Silicon Graphics 4D/35TG workstation.

The force field calculations involving the CVFF and the CHARMM 21.3 force field, were performed on a Silicon Graphics 210 GTXB workstation, using the INSIGHT/DISCOVER molecular modelling package version 3.0.0<sup>[6]</sup> and the QUANTA/CHARMM molecular modelling package version 3.2<sup>[7]</sup> respectively. The AMBER calculations were performed on the Alliant FX2816, using the AMBER 4.0 package<sup>[8]</sup>. The all atom force field was used and a dielectric constant of 1. All charges used in the AMBER calculations on the small derivatives of  $\text{NAD}^+/\text{NADH}$  were obtained through AM1 calculations. For the AMBER calculations on

NAD<sup>+</sup>/NADH (analogues) 6-31G\*\*/3-21G atomic charges were used (listed in Appendix 2).

### 4.3 Results

Table 4.1 lists the experimental gas-phase barriers and the calculated rotational energy barriers for all the moieties shown in Figure 4.2.

#### 4.3.1 Force field results

All force field methods (without adaptations) predict rotational barriers for nicotinamide and derivatives that are too high (Table 4.1). It is evident from these results that the force field programs are unable to describe proper rotational barriers for 1,3-substituted benzenes and pyridines, and therefore cannot be applied straightaway.

#### 4.3.2 Semiempirical methods

Most pyridinium structures have two minima: one global minimum for the planar *cis* conformation and another local minimum at the *trans* conformation. AM1 and PM3 calculations showed similar potential-energy curves. Whether the *trans* minimum is planar or not depends on the substituent. In the case of the aldehydes, we found a planar *trans* conformation as the local minimum. Conversely, 3-Methylbenzamide and acetyl and amide substituents of the pyridinium structures show a non-planar local *trans* minimum. This is in line with the experimental observation that benzamide exhibits an out-of-plane rotation of  $39 \pm 2^\circ$  in dioxane<sup>[9]</sup>.

The AM1 and PM3 calculated barriers have been collected in Table 4.1. All values are low compared with the available experimental data. Whereas the AM1 calculated barriers still show a reasonable fit, the PM3 values are more irregular. These observations are in agreement with the findings reported by Coussens et al.<sup>[4]</sup> who studied another series of aromatic moieties.

The use of the MMOK option in the MOPAC program, adding a molecular mechanics correction term for the torsional barrier of a peptide bond, did not result in a significant improvement of the aforementioned AM1 and PM3 results.

Coussens et al.<sup>[4]</sup> found that the AM1 calculated barriers for a number of small

**Table 4.1** Experimental rotational barriers and cis → trans rotational barriers calculated (kcal.mol<sup>-1</sup>) by force field, semiempirical and ab initio methods for the moieties shown in Figure 4.2.

	Force Field				Semiempirical			Ab initio		exp.
	CVVF	CHARMm	AMBER		AM1		PM3	6-31G**/6-31G*		
		21.3	4.0	adapted	scaled (×1.9)			scaled (×0.5)		
Benzaldehyde	12.6	9.5	9.7	4.9	2.7 <sup>a</sup>	5.1	1.6 <sup>a</sup>	8.9 <sup>a</sup>	4.5	4.9 <sup>b</sup>
3-Pyridinealdehyde	20.7	9.3	9.8	4.6	2.9	5.5	1.8	10.1	5.1	4.6 <sup>c</sup>
1-Me-3-pyridiniumaldehyde	18.6	10.2	9.9	4.7	2.7	5.1	1.4	8.6	4.3	
1-Me-3-acetylpyridinium	16.7	9.0	9.6	4.2	2.3	4.4	1.1			
Acetophenone	16.0	ND	9.5	3.1	1.6	3.0	0.4			3.1 <sup>d</sup>
3-Methylbenzamide	16.7	8.8	8.8	3.1	0.9	1.7	0.3			
1-Methylnicotinamide	16.2	9.2	7.4	3.0	1.8	3.4	2.0	5.1 <sup>e</sup>	2.6	
1-Me-1,4-dihydronicotinamide	5.0	8.6	10.3	4.7	2.9	5.5	1.0	7.8 <sup>e</sup>	3.9	

<sup>a</sup> See reference 4.

<sup>b</sup> Microwave results<sup>[10]</sup>. The observed barrier using far IR is 4.6 kcal.mol<sup>-1</sup> <sup>[11]</sup>.

<sup>c</sup> See reference 12.

<sup>d</sup> Rotational barrier for acetophenone in vapour phase<sup>[12]</sup>.

<sup>e</sup> See reference 13.

aromatic moieties having a  $\pi$ -conjugated substituent were too low by a factor of 1.9, as compared with average experimental values. The experimental data could be reproduced within 15% accuracy by multiplying the AM1 calculated barriers with this factor. In Table 4.1 the AM1 results given are corrected by scaling factor of 1.9. The values obtained in this way fit the experimental ones, which points to a systematic effect in AM1 for predicting too low barriers.

#### 4.3.3 *Ab initio* calculations

As *ab initio* calculations at the 6-31G\* level are very CPU-time consuming, we limited these calculations to the most interesting molecules in the context of this thesis, i.e., 3-pyridinealdehyde (for which the experimental value of the barrier is known) and 1-Me-3-pyridiniumaldehyde. Both the optimized 3-pyridinealdehyde and the optimized 1-Me-3-

**Table 4.2** Energy differences between the trans (*t*) and cis (*c*) conformers, the rotational barrier, and the out-of-plane value  $\theta$  for the minimal trans conformation of 1-methylnicotinamide and 1-Me-1,4-dihydronicotinamide. (Energies in kcal.mol<sup>-1</sup>,  $\theta$  in degrees).

	1-Methylnicotinamide			1-Me-1,4-dihydronicotinamide			Benzaldehyde
	t-c	barrier	$\theta(t)$	t-c	barrier	$\theta(t)$	barrier
<i>Ab initio</i>							
STO3G//STO3G <sup>a,b</sup>	1.6	3.1	0°	2.4	4.8	0°	5.9
3-21G//3-21G <sup>a,b</sup>	3.1	9.2	30°	4.7	12.1	0°	11.3
3-21G*//3-21G* <sup>c</sup>	3.1	8.7	0°	4.7	11.2	0-30°	
6-31G//3-21G <sup>a,b</sup>	3.1	6.7	30°	4.1	10.3	30°	9.4
6-31G*//3-21G <sup>a</sup>	1.8	5.1	20-30°	2.8	8.5	20-30°	9.0
6-31G*//3-21G* <sup>c</sup>	2.1	5.1	30°	3.0	8.5	30°	
6-31G*//6-31G* <sup>b,d</sup>	1.3	5.1	20-30°	1.7	7.8	20-30°	8.9
MP2/6-31G*//6-31G* <sup>b,d</sup>	0.9	3.1	20-30°	1.0	6.9	20-30°	8.6
AMBER adapted	1.7	3.0	31.6°	2.4	4.7	25.2°	4.9

<sup>a</sup> See reference 2. <sup>b</sup> See reference 4. <sup>c</sup> See reference 3. <sup>d</sup> See reference 13.



pyridiniumaldehyde show a global minimum at  $\theta=180^\circ$  (where  $\theta$  is defined as the O7-C7-C3-C4 dihedral angle,  $\theta=180^\circ$ : *cis* conformation), i.e. the conformation in which the carbonyl oxygen is directed toward the pyridine nitrogen (N1). A local minimum is observed at  $\theta=0^\circ$  (*trans* conformation). For 3-pyridinealdehyde and 1-Me-3-pyridiniumaldehyde the energy differences between the optimized *trans* conformer and the corresponding optimized *cis* conformer are 0.7 and 1.2 kcal.mol<sup>-1</sup>, respectively. The calculated barriers (*cis* → *trans*) for 1-Me-3-pyridiniumaldehyde and 3-pyridinealdehyde (Table 4.1), differ substantially from the experimental gas-phase value of the latter. The same conclusion can be drawn comparing the *ab initio* calculated barrier<sup>[4]</sup> and the experimental barrier<sup>[10]</sup> for benzaldehyde. For the latter molecule it has been reported that satisfactory agreement between calculated and experimental barriers can only be obtained by performing (very extensive) MCSCF calculations<sup>[4]</sup>.

In Table 4.2 the rotational energy barriers for 1-methylnicotinamide and 1-Me-1,4-dihydropyridin-2(1H)-one, calculated with several basis sets, are listed. Almost all *ab initio* results predict an absolute minimum at the planar *cis* configuration ( $\theta=180^\circ$ ) and a local minimum at the *trans* conformation, approximately 20-30° out-of-plane. Except for the STO-3G level, the *ab initio* calculations show a gradual decrease in barrier heights and energy differences between the *cis/trans* conformations, with increasing magnitude of the basis set. Similar trends are observed in the case of benzaldehyde<sup>[4]</sup>. With this molecule, even the MP2/6-31G\*\*/6-31G\* calculations are still a factor of 2 too high. A scaling factor of 2 can be derived from the ratio of experimental and 6-31G\* calculated barriers for benzaldehyde<sup>[4]</sup> (see also Table 4.1). Application of this scaling factor to the 6-31G\* calculated barrier presented in this paper for 3-pyridinealdehyde, results in a value close to the experimental one (Table 4.1).

#### 4.4 Discussion

The results presented above for a range of analogues of nicotinamide show that calculated side-chain barriers are either too large or too small, depending on the specific computational method used. If, for example, the barriers of 8 kcal.mol<sup>-1</sup> or even more are realistic values, then the  $\theta$  values of the molecules studied would be restricted in an enzymatic environment to almost those of the free molecules. However, the  $\theta$  values of the free molecules need not to be the most favourable ones in the enzymatic complex.

Based upon the available experimental data and the results reported by Coussens et al.<sup>[4]</sup>, the AM1 and the 6-31G\* calculated barriers were scaled, resulting in a reasonable agreement with each other and with the known experimental data (see Table 4.1). The scaled

barriers proved to be lower than  $5.5 \text{ kcal.mol}^{-1}$ , i.e. substantial fluctuations in the dihedrals can occur at ambient conditions, enabling the nicotinamide and related moieties to accommodate their conformation to the enzyme cavity.

In the past the AMBER program has been used for modelling studies on the horse liver alcohol dehydrogenase with  $\text{NAD}^+/\text{NADH}$  and its analogues<sup>[14,15]</sup>. The original AMBER parameter set results in high torsional barriers (Table 4.1) and forces the molecules studied into almost planar structures, due to the potential-energy equation used. It now appears from the results presented in this paper that the AMBER 4.0 force field can only be applied for such a purpose if the force field parameters are adapted in such a way that they are in conformity with the scaled AM1 and 6-31G\* barriers. It seems only necessary to adapt the parameters involved in the description of the dihedrals around the C3–C7 bond, i.e.  $V_n$  in the dihedral energy equation used (see also eq. 3.1):

$$\sum_{\text{dihedrals}} \frac{V_n}{2} (1 + \cos[n\phi - \gamma]) \quad (4.1)$$

By choosing the  $V_2$  values employed in the adapted AMBER force field in between 0.44 and

**Table 4.3** The (adapted) AMBER 4.0 parameters  $V_n/2$  for the dihedral barrier, the calculated rotational barrier and the out-of-plane value ( $\theta$ ) of the minima of the calculated structures. (Barriers and  $V_n/2$  in  $\text{kcal.mol}^{-1}$ ,  $\theta$  in degrees).

Substrate	original AMBER		adapted AMBER			
	barrier	$\theta$	$V_1/2$	$V_2/2$	barrier	$\theta$
Benzaldehyde	9.7	1	-	0.63	4.9	1
3-Pyridinealdehyde	9.8	0-2 <sup>a</sup>	-	0.58	4.6	0-4 <sup>a</sup>
1-Me-3-pyridiniumaldehyde	9.9	0-3 <sup>a</sup>	-	0.63	4.7	0-4 <sup>a</sup>
1-Me-3-acetylpyridinium	9.6	0-5 <sup>a</sup>	-	0.60	4.2	0-13 <sup>a</sup>
Acetophenone	9.5	0	-	0.44	3.1	3
3-Methylbenzamide	8.8	10-13 <sup>a</sup>	-	0.50	3.1	28 <sup>a</sup> -35
1-Methylnicotinamide	7.4	10-18 <sup>a</sup>	0.17	0.55	3.0	32 <sup>a</sup> -40
1-Me-1,4-dihydronicotinamide	10.3	0-11 <sup>a</sup>	0.19	0.59	4.7	0-25 <sup>a</sup>

<sup>a</sup> Indicates the *trans* minimum.

0.63 kcal.mol<sup>-1</sup> (Table 4.3), as compared with the standard value of 1.3 kcal.mol<sup>-1</sup> for all species in the original AMBER 4.0 force field, satisfactory agreement with the scaled *ab initio* and AM1 results is obtained (cf. Table 4.1). A low value for  $V_1$  is required in order to accommodate the *cis/trans* energy difference in the nicotinamides. The modification of the force field leads to larger values of  $\theta$ , coming closer to the calculated *ab initio*  $\theta$  values. Furthermore the adapted AMBER calculations indicate planar minimal structures for the aldehydes, whereas the compounds with acetyl or amide side-chains all show non-planar minima, i.e. significant out-of-plane rotations, in accordance with the semiempirical results.

#### 4.5 Determination of $V_n/2$ for NAD<sup>+</sup>/NADH and analogues

For the small derivatives a good estimation of the rotational barrier around the C3-C7 bond could be made by scaling AM1 and 6-31G\*\*/6-31G\* calculated values for the barriers. It is assumed that the calculated barriers for the small derivatives are the same as those for the corresponding NAD<sup>+</sup>/NADH (analogues). For the total NAD<sup>+</sup> and NADH coenzyme and the analogues 3-thionicotinamide, 3-acetylpyridine and 3-formylpyridine adenine dinucleotide, the  $V_n/2$  values were determined. The atomic charges were taken from 6-31G\*\*/3-21G *ab initio* calculations and therefore the parameters listed in Table 4.4 differ from the ones listed in Table 4.3.

**Table 4.4** The adapted AMBER 4.0 parameters  $V_n/2$  for the dihedral barrier of NAD<sup>+</sup>, NADH and analogues and the calculated rotational barrier (all values in kcal.mol<sup>-1</sup>).

Substrate	$V_1/2$	$V_2/2$	calculated barrier
NAD <sup>+</sup>	0.02	0.45	3.0
NADH	0.40	0.70	4.7
3-acetyl-PdAD <sup>+</sup>	—	0.39	4.2
3-formyl-PdAD <sup>+</sup>	—	0.505	4.7

These adapted parameters are also listed in Appendix 2 and will be applied in the MM and MD calculations as described in Chapter 5 and 6. For the thio analogue of NAD<sup>+</sup> (sNAD<sup>+</sup>) the standard AMBER parameters were used, resulting in a rotational barrier of 6.25 kcal.mol<sup>-1</sup> which is very close to the determined scaled AM1 calculated barrier of 6.3 kcal.mol<sup>-1</sup>. The minimum in energy was found at an out-of-plane value of 30° (*trans*).

## 4.6 Conclusions

Since the orientation of the carboxamide side-chain of the nicotinamide moiety in  $\text{NAD}^+/\text{NADH}$  dependent dehydrogenases seems to play an important role in the catalytic mechanism, a fundamental study of the rotational barriers of the side-chain of a series of coenzyme analogues, can significantly contribute to our understanding of the catalytic behaviour of these enzymes. It can be concluded that the computational methods used in this chapter all predict rotational barriers for the 1,3-substituted pyridines and benzenes (Figure 4.2) deviating more or less from the few experimentally data known (Table 4.1). Scaling of the results of semiempirical (AM1) and *ab initio* (6-31G\*) calculations provides values for the rotational barriers that are in good agreement with the experimental ones. Consequently, the AMBER force field parameters  $V_n/2$ , describing the rotational barriers, must be adjusted in order to bring the calculated barrier values into line with the scaled AM1 and *ab initio* results. At these values (lower than  $5.5 \text{ kcal.mol}^{-1}$ ) the out-of-plane rotation of the side-chain of  $\text{NAD}^+/\text{NADH}$ , suggested to be essential for the enzymatic activity, can easily be obtained at room temperature. The adapted AMBER 4.0 force field parameters will enable force field simulations of the  $\text{NAD}^+/\text{NADH}$  coenzyme and its analogues (see Chapter 5 and 6), improving the understanding of the catalytic mechanism of  $\text{NAD}^+/\text{NADH}$  dependent dehydrogenases.

## References

1. M.L. Frisch, M. Head-Gordon, G.W. Trucks, J.B. Foresman, H.B. Schlegel, K. Raghavachari, M.A. Robb, J.S. Binkley, C. Gonzalez, D.J. Defrees, D.J. Fox, R.A. Whiteside, R. Seeger, C.F. Melius, J. Baker, R.L. Martin, L.R. Kahn, J.J.P. Stewart, S. Topiol and J.A. Pople, GAUSSIAN 90, Gaussian Inc., Pittsburgh, Philadelphia, USA (1990).
2. P.L. Cummins and J.E. Gready, *J. Mol. Struct. (Theochem)* **183**, 161-174 (1989).
3. H. Li and B.M. Goldstein, *J. Med. Chem.* **35**, 3560-3567 (1992).
4. B. Coussens, K. Pierloot and R.J. Meier, *J. Mol. Struct. (Theochem)* **259**, 331-344 (1992).
5. QCPE Program No. 455, Quantum Chemistry Program Exchange, Indiana University, Bloomington, Indiana, USA (1991).
6. INSIGHT/DISCOVER, Biosym Inc., San Diego, California, USA.
7. QUANTA/CHARMM, Molecular Simulations Inc., Waltham, Massachusetts, USA.
8. D.A. Pearlman, D.A. Case, J.C. Caldwell, G.L. Seibel, U.C. Singh, P. Weiner and P.A. Kollman, AMBER 4.0, University of California, San Francisco, USA (1991).
9. R.K. Pierens and A.J. Williams, *J. Chem. Soc. Perkins Trans. 2*, 235-238 (1980).
10. R.K. Kakar, E.A. Rinehart, C.R. Quade and T. Kojima, *J. Chem. Phys.* **52**, 3803-3813 (1970).
11. J.R. Durig, H.D. Bist, K. Furic, J. Qiu and T.S. Little, *J. Mol. Struct.* **129**, 45-56 (1985).

12. F.A. Miller, W.G. Fateley and R.A. Wittkowski, *Spectrochim. Acta*, Part A, **23**, 891-908 (1967).
13. Y.-D. Wu and K.N. Houk, *J. Org. Chem.* **58**, 2043-2045 (1993).
14. N.A. Beijer, H.M. Buck, L.A.Æ. Sluyterman and E.M. Meijer, *Biochem. Biophys. Acta* **1039**, 227-233 (1990).
15. P.M.T. de Kok, N.A. Beijer, H.M. Buck, L.A.Æ. Sluyterman and E.M. Meijer, *Eur. J. Biochem.* **175**, 581-585 (1988).

---

*This chapter is based on:*

S.A.M. Vanhommerig, R.J. Meier, L.A.Æ. Sluyterman and E.M. Meijer, *J. Mol. Struct. (Theochem)* **304**, 53-59 (1994).

## 5

## Kinetic and modelling studies of polyethylene glycol bound $\text{NAD}^+$ versus native $\text{NAD}^+$

### 5.1 Introduction

A number of synthetically useful enzymatic reactions require cofactors such as nicotinamide adenine dinucleotide ( $\text{NAD}^+$ ). These cofactors are too expensive to be used as stoichiometric reagents. Retention and regeneration of the cofactors from the reaction (by-) products is thus required to make the process economically viable. Many procedures have been suggested to achieve efficient coenzyme recycling<sup>[1]</sup>. One of the systems investigated, the enzyme membrane reactor concept developed by Wandrey and co-workers<sup>[2,3]</sup>, shows commercially attractive features (see also Chapter 1). Little cofactor consumption in a membrane reactor has been achieved when  $\text{NAD}^+$  is covalently linked to polyethylene glycol (PEG- $\text{NAD}^+$ , Figure 5.1)<sup>[4]</sup>. Many other dehydrogenases accept the PEG- $\text{NAD}^+$  as coenzyme. So far, glucose dehydrogenase is the only enzyme known that is not active with PEG- $\text{NAD}^+$  <sup>[5]</sup>. Until now, the observed activities of PEG- $\text{NAD}^+$  with dehydrogenases are not understood at the molecular level. We tested the activity of PEG- $\text{NAD}^+$  with HLADH and in order to explain the kinetic results, several additional experiments were performed. As these could not be used to explain the kinetic data, we resorted to MD calculations, to examine possible changes in the structure caused by the PEG-tail.

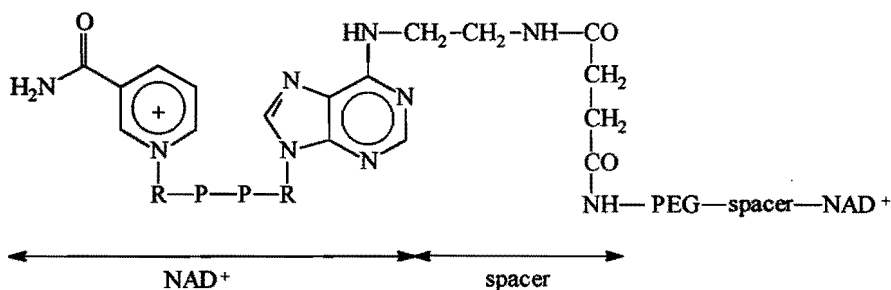


**Figure 5.1** Structure of polyethylene glycol bound  $\text{NAD}^+$ .  $R$ =ribose,  $P$ =phosphate, PEG=polyethylene glycol  $= (\text{CH}_2-\text{CH}_2-\text{O})_n$ .

## 5.2 Experimental

### 5.2.1 Materials

HLADH,  $\text{NMN}^+$  and  $\beta\text{-NAD}^+$  were purchased from Sigma. PEG-NADH was supplied by prof.dr. C. Wandrey and dr. U. Kragl from the Institute of Biotechnology in Jülich. The coenzyme  $\text{NAD}^+$  was lyophilised from distilled water. The PEG-NADH was oxidized to  $\text{PEG-NAD}^+$  as described by Bückmann et al.<sup>[6]</sup> The  $\text{PEG-NAD}^+$  was purified using a bacterial filter, with a pore size of 0.2  $\mu\text{m}$ . The coenzyme concentrations were determined spectrophotometrically using the following absorption coefficients: 18,000  $\text{M}^{-1}\text{cm}^{-1}$  at  $\lambda_{\text{max}}=260$  nm for  $\text{NAD}^+$ , 21,600  $\text{M}^{-1}\text{cm}^{-1}$  at  $\lambda_{\text{max}}=267.5$  nm for  $\text{PEG-NAD}^+$  and 6,220  $\text{M}^{-1}\text{cm}^{-1}$  at 340 nm in case of the reduced forms. Sodium dithionite was purchased from Janssen Pharmaceutical (purity  $\approx 80\%$ ;  $\epsilon=7,000$   $\text{M}^{-1}\text{cm}^{-1}$ ), potassium cyanide from Merck and Koshland reagent from Aldrich (purity 98%;  $\epsilon=18,000$   $\text{M}^{-1}\text{cm}^{-1}$  at  $\lambda=410$  nm and  $\text{pH}=10$ ).

### 5.2.2 Kinetic measurements

All kinetic experiments were carried out at  $25^\circ\text{C} \pm 0.1^\circ\text{C}$  in 47 mM phosphate buffer, 0.25 mM EDTA,  $\Gamma=0.1$ . The pH was adjusted to 8.0 with KOH. A Perkin-Elmer UV/Vis spectrophotometer Lambda 3B was used. Steady-state kinetics were carried out with coenzyme saturation (0.55 mM  $\text{NAD}^+$  or 0.59 mM  $\text{PEG-NAD}^+$ ) and a substrate concentration range from 1-10 mM in the case of ethanol and 10-100 mM in the case of isopropanol (see Appendix 1 for the equation used to determine the initial rates); the  $\text{NAD}^+$   $\text{PEG-NAD}^+$  concentrations were varied between 5-55  $\mu\text{M}$  at a constant ethanol concentration of 10 mM. The change of absorption at 340 nm was measured. The enzyme concentrations ranged from 0.03-0.52  $\mu\text{M}$  during the steady-state measurements. BSA was added to the enzyme stock solution to stabilize the HLADH. The interference of polyethylene glycol in the steady-state kinetics was checked using 1 mM PEG concentration (2% w/v), 10 mM ethanol and  $\text{NAD}^+$  or  $\text{PEG-NAD}^+$  as coenzyme.

### 5.2.3 Formation of adducts

The rates of formation of sulphinate adducts were determined at  $20.1^\circ\text{C}$  in a Hi-Tech Scientific stopped-flow spectrophotometer SF-51. Equal amounts of an anaerobic 0.20 mM sodium dithionite solution in 50 mM Tris/HCl buffer ( $\text{pH}=7.8$ ) and an anaerobic 1.32 mM coenzyme solution in phosphate buffer ( $\text{pH}=8.2$ ) were mixed, under an argon flush. The

total volume was 150  $\mu\text{L}$ . The formation of the sulphinate adduct was followed spectrophotometrically by measuring the change in absorption at 353 nm ( $\epsilon_{\text{adduct}}=3200 \text{ M}^{-1}\text{cm}^{-1}$ ). All the solutions used were made anaerobic by repeatedly flushing with purified argon<sup>[7]</sup>.

The formation of the cyanide adduct was carried out at 25°C in a 0.01 M KCN solution. The coenzyme concentration was 0.17 mM in a total volume of 2.5 mL. The reactions were followed spectrophotometrically by measuring the increase in absorption at 325 nm ( $\epsilon_{\text{adduct}}=6300 \text{ M}^{-1}\text{cm}^{-1}$ )<sup>[8]</sup>. A Perkin-Elmer UV/Vis spectrophotometer Lambda 3B was used.

### 5.2.4 Determination of the number of tryptophanes

Aqueous solutions of HLADH (with either buffer/NAD<sup>+</sup> or buffer/NAD<sup>+</sup>/polyethylene glycol ( $M_w=20,000$ ) or buffer/PEG-NAD<sup>+</sup> or plane phosphate buffer solution) were allowed to react in the dark with a solution of 50 mM 2-hydroxy-5-nitrobenzyl bromide dissolved in dried acetone<sup>[9]</sup>. The enzyme was separated from the excess of reagent, by column chromatography, using a 0.9 x 30 cm Sephadex (G25 medium) column, and phosphate buffer pH=8 as eluent. Absorption spectra were recorded on a Perkin-Elmer UV/Vis spectrophotometer Lambda 3B, after adjusting the pH of the fractions to 10, with KOH.

### 5.3 Computational methods

Energy calculations, total energy-minimizations and molecular dynamics simulations were performed with the molecular simulation package AMBER 4.0<sup>[10]</sup> on a Power Challenge SGI computer. The potential energy function used by AMBER is of the form:

$$\begin{aligned}
 V = & \sum_{\text{bonds}} k_r(r-r_e)^2 + \sum_{\text{angles}} k_\theta(\theta-\theta_e)^2 + \sum_{\text{dihedrals}} \frac{V_n}{2}(1+\cos[n\phi-\gamma]) \\
 & + \sum_{i < j} \left[ \frac{A}{r_{ij}^{12}} - \frac{B}{r_{ij}^6} + \frac{q_i q_j}{r_{ij}^\epsilon} \right] + \sum_{H \text{ bonds}} \left[ \frac{C}{r_{ij}^{12}} - \frac{D}{r_{ij}^{10}} \right] \quad (5.1) \\
 & \text{nonbonded}
 \end{aligned}$$

The crystallographic structure of the ternary complex of HLADH/NADH/DMSO<sup>[11]</sup> was used as a starting structure and obtained from the Protein Data Bank (PDB reference



number 6ADH). The cysteine residues 46, 103, 111 and 174 were defined as negatively charged cysteines, containing thiolate groups. All histidine residues were taken as HID except the His 51, which was taken HIP (diprotonated histidine) in the cases of the oxidized coenzyme complex. Ethoxide or isopropoxide was substituted at the position of DMSO. Nine water molecules were added manually, according to their subsequent presence in both the binary complex of HLADH (PDB file 5ADH)<sup>[12]</sup> and the X-ray structure of HLADH with NAD<sup>+</sup> and pentafluoro benzyl alcohol (PDB file 1HLD)<sup>[13]</sup>. Then more water was added in a range of 29 Å around the catalytic zinc ion, applying a minimum distance of 2.6 Å between the oxygen atom of a water molecule and the heavy atoms of the enzyme complex, resulting in approximately 1370 water residues in the shell around the enzyme. All water molecules were treated as TIP3P residues<sup>[14]</sup>. First the substrate and water molecules in the enzymatic complex were minimized in energy, keeping the rest fixed. Since the enzyme is too large to be minimized completely during the calculations, the 'belly' option was used so that only the amino acid residues within a radius of 15 Å around NAD<sup>+</sup> (see list in Appendix 2), the alkoxide, the catalytic zinc atom, NAD<sup>+</sup> and all water molecules were allowed to move freely (approximately 6825 atoms in the belly).

The three-dimensional starting structure of PEG-NAD<sup>+</sup> was constructed from the X-ray NAD<sup>+</sup> geometry to which the PEG-residues were linked using the program QUANTA/CHARMM 3.3.2<sup>[15]</sup>. Only 10 PEG residues plus the spacer group (see Figure 5.1) were coupled to the exocyclic adenine-NH<sub>2</sub> group. After the MD heating simulation (*vide infra*) the PEG-tail is positioned on the surface of the water shell.

All energy minimizations (MM-calculations, using 750 steps of steepest descent algorithm, followed by the conjugate gradient algorithm) were performed until the RMS gradient value of the energy was less than 0.1 kcal.Å<sup>-1</sup>, using a dielectric constant of 1 and treating all CH, CH<sub>2</sub> and CH<sub>3</sub> groups of the amino acids as united atoms. The nonbonded pair list had a cutoff of 12 Å and was updated every 25 time steps. The water cap was restrained at the 29 Å boundary by a harmonic potential with a force constant of 0.5 kcal.Å<sup>-1</sup> (positional constraints). Atomic charges of the nicotinamide moiety, the negatively charged cysteines, iPrO<sup>-</sup> and of EtO<sup>-</sup> were derived from 6-31G\*\*/3-21G *ab initio* calculations (Appendix 2). The zinc ions carried a charge of 1.45, according to the calculations by Tapia et al.<sup>[16]</sup>. Most harmonic force constants were obtained directly from the literature or extrapolated (see Appendix 2)<sup>[17,18]</sup>.

The molecular dynamics (MD) simulations up to 90 ps were carried out using a time step of 2.0 fs and the SHAKE procedure to constrain all the bond lengths. The following protocol was used: a heating phase of 5 ps to a final temperature of 300 K followed by 35 ps of equilibration and finally an observation period of 50 ps (250 conformations for analysis). Analysis of atomic trajectories was achieved with the CARNAL program<sup>[19]</sup>.

*Parameterization.* In order to maintain the tetracoordinated structure of the zinc ion, an explicit Zn-O bond and explicit angles of N-Zn-S, S-Zn-S and N-Zn-O were inserted between the zinc ion and its ligands (see Appendix 2). The parameters describing the torsional barrier for the carboxamide orientation of the side-chain of the nicotinamide moiety with 6-31G\* atom charges, were estimated<sup>[20]</sup> and applied as described in Chapter 4.

## 5.4 Results and discussion

### 5.4.1 Kinetic results

The kinetic behaviour of HLADH with both ethanol and isopropanol can be described by an extension of the Michaelis-Menten treatment<sup>[21]</sup> to those cases in which the enzyme, coenzyme and substrate combine into a ternary complex<sup>[22-24]</sup>. In this complex the reaction takes place. If NAD<sup>+</sup> is used as coenzyme and ethanol as substrate, the dissociation of the NADH from the enzyme is the rate limiting step, whereas in the case of the poor substrate isopropanol the rate of hydride-transfer is limiting as shown by pre steady-state measurements<sup>[25]</sup>. Table 5.1 summarizes the steady-state kinetic data obtained for

*Table 5.1 Kinetic constants of horse liver ADH using NAD<sup>+</sup> and PEG-NAD<sup>+</sup> respectively, as coenzymes. Initial velocities with varying concentrations of coenzymes or substrates were determined at 25°C, pH=8, by measuring the increase in absorption at 340 nm. Standard errors for the estimated  $k_{cat}$  and  $K_m$  values from a fit with HYPER<sup>[26]</sup> were less than 7% and 20% of the reported values, respectively.*

parameter		NAD <sup>+</sup>		PEG-NAD <sup>+</sup>	
$k_{cat}(\text{EtOH})$	s <sup>-1</sup>	1.14	(100%)	0.36	(32%)
$k_{cat}(\text{IPA})$	s <sup>-1</sup>	0.15	(13%)	0.038	(3%)
$K_m(\text{NAD}^+)^a$	μM	16.3		62.0	
$K_m(\text{EtOH})$	mM	0.46		1.13	
$K_m(\text{IPA})$	mM	12.3		16.8	
$k_{cat}(\text{EtOH})/K_m(\text{EtOH})$	s <sup>-1</sup> mM <sup>-1</sup>	2.48	(100%)	0.32	(13%)
$k_{cat}(\text{IPA})/K_m(\text{IPA})$	s <sup>-1</sup> mM <sup>-1</sup>	0.012	(4.8‰)	0.0023	(0.9‰)

<sup>a</sup> Determined with an ethanol concentration of 10 mM.

*Table 5.2 Dehydrogenases, substrates and the relative activity with PEG-NADH (\*=PEG-NAD<sup>+</sup>) compared with NADH (\*=NAD<sup>+</sup>) and the relative K<sub>m</sub> for PEG-NADH (\*=PEG-NAD<sup>+</sup>) compared to NADH (\*=NAD<sup>+</sup>).*

Enzyme	code	number of subunits	substrate	$\frac{k_{cat}(\text{PEG-NADH})}{k_{cat}(\text{NADH})}$	$\frac{K_m(\text{PEG-NADH})}{K_m(\text{NADH})}$
L-leucine DH <sup>[2]</sup>	1.4.1.9	6	keto isocaproate	0.9	2.5
leucine DH <sup>[5]</sup>	1.4.1.9	8	ketoleucine	0.9	0.9
formate DH <sup>[2]</sup>	1.2.1.2	2	NH <sub>4</sub> <sup>+</sup> formate	2.1*	1.1*
formate DH <sup>[27]</sup>	1.2.1.2	2	NH <sub>4</sub> <sup>+</sup> formate	1.0*	1.5*
L-hydroxy isocaproate DH <sup>[5]</sup>		4	ketoleucine	0.4	1.0
D-hydroxy isocaproate DH <sup>[5]</sup>		2	ketomethionine	0.9	1.4
mandelic acid DH <sup>[27]</sup>		2	phenylglyoxylic acid	0.4	2.5
mandelic acid DH <sup>[27]</sup>		2	mandelic acid	0.3*	1.7*
alanine DH <sup>[5]</sup>	1.4.1.1	2	pyruvate	0.5	58.6
L-lactate DH <sup>[5]</sup>	1.1.1.27	4/2	L-lactate	0.5	80.0
D-lactate DH <sup>[5]</sup>	1.1.1.27	4/2	D-lactate	0.1	0.2
phenylalanine DH <sup>[5]</sup>		?	phenylpyruvate	0.5	2.1
alcohol DH	1.1.1.1	2	ethanol	0.4	3.9

NAD<sup>+</sup> and PEG-NAD<sup>+</sup> with ethanol or isopropanol as substrate (see Appendix 1 for the equation used). The same mechanism as for NAD<sup>+</sup> is assumed to occur for PEG-NAD<sup>+</sup>. We found that HLADH exhibits substantially lower activity if PEG-NAD<sup>+</sup> is used instead of the native NAD<sup>+</sup>. The turnover number ( $k_{\text{cat}}$ ) appears to be three times lower for PEG-NAD<sup>+</sup>/ethanol compared to NAD<sup>+</sup>/ethanol. With isopropanol  $k_{\text{cat}}$  even drops by a factor of four. With most dehydrogenases similar results have been found (see Table 5.2)<sup>[2-5,27]</sup>. Only in a few cases comparable activities for NAD<sup>+</sup> and PEG-NAD<sup>+</sup> have been reported<sup>[3,4]</sup>. The value of the Michaelis-Menten constant  $K_m$  for PEG-NAD<sup>+</sup> is significantly larger than the  $K_m$  for NAD<sup>+</sup>, which has also been observed with other dehydrogenases<sup>[2,5,27]</sup>.

Since the PEG-NADH sample may contain up to 5% single substituted product (and thus a small amount of free, terminal OH-groups), the interference of polyethylene glycol in the ordinary enzymatic reaction was investigated. Based on experiments in which 2% w/v PEG ( $M_w=20,000$ ) was tested for its properties as substrate or inhibitor for HLADH, it could be concluded that the compound does not interfere in any way, neither with NAD<sup>+</sup> nor with PEG-NAD<sup>+</sup>.

In order to explain the kinetic results obtained for HLADH with PEG-NAD<sup>+</sup> as coenzyme we performed several studies including the determination of the intrinsic reactivity of PEG-NAD<sup>+</sup>, binding studies with the apo-enzyme, shifts in the monomer-dimer equilibrium of HLADH and modelling calculations directed at the coenzyme/apo-enzyme interactions.

#### 5.4.2 Measurements of intrinsic reactivities

The lower activity found with PEG-NAD<sup>+</sup> in enzymatic reactions with HLADH and many other dehydrogenases might be attributed to a lower intrinsic reactivity of PEG-NAD<sup>+</sup>. We therefore determined the intrinsic reactivities of NAD<sup>+</sup> and PEG-NAD<sup>+</sup> using sodium dithionite and potassium cyanide as reducing agents. These reducing agents form sulphinate and cyanide adducts with the cofactors<sup>[7,8]</sup>, respectively. From the results listed in Table 5.3 it is clear that PEG-NAD<sup>+</sup> shows a strongly reduced reactivity with both  $S_2O_4^{2-}$  and  $CN^-$  (31% and 43% of the reactivity of NAD<sup>+</sup>, respectively).

**Table 5.3** Determination of the intrinsic reactivities for various coenzymes. The formation of the sulphinate and cyanide adducts were followed spectrophotometrically at 353 nm and 325 nm respectively.

Coenzyme	relative $k(\text{SO}_2^-)$ %	relative $k(\text{CN}^-)$ %
NAD <sup>+</sup>	100 <sup>a</sup>	100 <sup>a</sup>
PEG-NAD <sup>+</sup>	31	43
NMN <sup>+</sup>	43	59

<sup>a</sup> The absolute rates at 0.1 mM dithionite and 10 mM KCN were 0.02 s<sup>-1</sup> and 0.0012 Abs. units.s<sup>-1</sup> respectively.

From NMR measurements it is known that free NADH in an aqueous environment can adopt a folded conformation, in which stacking occurs between the nicotinamide and adenine rings<sup>[28]</sup>. Such intramolecular stacking may very well enhance the reactivity of NAD<sup>+</sup>, as is nicely illustrated by the results obtained for the nicotinamide mononucleotide (NMN<sup>+</sup>), lacking the adenoside part of NAD<sup>+</sup> (see Table 5.3). It is conceivable that the polyethylene glycol tail attached to the adenine of PEG-NAD<sup>+</sup> prevents the stacking phenomenon in PEG-NAD<sup>+</sup>, resulting in the lower intrinsic reactivity observed.<sup>§</sup>

On the other hand it can be argued that the reactivities of NAD<sup>+</sup> and PEG-NAD<sup>+</sup>, once bound in the active site of the apo-enzyme, do not differ that much. In contrast with the conformational behaviour of free NAD<sup>+</sup>, the coenzyme solely binds in an extended conformation to HLADH as can be derived from the X-ray data<sup>[11,29]</sup>.

### 5.4.3 Binding studies

The HLADH dimer consists of two subunits, both of which contain one coenzyme binding site and one substrate binding site. Normally, two NAD<sup>+</sup> residues bind to the HLADH dimer in the coenzyme binding sites, plus two alcohol molecules in the substrate binding pockets. However, either by interactions of two PEG-chains, or after the binding of one PEG-NAD<sup>+</sup> molecule to a HLADH dimer, steric hindrance from the polyethylene glycol

<sup>§</sup> Unfortunately we were unable to carry out <sup>1</sup>H-NMR experiments on PEG-NAD<sup>+</sup> or PEG-NADH. Due to the low solubility of the polymer bound NAD<sup>+</sup>, the H4 signals could not be measured and no further information about the occurrence of the folded conformation of PEG-NAD<sup>+</sup> could be obtained.

tail, dangling outside the enzyme, with the second site might occur. From experimental data and a mathematical description concerning PEG-properties by Kambe et al.<sup>[30,31]</sup> it was calculated that the hydrodynamic radius  $R_h$  of polyethylene glycol with a  $M_w$  of 20,000 is 78 Å. As the linear distance between the entrances of the coenzyme pockets in the dimer is 38 Å, binding of a second PEG-NAD<sup>+</sup> might be prevented by steric hindrance. Therefore, the number of coenzyme binding sites available in HLADH after binding of one PEG-NAD<sup>+</sup> molecule were checked. There are three possibilities altogether after the binding of the first PEG-NAD<sup>+</sup>:

- 1) A second PEG-NAD<sup>+</sup> is able to bind.
- 2) Only NAD<sup>+</sup> is able to bind in the other coenzyme binding site, but not a second PEG-NAD<sup>+</sup>.
- 3) The other coenzyme binding site cannot bind NAD<sup>+</sup> either.

Distinction could be made between options 1/3 and 2 by measuring the competition between NAD<sup>+</sup> and PEG-NAD<sup>+</sup> (See Appendix 1 for theoretical background). Figure 5.2 shows the theoretical relative rates of coenzyme conversion for the options 1/3 and 2 at a fixed, saturating concentration of PEG-NAD<sup>+</sup> and a varying subsaturating NAD<sup>+</sup> concentration. If option 2 is operative and all dimers contain only one PEG-NAD<sup>+</sup> at saturating concentration, each dimer still has one coenzyme site available for binding NAD<sup>+</sup>. Adding NAD<sup>+</sup> should therefore cause a strong increase in rate, the more so as NAD<sup>+</sup> is more active than PEG-NAD<sup>+</sup>. If on the other hand options 1 or 3 are operative, the increase in rate will be limited, being due only to a partial, competitive replacement of PEG-NAD<sup>+</sup> by more reactive NAD<sup>+</sup>.

Actually, the experimental results, in which both NAD<sup>+</sup> and PEG-NAD<sup>+</sup> are exposed simultaneously to HLADH (see Figure 5.2), are in perfect agreement with options 1 and 3, i.e. PEG-NAD<sup>+</sup> and NAD<sup>+</sup> competing for the same binding site(s). Even if the polymer chain is confined within the volume of its hydrodynamic radius, (vide supra), its concentration is only 1.8% w/v, i.e. low enough not to prevent binding of ordinary NAD<sup>+</sup> in the neighbouring site. As already mentioned in the section dealing with the kinetic results, 2% w/v PEG in the bulk solution indeed does not affect the reaction rate. Therefore option 3 does not occur either, as far as blockage by the PEG-tail is concerned. The remote possibility might be considered that, despite of HLADH being no allosteric enzyme, the nonoptimal binding of the NAD part of PEG-NAD<sup>+</sup> is transmitted to the other site, causing a similar lower affinity for NAD there. If such were the case, the observed rates would have been intermediate between the two curves in Figure 5.2. This possibility can therefore be excluded too.

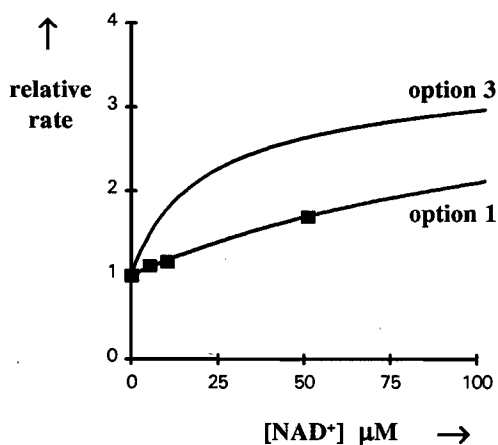


*Figure 5.2 Competition experiments between  $NAD^+$  and  $PEG-NAD^+$ ; calculated (lines, calculated using the eqs. in Appendix 1) and experimental relative rates (■), using a constant, high concentration of  $PEG-NAD^+$  (0.51 mM).*

In summary, the conclusion can be drawn that a situation in which the polyethylene glycol tail of  $PEG-NAD^+$  interferes with the coenzyme binding to HLADH seems highly unlikely.

#### 5.4.4 Check of the HLADH monomer-dimer equilibrium

It is known from immobilization experiments that HLADH is active only as a dimer<sup>[32]</sup>. The low activity with  $PEG-NAD^+$  might therefore be caused by an unfavourable shift in the monomer-dimer equilibrium, producing a partial dissociation of the dimer under the assay conditions. If such an equilibrium disturbance occurs, a decrease of the enzyme concentration at a constant  $PEG-NAD^+$  concentration would result in a larger amount of inactive HLADH monomer, implying a non-linear enzyme activity vs. enzyme concentration relationship. This possibility was checked by measuring the activity as a function of enzyme concentration in the relevant range of 0.03-0.15  $\mu\text{M}$ , using ethanol as substrate. Since both coenzymes ( $PEG-NAD^+$  and  $NAD^+$ ) proved to exhibit a linear relationship (results not shown), an equilibrium shift in the presence of  $PEG-NAD^+$  in the enzyme concentration range concerned, can be ruled out. Another approach to check the possible occurrence of an equilibrium shift is to determine the change in the number of tryptophans at the enzyme

surface. If the HLADH exists in the dimer conformation, only two tryptophans are at the enzyme surface (residues 15 from the A and B subunit) and the other two are buried deep inside the enzyme (residues 314, A and B). When the dimer would split into two monomers, the tryptophans which were buried inside the enzyme in the dimer conformation, will be at the surface of the monomer. By using the environmentally sensitive protein reagent 2-hydroxy-5-nitrobenzyl bromide (Koshland reagent), which is highly selective for tryptophan, the number of tryptophans at the surface can be determined (see Figure 5.3).

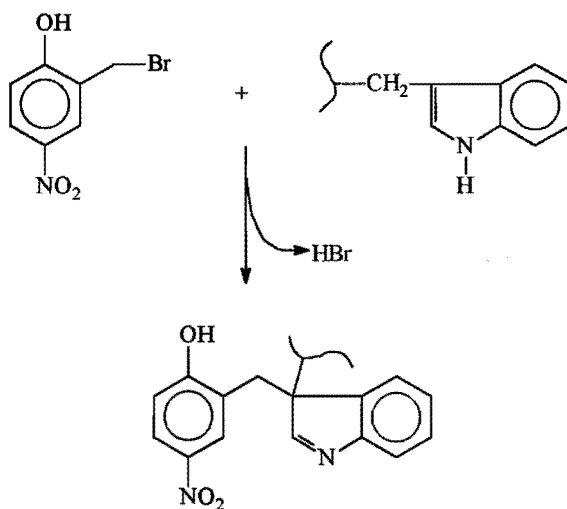


*Figure 5.3 Koshland reagent and its reaction with tryptophan.*

The unbound polyethylene glycol (PEG-20,000) does not seem to influence the HLADH conformation, because in both cases (using NAD<sup>+</sup> with or without PEG-20,000) the same number of tryptophans are found. Regrettably, PEG-NAD<sup>+</sup> is too large to be separated from HLADH on the G-25 Sephadex column and even with a G-200 Sephadex column we were not able to obtain separate fractions of PEG-NAD<sup>+</sup> and HLADH. This results in an unknown enzyme concentration in the case of PEG-NAD<sup>+</sup> and thus an unknown number of tryptophans at the enzyme surface. Comparing the relative concentrations of the reagent in the fractions of all four mixtures (Table 5.4), the numbers obtained with buffer/HLADH/PEG-NAD<sup>+</sup> mixtures do not differ substantially. Thus no evidence can be found for the destabilization of the HLADH dimer by PEG-NAD<sup>+</sup>.



**Table 5.4** Number of tryptophans determined when using Koshland reagent. The amounts of 50 mM Koshland reagent in acetone added to the solutions was 20  $\mu$ L in experiment 1 and 50  $\mu$ L in experiment 2. The enzyme concentration was determined spectrophotometrically at  $\lambda_{max} \approx 290$  nm. The reagent concentration was determined at  $\lambda_{max} = 405$ -410 nm. (Phosphate buffer pH=7.8 was used). The number of tryptophans was calculated from the ratio [reagent]:[enzyme].

Mixture	# TRP exp. 1	# TRP exp. 2
HLADH and buffer	1.52/1.46	2.65
HLADH, NAD <sup>+</sup> and buffer	1.81	3.07
HLADH, NAD <sup>+</sup> , PEG-20,000 and buffer	1.85	2.98
HLADH, PEG-NAD <sup>+</sup> and buffer	see text	see text

All factors investigated thus far are unable to explain the three to four times lower activity of PEG-NAD<sup>+</sup>. The change in  $k_{cat}$ (ethanol) suggests that the interaction between enzyme/coenzyme has changed. We therefore examined the possibility that the PEG-tail affects the interactions of the NAD<sup>+</sup> with the enzyme pocket by carrying out modelling calculations.

## 5.5 Modelling studies

In the past, a molecular mechanics approach has been used to study in detail the interactions of the coenzyme NAD<sup>+</sup> and a number of analogues in the active site of HLADH, in order to understand the essential factors involved in the productive binding between coenzyme and apo-enzyme<sup>[33-36]</sup>. It seemed worthwhile, however, to reconsider their results, utilizing recent X-ray data that show up more water molecules. In the following paragraph we present the results of improved modelling studies including molecular mechanics (MM) and dynamics (MD), to rationalize the kinetic data obtained.

Several X-ray crystallographic structures of binary and ternary complexes have been determined of HLADH<sup>[11-13,37-41]</sup>, which can be used as starting structures for MD-studies aiming at the elucidation of coenzyme/apo-enzyme interactions. The simulations with NADH, NAD<sup>+</sup> and PEG-NAD<sup>+</sup> positioned in the ternary complexes of HLADH/DMSO/coenzyme, HLADH/EtO<sup>-</sup>/coenzyme and HLADH/iPrO<sup>-</sup>/coenzyme, using the ternary crystal complex 6ADH<sup>[11]</sup>, will now be discussed.

### 5.5.1 Course of the simulations

Variations of the total potential energy of the MD alkoxide complexes as a function of time are reported in Figure 5.4. First the system is being warmed up (300 K) and the energy increases rapidly. Then in the next 45 ps the energy decreases and reaches an equilibrium after  $\pm 60$  ps and fluctuates with small deviations around a mean value during the rest of the simulation. Maximum deviations are 3% of the mean value, except for the van der Waals' energies where a maximum deviation of 6% is observed. Analyses based on the 40-90 ps period respectively the 50-90 ps period, did not lead to different results. Therefore, we used the data obtained from the 40-90 ps analysis period.

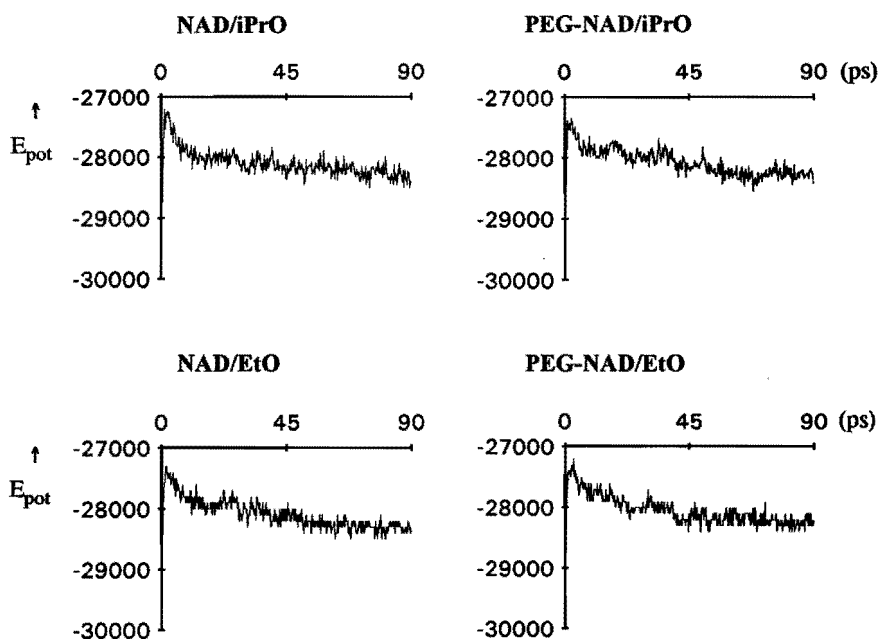


Figure 5.4 The total potential energy (in kcal.mol<sup>-1</sup>) versus time (in ps).

### 5.5.2 Overall structure

As the X-ray data on the ternary complexes of HLADH were obtained with NADH as coenzyme and DMSO as substrate analogue, MD calculations were initially carried out

with this complex. The results are listed in Table 5.5. Allowing one subunit to move freely during the calculations, results in RMS deviations almost twice as high as those obtained with the smaller belly (see methods), and therefore only the latter option was used for further calculations. Starting from the refined crystal structure at 1.8 Å resolution (PDB file 2OHX)<sup>[29]</sup> the MD-averaged structure remains closer to the crystal structure (Table 5.5). Since this crystal structure was published not earlier than December 1994, we were not able to use it throughout this thesis.

**Table 5.5** RMS deviations of the MD-averaged structures versus the crystal structure<sup>[11]</sup>.

NADH DMSO	NADH DMSO <sup>a</sup>	NADH DMSO <sup>b</sup>	NAD <sup>+</sup> iPrO <sup>-</sup>	PEG-NAD <sup>+</sup> iPrO <sup>-</sup>	NAD <sup>+</sup> EtO <sup>-</sup>	PEG-NAD <sup>+</sup> EtO <sup>-</sup>
RMS deviation backbone atoms						
1.35	2.43	1.06	1.45	1.27	1.66	1.28
average RMS deviation of some C $\alpha$ atoms near the coenzyme (see Table 5.7)						
0.85	1.84	0.69	0.96	0.92	1.25	0.81

<sup>a</sup> One subunit free during the calculations; all other data are related to the smaller belly option (see under methods).

<sup>b</sup> Starting from the refined crystal structure 2OHX<sup>[29]</sup>.

The minimized (PEG-)NAD<sup>+</sup> structures have a RMS deviation of the backbone atoms of the X-ray structures of 0.6 Å for all complexes compared with the X-ray structure. In contrast with the MM geometries, the MD simulations of NAD<sup>+</sup> and PEG-NAD<sup>+</sup> complexes (collected from 40-90 ps simulations) show some differences compared with the original X-ray structure, although the overall 3-dimensional structure is maintained (see Figure 5.6).

In Figure 5.5 the average RMS deviation of the backbone atoms during the 40-90 ps MD simulation are shown (only the atoms included in the belly option are included in the RMS deviation). In both cases a plateau has been reached: the plateau for the NAD<sup>+</sup>/EtO<sup>-</sup> complex is higher than the one for PEG-NAD<sup>+</sup>/EtO<sup>-</sup> (1.66 Å versus 1.28 Å). Thus the MD-averaged NAD<sup>+</sup> complex is further away from the original X-ray structure. A similar situation exists for the iPrO<sup>-</sup> complexes (see Figure 5.5). The oxygen atoms of the nine water molecules explicitly added in the active site show RMS deviations from 1.0 to 4.3 Å. Similar RMS deviations as reported above, have been communicated by other groups performing MD simulations on proteins<sup>[42]</sup>.

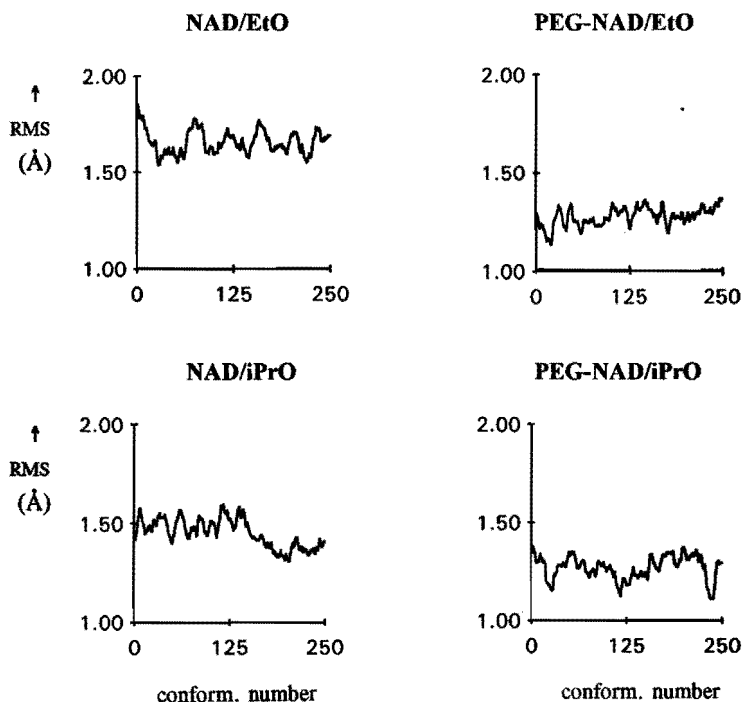


**Figure 5.5** The RMS deviations (in Å) of the backbone atoms for the 250 conformations over 40-90 ps simulation period. On the left the RMS values for the NAD<sup>+</sup> complexes; on the right the ones for the PEG-NAD<sup>+</sup> complexes.

It is worth mentioning that between the subunits of the X-ray structure of HLADH/NADH/DMSO RMS differences have been observed for the main and side-chain atoms of 0.7 and 1.0 Å respectively<sup>[61]</sup>. The refined crystal structure of the latter HLADH complex shows RMS deviations of 0.22 Å and 0.34 Å for the backbone atoms and the side-chains<sup>[29]</sup>. In the recently determined ternary crystal structure with pentafluoro benzylalcohol a RMS difference of 0.24 Å between the two subunits has been observed<sup>[13]</sup>.

### 5.5.3 Change in the coenzyme position

The primary effect of the PEG-tail is quite evident in Figure 5.7, which shows the positions of NAD<sup>+</sup> and PEG-NAD<sup>+</sup>, in case iPrO<sup>-</sup> is substrate. It is quite evident that the

polymer tail pulls the adenine moiety in the outside direction by about 2 Å, dragging along with it the other parts of the coenzyme. A similar results was obtained with ethanol as substrate. This primary effect will of course induce small but significant conformational changes in the coenzyme itself and in the surrounding peptide chain. Some of these will next be treated in detail.

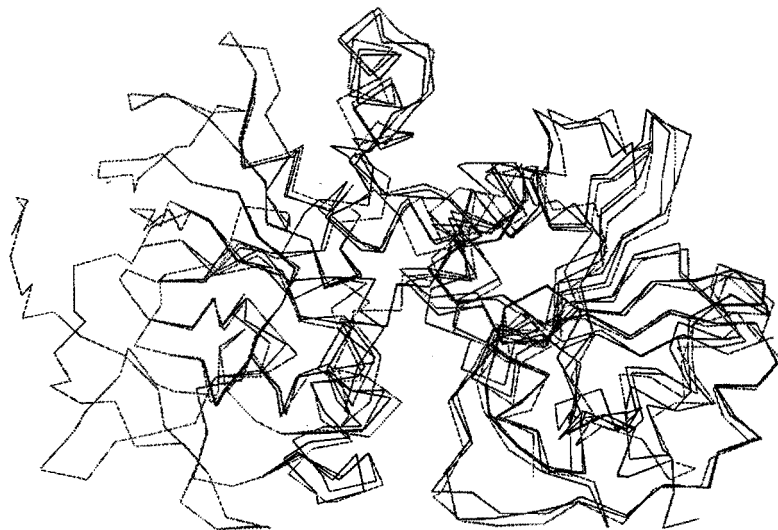


**Figure 5.6** MD-averaged structures of the  $\text{NAD}^+/\text{EtO}^-$  (---) and  $\text{PEG-NAD}^+/\text{EtO}^-$  (—) complex and the crystal structure<sup>[11]</sup> (.....). The left side is fixed during the calculations.

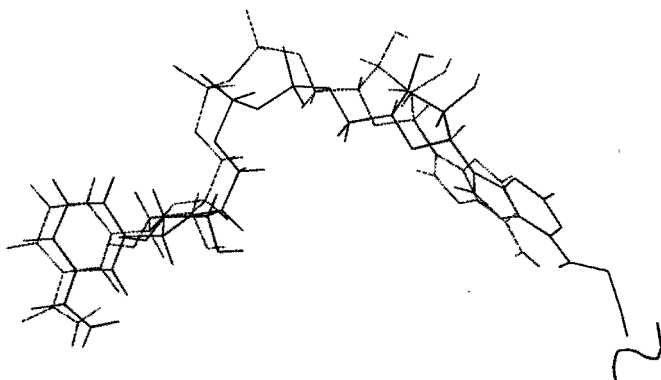


**Figure 5.7** Stick plot of the MD averaged structures of NAD (-----) and PEG-NAD from the  $\text{iPro}^-$  (—) complexes.



**Table 5.6** Overview of torsion angles <sup>a</sup> (in degrees) for NAD<sup>+</sup>, PEG-NAD<sup>+</sup> as derived from modelling calculations (MM and MD), and the X-ray structures (NADH/HLADH/DMSO, 6ADH [11] and 2OHX [29]). The MD time-averaged values are taken from 250 conformations over 40-90 ps.

Coenzyme	$\theta$	$\chi_N$	$\gamma_N$	$\beta_N$	$\alpha_N$	$\zeta_N$	$\zeta_A$	$\alpha_A$	$\beta_A$	$\gamma_A$	$\chi_A$
NADH (X-ray 2ohx)	23	263	49	191	61	193	95	76	156	292	257
NADH (2ohx) MM <sup>b</sup>	9	252	62	185	72	196	82	58	165	300	249
NADH (2ohx) MD <sup>b</sup>	21	218	61	176	70	192	80	51	176	292	242
<hr/>											
NADH (X-ray 6adh)	34	258	39	214	59	207	85	106	147	281	264
<hr/>											
<b>MM-results</b>											
<hr/>											
NADH/DMSO	26	248	64	180	69	218	70	69	150	296	252
NADH/DMSO <sup>c</sup>	24	249	65	180	68	220	66	69	148	297	251
NAD <sup>+</sup> /iPrO <sup>-</sup>	13	250	59	181	72	208	79	62	158	296	250
PEG-NAD <sup>+</sup> /iPrO <sup>-</sup>	13	251	59	183	69	209	71	61	146	309	254
NAD <sup>+</sup> /EtO <sup>-</sup>	13	250	58	181	71	206	80	61	157	294	250
PEG-NAD <sup>+</sup> /EtO <sup>-</sup>	13	252	59	184	68	211	69	63	146	309	255
<hr/>											
<b>MD-results</b>											
<hr/>											
NADH/DMSO	9	224	71	176	69	204	73	47	157	302	242
NADH/DMSO <sup>c</sup>	16	248	58	166	75	311	328	150	81	287	281
NAD <sup>+</sup> /iPrO <sup>-</sup>	37	242	72	176	76	196	77	43	163	298	251
PEG-NAD <sup>+</sup> /iPrO <sup>-</sup>	18	251	54	195	68	198	68	66	145	309	254
NAD <sup>+</sup> /EtO <sup>-</sup>	3	230	76	177	62	198	76	43	150	306	252
PEG-NAD <sup>+</sup> /EtO <sup>-</sup>	10	248	39	182	84	318	299	159	122	293	263

<sup>a</sup> According to IUPAC nomenclature<sup>[43]</sup>.

<sup>b</sup> Started from the refined crystal structure 2OHX<sup>[29]</sup>.

<sup>c</sup> One subunit free during the calculations.

group. The average MD-values (Table 5.6) for  $\chi_N$  of 230° (NAD<sup>+</sup>/EtO<sup>-</sup>), 248° (PEG-NAD<sup>+</sup>/EtO<sup>-</sup>) 242° (NAD<sup>+</sup>/iPrO<sup>-</sup>) and 251° (PEG-NAD<sup>+</sup>/iPrO<sup>-</sup>), correspond to an *anti* conformation of the ribose and nicotinamide rings with all complexes simulated, similar to the conformation observed in the X-ray structure<sup>[11]</sup>.

The puckering of the ribose moieties is valued by the size of torsion angles  $\nu_2(N)$  and  $\nu_2(A)$  of the nicotinamide and adenine ribose respectively. The MM and MD structures all show  $\nu_2(N)$  values similar to the X-ray value of -37°. The  $\nu_2(A)$  values are smaller in the simulated complexes than in the X-ray structure.

**Table 5.7** Substrate-coenzyme distance and the puckering values of the nicotinamide ring and ribose rings. The MD time-averaged values are taken from 250 conformations over 40-90 ps. The X-ray data are taken from the ternary complex with HLADH/NADH/DMSO <sup>[11]</sup>.

	X-ray NADH	NAD <sup>+</sup> iPrO <sup>-</sup>	PEG-NAD <sup>+</sup> iPrO <sup>-</sup>	NAD <sup>+</sup> EtO <sup>-</sup>	PEG-NAD <sup>+</sup> EtO <sup>-</sup>
	Minimized structures				
C4 (NAD)–C1 (RO <sup>-</sup> ) (Å)	4.18 <sup>a</sup>	3.37	3.38	3.42	3.44
C1(RO <sup>-</sup> )–C4(NAD)–N1(NAD)	93° <sup>b</sup>	104°	104°	107°	107°
$\alpha_C$ (degrees)	0	-4	-4	-3	-4
$\alpha_N$ (degrees)	0	3	3	3	3
$\nu_2(N)$ (degrees)	-37	-38	-38	-38	-38
$\nu_2(A)$ (degrees)	-37	-24	-21	-24	-22
	MD-averaged structures				
C4 (NAD)–C1 (RO <sup>-</sup> ) (Å)	4.18 <sup>a</sup>	3.46	3.57	3.56	3.57
C1(RO <sup>-</sup> )–C4(NAD)–N1(NAD)	93° <sup>b</sup>	106°	103°	124°	97°
$\alpha_C$ (degrees)	0	4	7	7	10
$\alpha_N$ (degrees)	0	-2	1	2	2
$\nu_2(N)$ (degrees)	-37	-32	-34	-33	-36
$\nu_2(A)$ (degrees)	-37	-20	-15	-20	-21

<sup>a</sup> The C4 (NAD)–S (DMSO) distance is used for the crystal structure.

<sup>b</sup> The S–C4–N1 angle is used.



The deformation angles  $\alpha_C$  and  $\alpha_N$  (defined as C2-C6-C3-C4 and C3-C5-C6-N1 respectively) reflect the extent of bending of the nicotinamide ring towards a boat conformation (Table 5.7). This puckering of the nicotinamide ring places one of the C4-hydrogens of NADH in a pseudoaxial position, which could favour the hydride-transfer rate<sup>[44]</sup>. In Table 5.7 the average values for  $\alpha_C$  and  $\alpha_N$  for NAD<sup>+</sup> are listed. Plots of these calculated  $\alpha_C$  angles versus the calculated  $\alpha_N$  angles are shown in Appendix 3. Only minor differences can be observed between the complexes.

### 5.5.5 Changes of the polypeptide chain

Due to some changes in the coenzyme position and geometry, the surrounding peptide chains also exhibit small, conformational changes. Deviations of a few amino acids are listed in Table 5.8. Some Ca's of the coenzyme neighbouring amino acids are displaced by 1-2 Å. Near the enzyme surface sometimes large deviations are observed.

The average RMS deviations between the MD-averaged structures of the surrounding peptides of the NAD<sup>+</sup> and the PEG-NAD<sup>+</sup> complexes are 0.81 and 0.93, respectively (Table 5.8). Though small, they seem significant, because a second NAD<sup>+</sup>/iPrO<sup>-</sup> calculation showed a RMS=0.32 deviation from the first one.

### 5.5.6 Changes in the interactions between enzyme and coenzyme

These changes can best be described in terms of H-bonding patterns. The most pronounced differences occur around the phosphate groups. Near these phosphate groups strong electrostatic forces play an important role in the interaction between coenzyme and enzyme. The changes in interactions are evident from the hydrogen-bonds listed in Table 5.9. The encased H-bonds are maintained during the simulations. The NAD<sup>+</sup>/iPrO<sup>-</sup> complex still has three H-bonds as found in the X-ray structure; with PEG-NAD<sup>+</sup>/iPrO<sup>-</sup> only 1 and with NAD<sup>+</sup>/EtO<sup>-</sup> and PEG-NAD<sup>+</sup>/EtO<sup>-</sup> 2 H-bonds are similar to those found in the X-ray structure. Furthermore three complexes have H-bonds between O2P<sub>A</sub> and two water molecules (which are also present in the refined crystal structure<sup>[29]</sup>) and only the PEG-NAD<sup>+</sup>/EtO<sup>-</sup> lacks these interactions. This is due to a new electrostatic interaction of the phosphate group with the Arg 47 side-chain in the latter complex. In the NAD<sup>+</sup>/EtO<sup>-</sup> complex the HN11 of Arg 47 interacts with the O1P(A) oxygen (Table 5.9); in the case of PEG-NAD<sup>+</sup>/EtO<sup>-</sup> this is replaced by O2P(A). A similar change from O1P(N) to O2P(N) occurs in the hydrogen-bond with HN (203) for the EtO<sup>-</sup> complexes.

**Table 5.8** RMS deviations of the MD-averaged structures from the crystal structure<sup>[11]</sup>.

	versus Crystal structure				MD PEG-NAD <sup>+</sup> versus MD NAD <sup>+</sup>	
	NAD <sup>+</sup> iPrO <sup>-</sup>	PEG-NAD <sup>+</sup> iPrO <sup>-</sup>	NAD <sup>+</sup> EtO <sup>-</sup>	PEG-NAD <sup>+</sup> EtO <sup>-</sup>	iPrO <sup>-</sup> complex	EtO <sup>-</sup> complex
<b>C<math>\alpha</math>'s of residues near coenzyme</b>						
Cys 46	0.98	0.91	1.79	0.98	0.46	0.85
Arg 47	0.98	0.57	1.92	0.63	0.41	1.30
Ser 48	0.65	0.26	1.89	0.40	0.40	1.73
His 51	0.47	0.20	1.56	0.41	0.32	1.55
His 67	0.13	0.47	0.11	0.13	0.52	0.20
Cys 174	1.06	0.90	1.17	0.84	0.84	0.86
Thr 178	1.64	1.06	1.28	1.07	0.95	0.40
Gly 202	0.78	0.81	0.98	0.68	1.46	1.10
Val 203	0.83	0.84	0.89	0.68	1.15	0.71
Val 292	0.33	0.33	0.35	0.43	0.43	0.63
Ala 317	0.51	0.46	0.69	0.56	0.30	0.13
Phe 319	1.91	1.86	1.31	1.55	0.57	0.25
Arg 369	0.47	1.56	0.69	1.05	1.37	0.52
average RMS	0.96	0.92	1.25	0.81	0.81	0.93
<b>C<math>\alpha</math>'s of residues near enzyme surface</b>						
227	2.46	1.41	2.47	1.02	1.29	2.17
248	3.83	1.36	6.39	2.28	3.36	4.42
297	2.77	3.57	3.16	0.80	1.69	2.48

Although there is little change in the angles around the phosphate residues with iPrO<sup>-</sup> as substrate (see section 5.5.4), some of the interactions do change: hydrogen-bonds of O1P(N) with HN12 (Arg 369) and HN (203) (Table 5.9) are replaced by those with water,

**Table 5.9** Hydrogen-bonding pattern and electrostatic interactions around the phosphate groups of the coenzyme for the time-averaged MD structures and crystal structure. 'WAT' denotes a water molecule. (distances in Å).

	X-ray	NAD <sup>+</sup>		PEG-NAD <sup>+</sup>	
		iPrO <sup>-</sup>	iPrO <sup>-</sup>	EtO <sup>-</sup>	EtO <sup>-</sup>
O1P <sub>N</sub> (NAD)-HN12 (Arg 369)	2.95	1.72		1.82	1.83
O1P <sub>N</sub> (NAD)-H (WAT 757)			1.74		
O1P <sub>N</sub> (NAD)-H (WAT)			1.69		
O1P <sub>N</sub> (NAD)-HN (Val 203)		1.99		2.02	
O2P <sub>N</sub> (NAD)-HN (Gly 202)	3.19				
O2P <sub>N</sub> (NAD)-HN (Val 203)	3.21				1.83
O2P <sub>N</sub> (NAD)-HN (204)		2.14	2.16	1.90	2.14
O1P <sub>A</sub> (NAD)-HN11 (Arg 47)	2.91	1.68	1.98	1.70	
O1P <sub>A</sub> (NAD)-H (WAT)				1.83	
O1P <sub>A</sub> (NAD)-H (WAT)		1.88	2.07	1.83	1.64
O2P <sub>A</sub> (NAD)-HN11 (Arg 47)					1.86
O2P <sub>A</sub> (NAD)-H (WAT)		2.39	1.65	1.75	
O2P <sub>A</sub> (NAD)-H (WAT)		2.11	2.21	1.88	
O2P <sub>A</sub> (NAD)-HN (Gly 202)		2.32		2.19	
O2P <sub>A</sub> (NAD)-HNZ1 (Lys 228)	3.29	1.97			

and those of O2P(A) with HN (202) and HNZ1 (Lys 228) are removed.

In general it can be concluded that there are fewer direct interactions of amino acid residues with the phosphates of PEG-NAD<sup>+</sup> than with those of NAD<sup>+</sup>, with both substrates. All of these changes are likely to affect the binding of the coenzyme and the rates of the concomitant conformational changes, that have to take place during coenzyme association to and dissociation from the apo-enzyme, contributing to the observed decrease in  $k_{\text{cat}}$  of ethanol oxidation. This will be further discussed in Chapter 6.

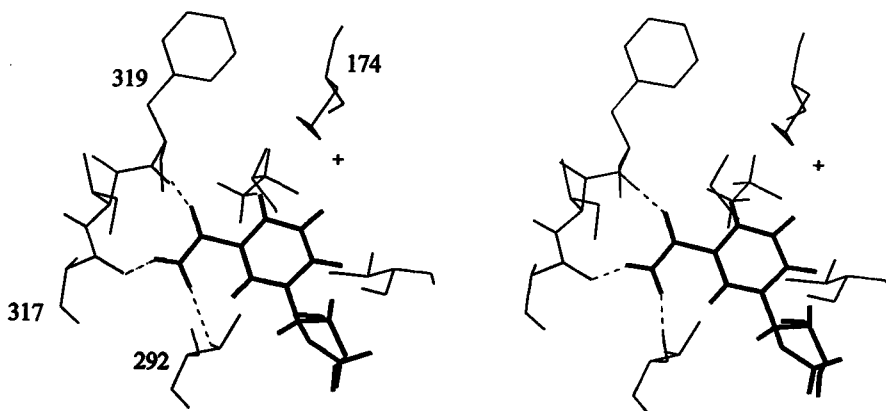


**Figure 5.9** Stereo-pair of the active site of the crystal structure after optimization of the water and substrate molecules, showing the hydrogen-bonding patterns of the carboxamide side-chain with the enzyme.

**Table 5.10** Hydrogen-bonding pattern of the carboxamide side-chain of the coenzyme with neighbouring amino acids. X-ray distances are taken from the crystal conformation <sup>[11]</sup>; distances for the MD are averaged for 250 conformations over 40-90 ps. (distances in Å).

H-(Donor) – Acceptor	X-ray <sup>a</sup>	NAD <sup>+</sup> iPrO <sup>-</sup>	PEG-NAD <sup>+</sup> iPrO <sup>-</sup>	NAD <sup>+</sup> EtO <sup>-</sup>	PEG-NAD <sup>+</sup> EtO <sup>-</sup>
Minimized structures					
HN (Phe 319) - O7 (NAD)	2.83	1.86	1.86	1.85	1.85
HNA (NAD) - O (Ala 317)	2.60	1.99	1.97	1.99	1.97
HNB (NAD) - O (Val 292)	2.53	1.87	1.89	1.87	1.88
MD-averaged structures					
HN (Phe 319) - O7 (NAD)	2.83	2.02	1.89	1.93	1.98
HNA (NAD) - O (Ala 317)	2.60	1.90	1.91	1.87	1.93
HNB (NAD) - O (Val 292)	2.53	2.51	1.89	1.95	1.92

<sup>a</sup> The Donor - Acceptor distances were taken, because there are no hydrogens present in the X-ray structure.

In the H-bonding interactions between the carboxamide side-chain of the nicotinamide moiety and the enzyme three amino acids are involved, namely Phe 319, Ala 317 and Val 292. They are shown in Figure 5.9 and Table 5.10. H-bonds are assigned if the donor (D) – acceptor (A) distance is, at least temporary, smaller than 3.5 Å and the D-H – A angle value lies between 90° and 180°. An H–A bond of  $\leq 2.5$  Å will be considered as being stable<sup>[45]</sup>.

Figure 5.10 shows the fluctuations in the three hydrogen-bonds in these complexes.

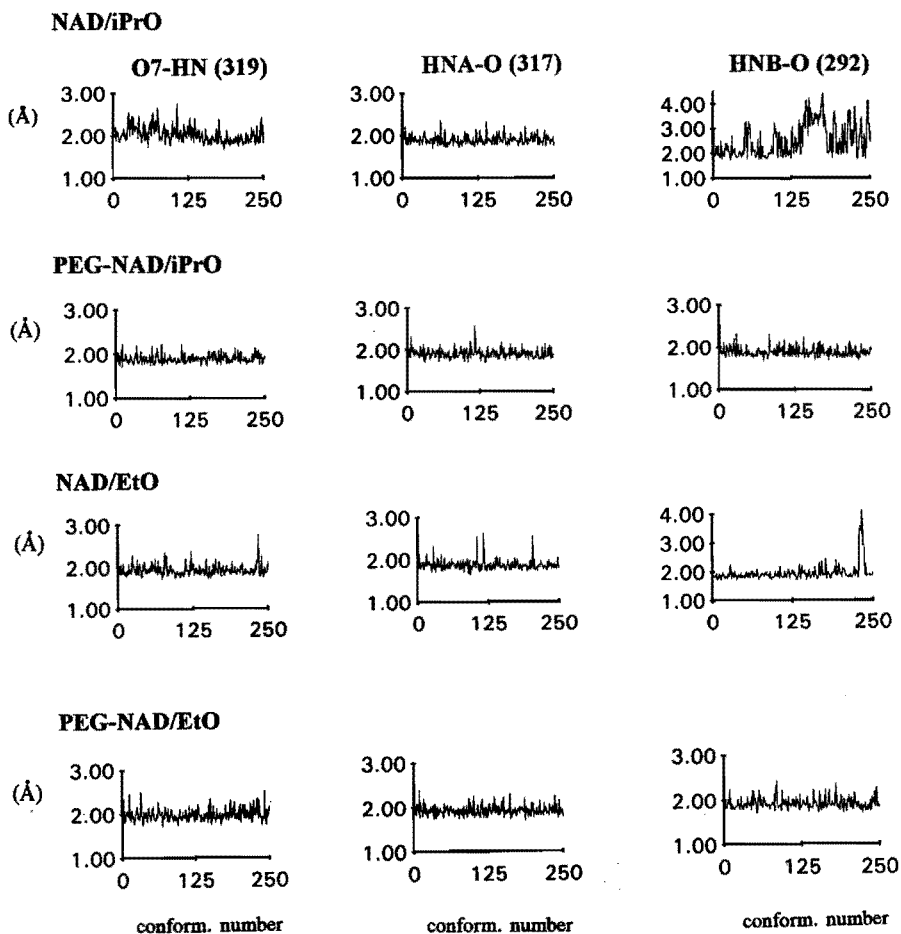


**Figure 5.10** Hydrogen-bonding distance fluctuations (in Å) between the carboxamide side-chain and HLADH residues Phe 319 (left), Ala 317 (middle) and Val 292 (right).

During the MD simulations all three H-bonds are largely kept intact both in the NAD<sup>+</sup> and in the PEG-NAD<sup>+</sup> complexes, with the exception of the NAD<sup>+</sup>/iPrO<sup>-</sup> Val 292 bond, which is not quite stable (see also paragraph 5.5.8).

### 5.5.7 The proton relay system

It is known that the substrate, coordinated to the catalytic zinc ion, is also involved in a H-bonding system, essential for the enzymatic activity. The O1 of the alkoxide is at H-bonding distance of HOG (Ser 48) and from the crystal structure the following path along which the proton may be released can be envisioned:

OG (Ser 48) - HO2' (N-ribose NAD<sup>+</sup>), O2' (NAD<sup>+</sup>) - HNE (His 51), HNE (His 51) - O3' (NAD<sup>+</sup>), HND (His 51)- H<sub>2</sub>O's at protein surface, HO3' (NAD<sup>+</sup>) - O (Ile 269) (see Figure 5.11).

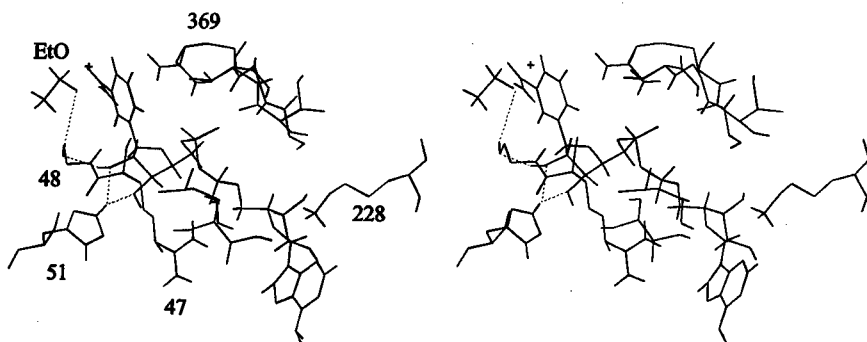


**Figure 5.11** Stereo-pair of the active site around the phosphate groups and the amino acids involved in the proton relay system (crystal structure) after optimization of the water and substrate molecules.

Table 5.11 lists this hydrogen-bonding pattern for the minimized and averaged dynamics structures. In the minimized structures all H-bonds are stable, whereas a different picture emerges from the MD calculations. With all four modelled complexes, the first three hydrogen-bonds are quite stable. In all MD structures, although the frequency may differ, the HO3'-O (Ile 269) H-bond is frequently broken. From these modelling experiments it might be concluded that the proton relay systems in the PEG-NAD<sup>+</sup> complexes are as (in)efficient as in the case of the NAD<sup>+</sup> complexes.

**Table 5.11** Hydrogen-bonding pattern of the proton relay system (distances in Å).

H-Donor – Acceptor	X-ray <sup>a</sup>	NAD	PEG	NAD	PEG
		IPRO	IPRO	ETO	ETO
Minimized structures					
HOG (Ser 48)-O1 (RO <sup>-</sup> ) <sup>b</sup>	3.93	1.76	1.76	1.76	1.77
HO2' (NAD)-OG (Ser 48)	2.73	1.83	1.85	1.84	1.86
HNE (His 51)-O2' (NAD)	2.85	1.88	1.88	1.87	1.89
HNE (His 51)-O3' (NAD)	2.94	1.97	1.96	1.96	1.95
HO3' (NAD)-O (Ile 269)	2.73	1.81	1.81	1.81	1.81
MD-averaged structures					
HOG (Ser 48)-O1 (RO <sup>-</sup> ) <sup>b</sup>	3.93	1.80	1.80	1.89	1.79
HO2' (NAD)-OG (Ser 48)	2.73	1.99	1.96	2.05	1.92
HNE (His 51)-O2' (NAD)	2.85	1.88	1.92	2.04	1.93
HNE (His 51)-O3' (NAD)	2.94	2.89	2.32	2.23	2.31
HO3' (NAD)-O (Ile 269)	2.73	3.13	2.16	2.39	2.57

<sup>a</sup> The Donor - Acceptor distances were taken, because there are no hydrogens visible in the X-ray structure.

<sup>b</sup> RO<sup>-</sup> denotes the alkoxide

### 5.5.8 The hydride-transfer

Among the factors affecting the rate of hydride-transfer are the distance to be tided over and the out-of-plane orientation of the carboxamide side-chain. As far as the first factor is concerned, the data in Table 5.7 are relevant. The average distances between the C4 of NAD<sup>+</sup> or PEG-NAD<sup>+</sup> and the C1 atoms of EtO<sup>-</sup> and iPrO<sup>-</sup> turn out to be almost equal to the 3.40 Å found by semiempirical calculations (Chapter 2, Table 2.4). The angles of approach, N1-C4-C1 are also reasonably close; 107° versus 114° for ethanol and 104° versus 89° for isopropanol for MD and quantum chemical calculations, respectively. The PEG-tails do not change the MD values. Apparently all of these data do not provide an

explanation for a reduced rate of hydrogen-transfer.

As far as the second factor is concerned, the out-of-plane values  $\theta$  (O7-C7-C3-C4, Figure 5.8) of NAD<sup>+</sup> and PEG-NAD<sup>+</sup> complexes during the simulation period are shown in Figure 5.12. For the NAD<sup>+</sup>/iPrO<sup>-</sup> complex a time-weighted average value of 37° (Table 5.6) can be calculated, i.e. a positioning of the carboxamide side-chain on the A-side of the nicotinamide plane, which is in nice agreement with the observed X-ray value of 34° and the 30° calculated by semiempirical studies (Chapter 2, Table 2.6). On the other hand, the fluctuations in  $\theta$  in this case (left top of Figure 5.8) are larger than those of the other complexes. These fluctuations are accompanied by lengthening of the H-bond with Val 292 (right top of Figure 5.10). A second and third MD calculation were therefore carried out. It turned out that of all torsional angles only  $\theta$  changed substantially, i.e. 76° and 32° for the second and third run respectively (see Figure 5.12), versus 37° in the first run.

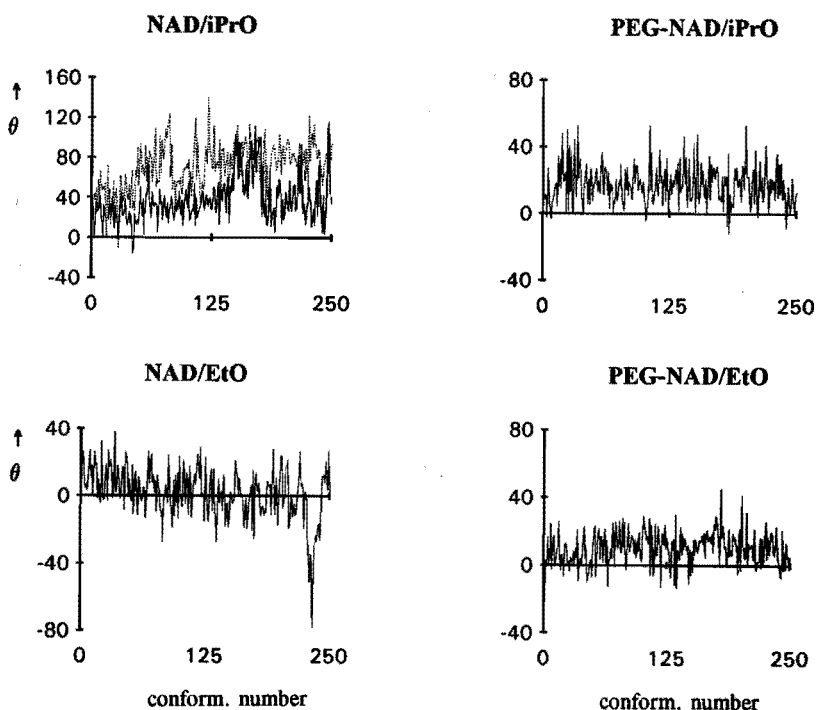


**Figure 5.12** Variation of  $\theta$  (in degrees) of (PEG)-NAD<sup>+</sup> in HLADH for the 250 conformations during the 40-90 ps sampling phase.



Apparently the positioning of the carboxamide side-chain is quite flexible, the favourable conformation of  $\theta \approx 35^\circ$  occurring for about two thirds of the time.

The  $i\text{PrO}^-$  complex with the PEG-NAD<sup>+</sup> coenzyme has a smaller average  $\theta$  than the complex with NAD<sup>+</sup>. Referring to the earlier mentioned relationship between the hydride-transfer rate and the orientation of the carbonyl dipole, this seems to be in agreement with the observed, reduced rate of the hydride-transfer in the case of PEG-NAD<sup>+</sup> [44,46,47].

Not satisfying is the average value of  $\theta$  of only  $3^\circ$ , found for NAD<sup>+</sup>/EtO<sup>-</sup>. It deviates not only from the X-ray value (which might be explained by the fact that ethanol does not resemble DMSO, present in the crystal structure, as well as isopropanol), but also from the results of the quantum calculations. However, the changes we try to explain are very subtle ones. It may be worthwhile to re-examine this detail by repeating the MD calculation starting from the 2OHX file.

A change in rate of hydrogen-transfer when ethanol is the substrate is not detectable as long as the dissociation of the coenzyme from the enzyme is the rate limiting step. As mentioned in paragraph 5.5.6, the latter rate could well be decreased, owing to the changed interactions between enzyme and coenzyme, particularly in the case of ethanol, causing some changes in the rates of association, dissociation and the concomitant conformational changes of the enzyme, as will be discussed in the next chapter.

## 5.6 Conclusions

HLADH appears to be three to four times less active with PEG-NAD<sup>+</sup> than native NAD<sup>+</sup>. The following explanations for the kinetic behaviour of PEG-NAD<sup>+</sup> can be ruled out:

- A lower intrinsic reactivity
- Interference of single substituted polyethylene glycol in the enzymatic reaction
- Steric hindrance exerted by the polyethylene glycol tail
- Destabilization of the HLADH dimer.

The reported MD calculations indicate that the PEG-tail of enzyme-bound PEG-NAD<sup>+</sup> causes shifts in the positioning of the coenzyme, owing to the pulling action of the polymer chain. Such changes are evident with both substrates, ethanol and isopropanol. As a consequence, differences are found in some H-bonds, the out-of-plane angle  $\theta$ , the dihedral angles of the pyrophosphate moiety and the interactions with the peptide chains around the phosphates. The MD calculations on the ternary complexes of HLADH/(PEG-)NAD<sup>+</sup>/alkoxide no essential differences in the overall structure of the polypeptide chain, the C4(NAD)-C1(alc.) distances, and the angle N1-C4-C1.

## References

1. S.S. Wang and C.-K. King, *Adv. Biochem. Engin.* **12**, 119-146 (1979).
2. R. Wichmann, C. Wandrey, A.F. Bückmann and M.-R. Kula, *Biotechn. Bioeng.* **23**, 2789-2802 (1981).
3. C. Wandrey and R. Wichmann, *Biotechnology series*, **5**, 177-208 (1985).
4. C. Wandrey in "Proceedings 4th European Congress on Biotechnology", (O.M. Neijssel, R.R. van der Meer and K.Ch.A.M. Luyben, eds.) Elsevier, Amsterdam, vol. 4, p. 171-188 (1987).
5. M.-R. Kula and C. Wandrey, *Methods in Enzymology* **136**, 9-21 (1987).
6. A.F. Bückmann, M.-R. Kula, R. Wichmann and C. Wandrey, *J. Applied Biochem.* **3**, 301-315 (1981).
7. G. Blankenhorn and E.G. Moore, *J. Am. Chem. Soc.* **102**, 1092-1098 (1980).
8. S.P. Colowick, N.O. Kaplan and M.M. Ciotti, *J. Biol. Chem.* **191**, 447-459 (1951).
9. H.R. Horton and D.E. Koshland, Jr., *J. Am. Chem. Soc.* **87**, 1126-1132 (1965).
10. D.A. Pearlman, D.A. Case, J.C. Caldwell, C.L. Seibel, U.C. Singh, P. Weiner and P.A. Kollman, AMBER 4.0, University of California San Francisco, California, USA (1991).
11. H. Eklund, J.-P. Samama and T.A. Jones, *Biochemistry* **23**, 5982-5996 (1984).
12. H. Eklund, J.-P. Samama, L. Wallén, C.-I. Brändén, Å. Åkeson and T.A. Jones, *J. Biol. Chem.* **261**, 15273-15280 (1981).
13. S. Ramaswamy, H. Eklund and B.V. Plapp, *Biochemistry* **33**, 5230-5237 (1994).
14. W.L. Jorgensen, J. Chandrasekar, J.D. Madura, R.W. Impey and M.L. Klein, *J. Chem. Phys.* **79**, 926-935 (1983).
15. QUANTA/CHARMM 3.3.2, Molecular Simulations Inc., Waltham, Massachusetts, USA.
16. O. Tapia, R. Cardenas, J. Andres, J. Krechl, M. Campillo and F. Colonna-Cesari, *Int. J. Quant. Chem.* **39**, 767-786 (1991).
17. S.J. Weiner, P.A. Kollman, D.A. Case, U.C. Singh, C. Ghio, G. Alagona, S. Profeta and P.K. Weiner, *J. Am. Chem. Soc.* **106**, 765-784 (1984).
18. S.J. Weiner, P.A. Kollman, D.T. Nguyen and D.A. Case, *J. Comp. Chem.* **7**, 230-252 (1986).
19. CARNAL (beta release) is a coordinate analysis program by W.S. Ross, Dept. of Pharmaceutical Chemistry, UCSF, San Francisco, California, USA.
20. S.A.M. Vanhommerig, R.J. Meier, L.A.Æ. Sluyterman and E.M. Meijer, *J. Mol. Struct. (Theochem)* **304**, 53-59 (1994).
21. M. Dixon and E.C. Webb in "Enzymes", 3rd edition, Longman Group Ltd, p. 90-95 (1979).
22. C.C. Wratten and W.W. Cleland, *Biochemistry* **2**, 935-941 (1963).
23. F.B. Rudolph and H.J. Fromm, *Biochemistry* **9**, 4660-4665 (1970).
24. K. Dalziel and F.M. Dickinson, *Biochem. J.* **100**, 34-46 (1966).
25. R.L. Brooks and J.D. Shore, *Biochemistry* **10**, 3855-3858 (1971).
26. W.W. Cleland, *Methods Enzymol.* **63**, 103-138 (1979).
27. Dj. Vasic-Racki, M. Jonas, C. Wandrey, W. Hummel and M.-R. Kula, *Appl. Microbiol. Biotechnol.* **31**, 215-222 (1989).
28. N.J. Oppenheimer, L.J. Arnold Jr. and N.O. Kaplan, *Biochemistry* **17**, 2613-2619 (1978).

29. S. Al-Karadaghi, E.S. Cedergren-Zeppezauer and S. Hövmoller, *Acta Cryst.* **D50**, 793-807 (1994).
30. Y. Kambe and C. Honda, *Polymer Communications* **24**, 208-210 (1983).
31. Y. Kambe and C. Honda, *Polymer Communications* **25**, 154-157 (1984).
32. K. Mosbach and L. Andersson in "Pyridine Nucleotide-dependent Dehydrogenases", (H. Sund ed.), Walter de Gruyter & co, Berlin, Germany, p. 173-179 (1977).
33. P.M.T. De Kok, N.A. Beijer, H.M. Buck, L.A.Æ. Sluyterman and E.M. Meijer, *Recl. Trav. Chim. Pays-Bas* **107**, 355-361 (1988).
34. P.M.T. De Kok, N.A. Beijer, H.M. Buck, L.A.Æ. Sluyterman and E.M. Meijer, *Eur. J. Biochem.* **175**, 581-585 (1988).
35. N.A. Beijer, H.M. Buck, L.A.Æ. Sluyterman and E.M. Meijer, *Biochim. Biophys. Acta* **1039**, 227-233 (1990).
36. N.A. Beijer, H.M. Buck, L.A.Æ. Sluyterman and E.M. Meijer, *Ann. N. Y. Ac. Sc.* **613**, 494-500 (1990).
37. H. Eklund, B. Nordström, E. Zeppezauer, G. Söderlund, I. Ohlsson, T. Boiwe, B.-O. Söderberg, O. Tapia and C.-I. Brändén, *J. Mol. Biol.* **102**, 27-59 (1976).
38. H. Eklund, J.-P. Samama and L. Wallén, *Biochemistry* **21**, 4858-4866 (1982).
39. E. Cedergren-Zeppezauer, J.-P. Samama and H. Eklund, *Biochemistry* **21**, 4895-4908 (1982).
40. B.V. Plapp, H. Eklund, T.A. Jones and C.-I. Brändén, *J. Biol. Chem.* **258**, 5537-5547 (1983).
41. E. Cedergren-Zeppezauer, *Biochemistry* **22**, 5761-5772 (1983).
42. D. Rognan, N. Zimmermann, G. Jung and G. Folkers, *Eur. J. Biochem.* **208**, 101-113 (1992). And references mentioned within this article.
43. IUPAC-IUB Nomenclature, *Eur. J. Biochem.* **131**, 9-15 (1983).
44. O. Almarsson and T.C. Bruice, *J. Am. Chem. Soc.* **115**, 2124-2138 (1993).
45. D-A < 3.5 Å and H-A < 2.5 Å is normally used also in QUANTA.
46. H. Dutler in "Pyridine Nucleotide-dependent Dehydrogenases", (H. Sund ed.), Walter de Gruyter & Co, Berlin, Germany, p. 339-350 (1977).
47. M.C.A. Donkersloot and H.M. Buck, *J. Am. Chem. Soc.* **103**, 6554-6558 (1981).

---

*This chapter is based on:*

S.A.M. Vanhommerig, L.A.Æ. Sluyterman and E.M. Meijer, *Biochim. Biophys. Acta*, in preparation.

## 6

# Kinetic and modelling studies of $NAD^+$ analogues, modified in the C3 side-chain

## 6.1 Introduction

In this chapter the  $NAD^+$  analogues thionicotinamide adenine dinucleotide ( $sNAD^+$ ), 3-acetylpyridine adenine dinucleotide ( $acPdAD^+$ ) and 3-formylpyridine adenine dinucleotide ( $fPdAD^+$ ) carrying the pyridine side-chains  $C(S)NH_2$ ,  $C(O)CH_3$  and  $C(O)H$  respectively (see Figure 6.1), are studied in their interaction with HLADH. Since X-ray data of the corresponding HLADH/coenzyme complexes are not available, we resorted to modelling studies in earlier work<sup>[1-4]</sup>. In the present study we use the molecular mechanics/ dynamics model as described in Chapter 5, to assess the geometry of the  $NAD^+$  analogues and their interactions with the apo-enzyme. The modelling results will be discussed together with the available kinetic data and other experimental information.

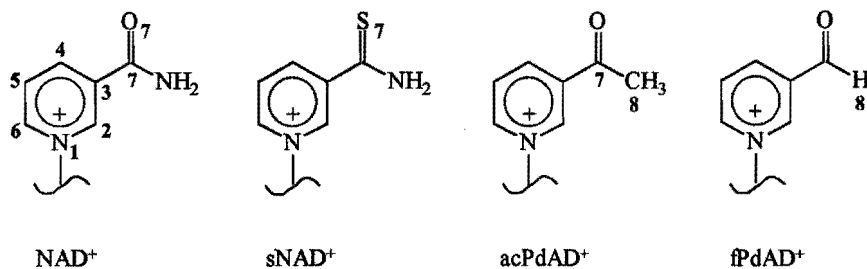


Figure 6.1 The nicotinamide part of  $NAD^+$  and analogues;  $sNAD^+$  = thionicotinamide,  $acPdAD^+$  = 3-acetylpyridine,  $fPdAD^+$  = 3-formylpyridine

## 6.2 Experimental

### 6.2.1 Materials

HLADH, sNAD<sup>+</sup>, acPdAD<sup>+</sup>, fPdAD<sup>+</sup> and  $\beta$ -NAD<sup>+</sup> were purchased from Sigma. The coenzyme NAD<sup>+</sup> was lyophilised from distilled water. The coenzyme concentrations were determined spectrophotometrically using the following absorption coefficients: 18,000 M<sup>-1</sup>cm<sup>-1</sup> at  $\lambda_{\max}$ =260 nm for NAD<sup>+</sup>,  $\epsilon$ =19,700 M<sup>-1</sup>cm<sup>-1</sup> at  $\lambda_{\max}$ =259 nm for sNAD<sup>+</sup>,  $\epsilon$ =16,220 M<sup>-1</sup>cm<sup>-1</sup> at  $\lambda_{\max}$ =260 nm,  $\epsilon$ =18,200 M<sup>-1</sup>cm<sup>-1</sup> at  $\lambda_{\max}$ =260 nm. For the reduced forms: NADH:  $\epsilon$ =6,220 M<sup>-1</sup>cm<sup>-1</sup> at 340 nm, sNADH:  $\epsilon$ =11,900 M<sup>-1</sup>cm<sup>-1</sup> at 398 nm, acPdADH:  $\epsilon$ =9,120 M<sup>-1</sup>cm<sup>-1</sup> at 363 nm and fPdADH:  $\epsilon$ =9,330 M<sup>-1</sup>cm<sup>-1</sup> at 358 nm.

### 6.2.2 Kinetic measurements

All kinetic experiments were carried out at 25°C  $\pm$  0.1°C in 47 mM phosphate buffer, 0.25 mM EDTA,  $\Gamma$ =0.1. The pH was adjusted to 8.0 with KOH. A Perkin-Elmer UV/Vis spectrophotometer Lambda 3B was used. Steady-state kinetics were carried out with coenzyme saturation and varying the alcohol concentration or vice versa (0.55 mM NAD<sup>+</sup>, 0.065 mM sNAD<sup>+</sup>, 0.125 mM fPdAD<sup>+</sup>, 0.10 mM acPdAD<sup>+</sup> in the presence of 1-10 mM ethanol or 0.55 mM NAD<sup>+</sup>, 0.065 mM sNAD<sup>+</sup>, 0.10 mM acPdAD<sup>+</sup> in the presence of 10-100 mM isopropanol; with fPdAD<sup>+</sup> a coenzyme concentration of 5.2 mM was used varying the isopropanol concentration between 38-760 mM; at constant ethanol concentration of 10 mM the NAD<sup>+</sup> and sNAD<sup>+</sup> concentrations were varied between 5-55  $\mu$ M and 6-65  $\mu$ M respectively; with the fPdAD<sup>+</sup> (from 20-201  $\mu$ M) and acPdAD<sup>+</sup> (from 10-100  $\mu$ M) a constant ethanol concentration of 130 mM was used; a constant value 100 mM isopropanol was used when varying the concentrations of NAD<sup>+</sup> (5-55  $\mu$ M), sNAD<sup>+</sup> (6-65  $\mu$ M) and acPdAD<sup>+</sup> (10-100  $\mu$ M); with fPdAD<sup>+</sup> (from 0.2-0.7 mM) an isopropanol concentration of 2 M was used). The change of absorption was measured at  $\lambda_{\max}$  of the corresponding reduced coenzyme. The enzyme concentrations ranged from 0.01-0.23  $\mu$ M during the steady-state measurements. The fPdAD<sup>+</sup> with isopropanol measurements required the highest enzyme concentration. BSA was added to the enzyme stock solution to stabilize the HLADH.

## 6.3 Modelling calculations

As starting structure the crystallographic data of the ternary complex of HLADH/NADH/DMSO as reported by Eklund and co-workers (2.9 Å resolution)<sup>[5]</sup> was

used. Water molecules were added as described in the previous chapter. MM calculations were performed until the RMS gradient value of the energy was less than 0.1 kcal.Å, using an  $\epsilon=1$ . MD calculations up to 90 ps were carried out using a time step of 2 fs and the SHAKE procedure<sup>[6]</sup> to constrain all bond length. The final temperature was 300 K and 250 conformations were used for analysis, taken from the last period of 50 ps. In the case of the fPdAD<sup>+</sup> complexes, one additional water molecule was added near the carboxamide side-chain, filling the extra space resulting from substituting a -NH<sub>2</sub> or -CH<sub>3</sub> group with a hydrogen. Without this extra water residue, the calculations appeared to show less agreement with the X-ray structure. The three-dimensional structures of the NAD<sup>+</sup> analogues were derived from the X-ray NADH geometry, using the modelling package QUANTA/CHARMM<sup>[7]</sup>. In Appendix 2 the parameters are given that have been added to the AMBER data set. Also the calculated *ab initio* 6-31G\*/3-21G atomic charges are listed there. All calculations were performed on a Power Challenge SGI computer using AMBER 4.0<sup>[8]</sup>. The same procedures are used as described in Chapter 5.

## 6.4 Results

### 6.4.1 Kinetic experiments

Table 6.1 and 6.2 summarizes the steady-state kinetic data obtained for NAD<sup>+</sup> and its analogues with ethanol and isopropanol as substrates (see Appendix 1 for the equation used). With ethanol the dissociation of NADH from the binary complex is rate-limiting, with isopropanol the actual hydride-transfer step is rate-limiting (see also Chapter 5).

Both sNAD<sup>+</sup> and acPdAD<sup>+</sup> are more reactive than NAD<sup>+</sup>, 2.4 and 6.5 times, respectively in the case of ethanol and 4.1 and 1.9 times in the case of isopropanol (Table 6.2). On the contrary fPdAD<sup>+</sup> is less active (approximately 20% of the activity of NAD<sup>+</sup>). In the case of the fPdAD<sup>+</sup>/ethanol system the dissociation step is possibly not the rate-determining step any more, as the  $k_{\text{cat}}$  value of 0.23 approaches  $k_{\text{cat}}=0.15$  of NAD<sup>+</sup>/IPA (Table 6.1), where the hydride-transfer is known to be the rate-limiting step. In the past, different values and ratios of the  $k_{\text{cat}}$ 's and  $K_{\text{m}}$ 's have been reported, although the acPdAD<sup>+</sup> and sNAD<sup>+</sup> coenzymes always appear to have higher  $k_{\text{cat}}$ 's and the fPdAD<sup>+</sup> coenzyme a lower  $k_{\text{cat}}$  than the native NAD<sup>+</sup> [9-12].

Three factors govern the rate of hydride-transfer ( $=k_{\text{H}}$ ) in the enzyme: firstly the spatial relationship between coenzyme and enzyme and between coenzyme and substrate, secondly the intrinsic reactivity of the pyridinium moiety, and, thirdly the accessibility of C4 taking into account the possible steric hindrance exerted by the C3 substituent.

**Table 6.1** Kinetic constants of horse liver ADH using  $\text{NAD}^+$  and  $\text{NAD}^+$  analogues. Initial velocities with varying concentrations of coenzymes or substrates were determined at  $25^\circ\text{C}$ ,  $\text{pH}=8$ , measuring the increase in absorption at 340 nm. Standard errors for the estimated  $k_{\text{cat}}$  and  $K_m$  values from a fit with HYPER<sup>[13]</sup> were less than 7% and 20% respectively of the reported values, except in the case of <sup>a</sup> (standard error 53%).

	Ethanol			Isopropanol		
	$k_{\text{cat}}$ ( $\text{s}^{-1}$ )	$K_{\text{mA}}$ ( $\mu\text{M}$ )	$K_{\text{mB}}$ (mM)	$k_{\text{cat}}$ ( $\text{s}^{-1}$ )	$K_{\text{mA}}$ ( $\mu\text{M}$ )	$K_{\text{mB}}$ (mM)
$\text{NAD}^+$	1.14	16.3	0.46	0.15	20.7	12.3
s $\text{NAD}^+$	2.72	28.7	4.03	0.61	33.6	23.9
acPdAD <sup>+</sup>	7.36	73.2	9.44	0.28	65.0	57.1
fPdAD <sup>+</sup>	0.23	97.5	7.89	0.022	664 <sup>a</sup>	154

**Table 6.2** The intrinsic reactivities for various  $\text{NAD}^+$  (analogues) and the relative  $k_{\text{cat}}$  with ethanol and isopropanol.

Coenzyme	relative $k(\text{SO}_2^{\ominus})$	relative $k_{\text{cat}}$ ethanol	relative $k_{\text{cat}}$ isopropanol	$k_{\text{cat}}(\text{IPA})/$ $k(\text{SO}_2^{\ominus})$	electro- negativity <sup>d</sup>
$\text{NAD}^+$	1 <sup>a</sup>	1	1	1	3.680
s $\text{NAD}^+$	3 <sup>a</sup>	2.4	4.1	1.4	
acPdAD <sup>+</sup>	22 <sup>a</sup>	6.5	1.9	0.09	3.938
fPdAD <sup>+</sup>	18 <sup>b</sup>	0.21	0.15	0.01	4.005
cnPdAD <sup>+</sup>	55 <sup>b</sup>		<0.01 <sup>c</sup>	~0	3.991

<sup>a</sup> From reference 14; rate constants for the sulphinate adduct formation:  $\text{NAD}^+$ :  $47 \text{ M}^{-1}\text{s}^{-1}$ , acPdAD<sup>+</sup>:  $1050 \text{ M}^{-1}\text{s}^{-1}$  and s $\text{NAD}^+$ :  $150 \text{ M}^{-1}\text{s}^{-1}$ .

<sup>b</sup> A linear relationship between  $\log k(\text{SO}_2^{\ominus})$  and the redox potential is assumed, showing a higher rate of dithionite reduction with increasing redox potential<sup>[14]</sup>. For fPdAD<sup>+</sup> with a redox potential of  $-262 \text{ mV}$ <sup>[15]</sup> an intrinsic reactivity of  $830 \text{ M}^{-1}\text{s}^{-1}$  can be calculated; for cnPdAD<sup>+</sup> with a redox potential of  $-240 \text{ mV}$ <sup>[16]</sup> this results in  $k(\text{SO}_2^{\ominus})=2593 \text{ M}^{-1}\text{s}^{-1}$ .

<sup>c</sup> See references 12 and 16.

<sup>d</sup> Calculated absolute electronegativity of 1-methyl-3-substituted-1,4-dihydropyridines<sup>[17]</sup>.

As the hydride-transfer is known to be the rate-limiting reaction when isopropanol is the substrate and NAD<sup>+</sup> the coenzyme, the same may be expected when NAD is replaced by close analogues. If the geometries of the enzyme/coenzyme/substrate complexes are identical in all cases, the  $k_{\text{cat}}$  values of the analogues should correlate with the intrinsic reactivities. This is approximately true only for sNAD<sup>+</sup>. The acetyl- and formyl analogues, however, are slower than expected by one and two orders of magnitude respectively. This suggests that there is some essential difference in structure of the ternary complexes of NAD<sup>+</sup> and sNAD<sup>+</sup> on the one hand and of the acyl analogues on the other hand. Unfortunately, no crystal structures have been elucidated with any of the above mentioned analogues. We therefore resorted to modelling calculations.

#### 6.4.2 Modelling studies

Both MM and MD calculations have been applied. The torsional angles of the coenzymes are shown in Table 6.3. In the MM calculations the values of the out-of-plane rotation  $\theta$  of the side-chain of the pyridinium moiety for acyl analogues deviate from the values of the other coenzymes in being negative. This is far more pronounced in the MD calculations; in three of the cases the carbonyl group even turns nearly 180° compared with NAD<sup>+</sup>. These rotations are possible of course owing to the impossibility of hydrogen-bonding the other atoms of the side-chain.

The methyl group of the acetyl analogue is in van der Waals contact with the phenyl group of Phe 93, the side-chains of Cys 174 and Thr 178, the backbone atoms of Phe 319 and C1 of the ethanolate. The ethanolate is small enough to permit the full rotation of the acetyl group to  $\theta = -151^\circ$  (see Figure 6.2). Notwithstanding this rotation the O7-HN (Phe

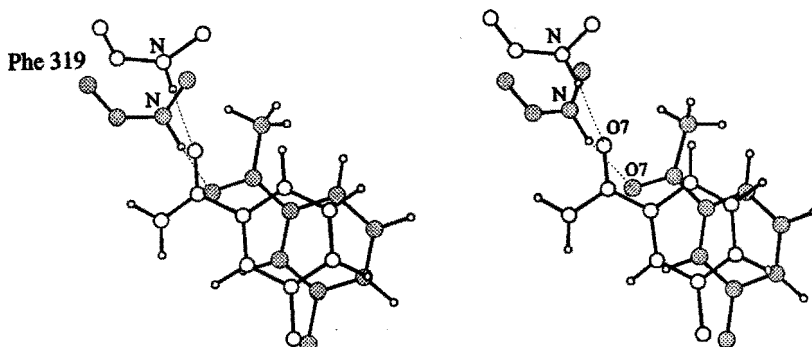


**Figure 6.2** Stereo-pair of the MD-averaged structures of the ethanolate complexes of NAD<sup>+</sup> (blank atoms) and acPdAD<sup>+</sup> (dotted atoms). The H-bond O7–HN (Phe 319) is shown.



**Table 6.3** Overview of torsion angles<sup>a</sup> (in degrees) for NAD<sup>+</sup> and NAD<sup>+</sup> analogue as derived from modelling calculations (MM and MD), and the X-ray structure (NADH/DMSO/HLADH)<sup>[5]</sup>. The MD time-averaged values are taken from 250 conformations over 40-90 ps.

Coenzyme	$\theta$	$\chi_N$	$\gamma_N$	$\beta_N$	$\alpha_N$	$\zeta_N$	$\zeta_A$	$\alpha_A$	$\beta_A$	$\gamma_A$	$\chi_A$
NADH (X-ray)	34	258	39	214	59	207	85	106	147	281	264
<b>MM-results</b>											
NAD <sup>+</sup> /iPrO <sup>-</sup>	13	250	59	181	72	208	78	62	158	296	250
sNAD <sup>+</sup> /iPrO <sup>-</sup>	12	253	59	185	68	214	67	64	148	308	251
acPdAD <sup>+</sup> /iPrO <sup>-</sup>	-15	244	59	184	69	213	66	64	147	312	249
fPdAD <sup>+</sup> /iPrO <sup>-</sup>	-3	243	58	187	64	198	82	65	153	303	254
NAD <sup>+</sup> /EtO <sup>-</sup>	13	250	58	181	71	206	80	61	157	294	250
sNAD <sup>+</sup> /EtO <sup>-</sup>	11	252	59	182	70	220	60	65	137	314	252
acPdAD <sup>+</sup> /EtO <sup>-</sup>	-11	247	58	184	70	209	70	62	144	312	252
fPdAD <sup>+</sup> /EtO <sup>-</sup>	-3	243	59	185	64	201	80	64	149	302	255
fPdAD <sup>+</sup> /EtO <sup>-</sup> <sup>b</sup>	-11	243	61	183	65	201	78	62	151	303	254
<b>MD-results</b>											
NAD <sup>+</sup> /iPrO <sup>-</sup>	35 <sup>c</sup>	242	72	176	76	196	77	43	163	298	251
sNAD <sup>+</sup> /iPrO <sup>-</sup>	21	236	56	186	63	190	89	60	146	311	296
acPdAD <sup>+</sup> /iPrO <sup>-</sup>	-35	236	51	171	86	<b>316</b>	<b>313</b>	<b>160</b>	<b>125</b>	289	258
fPdAD <sup>+</sup> /iPrO <sup>-</sup>	-157	229	54	161	72	<b>326</b>	<b>323</b>	<b>161</b>	<b>72</b>	278	294
NAD <sup>+</sup> /EtO <sup>-</sup>	3	230	76	177	62	198	76	43	150	306	252
acPdAD <sup>+</sup> /EtO <sup>-</sup>	-151	233	63	162	75	<b>309</b>	<b>332</b>	<b>148</b>	<b>82</b>	288	274
fPdAD <sup>+</sup> /EtO <sup>-</sup>	-141	225	58	173	83	<b>283</b>	<b>359</b>	<b>141</b>	<b>90</b>	293	264
fPdAD <sup>+</sup> /EtO <sup>-</sup> <sup>b</sup>	-139	238	55	174	90	<b>302</b>	<b>324</b>	<b>161</b>	<b>72</b>	278	300

<sup>a</sup> According to IUPAC nomenclature<sup>[18]</sup> (see also p. 75).

<sup>b</sup> No extra water molecule present.

<sup>c</sup> This average value of  $\theta$  is found for two thirds of the time (see also section 5.5.8).

319) H-bond is retained (Table 6.4), causing a small shift in the position of the pyridinium moiety. When isopropanol is the substrate, however, its additional methyl group restricts the rotation of the acetyl group to  $\theta = -35^\circ$  (Table 6.3), due to steric hindrance between the additional methyl group of the substrate and the methyl group of the acetyl pyridinium side-chain. The formyl side-chain, lacking a methyl group, is free to turn around to  $\theta \approx -150^\circ$  with both substrates. The formyl analogue even leaves room for a water molecule which, if present, is hydrogen-bonded to the backbone oxygens of Phe 319 and Ala 317 (like the NH<sub>2</sub>

**Table 6.4** Hydrogen-bonding pattern of the carboxamide side-chain of the coenzyme with neighbouring amino acids. X-ray distances are taken from the crystal conformation 6ADH<sup>[5]</sup>; MD distances are averaged for 250 conformations over 40-90 ps. (distances in Å).

	Minimized structures			MD-averaged structures		
	O7-HN <sup>a</sup>	HNA-O <sup>b</sup>	HNB-O <sup>c</sup>	O7-HN <sup>a</sup>	HNA-O <sup>b</sup>	HNB-O <sup>c</sup>
NAD <sup>+</sup> /iPrO <sup>-</sup>	1.86	1.99	1.84	2.02	1.90	2.51
sNAD <sup>+</sup> /iPrO <sup>-</sup>	2.35 <sup>f</sup>	2.09	1.84	2.56 <sup>f</sup>	2.31	1.91
acPdAD <sup>+</sup> /iPrO <sup>-</sup>	1.90	3.57 <sup>d</sup>	3.31 <sup>d</sup>	2.17	4.07 <sup>d</sup>	3.93 <sup>d</sup>
fPdAD <sup>+</sup> /iPrO <sup>-</sup>	1.97	3.80 <sup>e</sup>	3.57 <sup>e</sup>	3.55	6.34 <sup>e</sup>	5.38 <sup>e</sup>
NAD <sup>+</sup> /EtO <sup>-</sup>	1.85	1.99	1.87	1.93	1.87	1.95
sNAD <sup>+</sup> /EtO <sup>-</sup>	2.36 <sup>f</sup>	2.15	1.84	ND	ND	ND
acPdAD <sup>+</sup> /EtO <sup>-</sup>	1.92	3.58 <sup>d</sup>	3.26 <sup>d</sup>	1.88	6.00 <sup>d</sup>	6.36 <sup>d</sup>
fPdAD <sup>+</sup> /EtO <sup>-</sup>	1.96	3.39 <sup>e</sup>	3.57 <sup>e</sup>	2.56	7.34 <sup>e</sup>	5.76 <sup>e</sup>
fPdAD <sup>+</sup> /EtO <sup>-</sup> §	1.89	3.39 <sup>e</sup>	3.57 <sup>e</sup>	2.43	5.44 <sup>e</sup>	5.92 <sup>e</sup>
X-ray <sup>h</sup>	2.83	2.60	2.53	2.83	2.60	2.53

<sup>a</sup> O7 (NAD<sup>+</sup>) – HN (Phe 319)

<sup>b</sup> HNA (NAD<sup>+</sup>) – O (Ala 317)

<sup>c</sup> HNB (NAD<sup>+</sup>) – O (Val 292)

<sup>d</sup> The O (amino acid) – C8 (acPdAD<sup>+</sup>, side-chain) distance is taken.

<sup>e</sup> The O (amino acid) – H8 (fPdAD<sup>+</sup>, side-chain) distance is taken.

<sup>f</sup> Here the S7 (sNAD<sup>+</sup>) – HN (Phe 319) distance is taken.

§ No extra water molecule present near the formyl side-chain of the coenzyme.

<sup>h</sup> The donor-acceptor (N–O) distances are taken.

group of  $\text{NAD}^+$ ), and another water molecule.

Furthermore it is evident from the MD-results reported in Table 6.3 (italic values), that pronounced differences of more than  $100^\circ$  occur in the torsional angles  $\zeta_{\text{N}}$ ,  $\zeta_{\text{A}}$  and  $\alpha_{\text{A}}$  around the phosphate groups of the acetyl and formyl analogues. They are strikingly similar to those reported in the previous chapter (Table 5.6), on proceeding from  $\text{PEG-NAD}^+/\text{iPrO}^-$  to  $\text{PEG-NAD}^+/\text{EtO}^-$ . This rather confirms the suggestion of there being two main types of conformations, all values for  $\zeta_{\text{N}}$ ,  $\zeta_{\text{A}}$  and  $\alpha_{\text{A}}$  being low or high. The concomitant changes in H-bonding of the phosphates to the surrounding peptide are partly different from the earlier ones, as is evident on comparing the data of Table I in Appendix 4 with those of Table 5.9. The differences may be due to the fact that there are also changes, from  $50^\circ$  to  $90^\circ$ , of  $\beta_{\text{A}}$  in the present cases. The various coenzymes and substrates of course affect somewhat the position of the surrounding peptide chain as evident from the RMS deviation of the structure of each combination from the X-ray structure (Table II in Appendix 4). As to be expected the changes in enzyme-coenzyme interactions are attended by small but significant changes in interaction energies. They are shown in Table 6.6 (which is discussed in more detail later), including the one of  $\text{PEG-NAD}^+$  (not mentioned in Chapter 5).

The spatial relationship between coenzyme and substrate is greatly governed by the distance between C1 of the substrate and C4 of the coenzyme, and the related angle N1-C4-C1. They are shown in Table 6.5. There are no marked differences in either factor, with the possible exception of the C4-C1 distance in  $\text{acPdAD}^+/\text{EtO}^-$  in the MD structure. Neither are there any significant differences in the puckering of the nicotinamide ring and ribose rings (Table 6.5, values of  $\alpha_{\text{C}}$ ,  $\alpha_{\text{N}}$ ,  $\nu_2(\text{N})$  and  $\nu_2(\text{A})$ ).

## 6.5 Discussion

It is known that the distance to be travelled by the hydride ion, from C1 (substrate) to C4 (coenzyme), and the direction concerned, the angle C1-C4-N1 (coenzyme), are among the factors that determine the effectiveness of the catalytic reaction. As shown in Table 6.5 they are mainly the same in all cases. The MM calculated distance of 3.4 Å is equal to the 3.4 Å found with the AM1 calculations in the alcohol state (Table 2.4); the MD calculated mean distance of 3.7 Å is reasonably close to it. The same holds for the angles, being  $108^\circ$ ,  $109^\circ$ , and  $89^\circ$  to  $114^\circ$  in the MM, MD and AM1 calculations respectively. In the X-ray structure of the DMSO/NADH complex the distance is 4.18 Å (somewhat larger, owing to the size of the S atom) and the angle  $93^\circ$  (Table 6.5).

The distances and angles being rather constant, the differences in activity are mainly to be found in another factor, the out-of-plane rotation of the carbonyl group of the

**Table 6.5** Substrate-coenzyme distance and the puckering values of the nicotinamide ring and ribose rings. The MD time-averaged values are taken from 250 conformations over 40-90 ps. The X-ray data are taken from the ternary complex with NADH/DMSO/HLADH<sup>f</sup> <sup>51</sup>.

	X-ray NADH	NAD iPrO	acPdAD iPrO	fPdAD iPrO	sNAD iPrO	NAD EtO	acPdAD EtO	fPdAD EtO	fPdAD EtO <sup>a</sup>	sNAD EtO
<b>Minimized structures</b>										
C4(NAD)–C1(RO <sup>-</sup> ) (Å)	4.18 <sup>b</sup>	3.37	3.33	3.31	3.40	3.42	3.41	3.38	3.38	3.46
N1–C4–C1 (degrees)	93	104	106	104	110	107	111	109	108	112
$\alpha_C$ (degrees) <sup>c</sup>	0	-4	-7	-8	2	-3	-7	-9	-9	-7
$\alpha_N$ (degrees) <sup>c</sup>	0	3	-1	-2	-6	3	-1	-2	-2	2
$\nu_2(N)$ (degrees) <sup>d</sup>	-37	-38	-36	-33	-38	-38	-37	-34	-34	-38
$\nu_2(A)$ (degrees) <sup>d</sup>	-37	-24	-22	-23	-22	-24	-20	-22	-22	-19
<b>MD-averaged structures</b>										
C4(NAD)–C1(RO <sup>-</sup> ) (Å)	4.18 <sup>b</sup>	3.46	3.52	3.49	3.49	3.56	4.35	3.79	4.10	ND
N1–C4–C1 (degrees)	93	106	102	104	101	124	88	103	106	ND
$\alpha_C$ (degrees) <sup>c</sup>	0	4	1	-4	9	7	-6	-3	-5	ND
$\alpha_N$ (degrees) <sup>c</sup>	0	-2	-3	-7	1	2	-5	-6	-6	ND
$\nu_2(N)$ (degrees) <sup>d</sup>	-37	-32	-33	-31	-33	-33	-35	-29	-31	ND
$\nu_2(A)$ (degrees) <sup>d</sup>	-37	-20	-19	-33	-19	-20	-20	-18	-16	ND

<sup>a</sup> No extra water molecule present near the formyl side-chain of the coenzyme.

<sup>b</sup> The C4 (NAD)–S (DMSO) distance in the crystal structure.

<sup>c</sup>  $\alpha_C$  = C2–C6–C3–C4 (atoms of the nicotinamide ring), and  $\alpha_N$  = C3–C5–C6–N1.

<sup>d</sup>  $\nu_2(N)$  = C1'–C2'–C3'–C4' of the nicotinamide ribose;  $\nu_2(A)$  = C1'–C2'–C3'–C4' of the adenine ribose.

pyridinium moiety. This will now be discussed.

First the aspects of the substrate isopropanol will be discussed, as its  $k_{cat}$  values can be considered to be equal to the rate of hydrogen-transfer  $k_H$ . As mentioned in paragraph 6.4.1, the higher  $k_{cat}$  value of sNAD<sup>+</sup> compared with that of NAD<sup>+</sup> can reasonably be explained by its intrinsic reactivity. Both compounds have a positive value of  $\theta$  in the ternary complex, according to MD calculations (Table 6.3) and their geometries resemble each other quite well. Such positive values of  $\theta$  are supported by X-ray data of ternary complexes of the

enzyme with NADH and three different substrate analogues (DMSO<sup>[5]</sup>, F<sub>5</sub> benzyl-alcohol<sup>[19]</sup> and pyrazole<sup>[20]</sup>). Furthermore similar positive values of  $\theta$  are shown up in AM1 calculations on a simplified enzyme model, both in transition state and, when provided with the proper H-bonds, in the initial state (Tables 2.5 and 2.6).

The most remarkable results of this chapter are the negative values of  $\theta$  when the acyl analogues are used as coenzyme, quite clear in the MD calculations (Table 6.3). Here again the AM1 calculations show the same trend, though less pronounced.

The  $k_{\text{cat}}$  when isopropanol is the substrate and the acetyl analogue is the coenzyme can now be explained; the carbonyl group being on the wrong side of the pyridinium ring, cannot directly assist the hydrogen-transfer. The advantage of the high intrinsic activity of the cofactor is therefore almost neutralized.

When the formyl analogue is the coenzyme,  $k_{\text{cat}}$  is further reduced. This is accompanied by  $\theta = -157^\circ$ , i.e. the C=O group points in almost exactly the opposite direction from its position in NAD<sup>+</sup>. Instead of aiding the hydride-transfer as it does in NAD<sup>+</sup>, it will now counteract it, causing overcompensation of the high intrinsic activity, resulting in a low value of  $k_{\text{cat}}$ .

In the case of ethanol as the substrate there is a complication in that the rate of dissociation of the coenzyme (including the concomitant conformational change of the enzyme) is limiting when NAD<sup>+</sup>, sNAD<sup>+</sup> and the acetyl analogue are utilized as coenzyme. A change of  $k_{\text{H}}$  is therefore not detected, unless  $k_{\text{H}}$  is greatly reduced. This seems to occur when the formyl analogue is used; in this case, as pointed out in paragraph 6.4.1,  $k_{\text{cat}}$  is lowered to such an extent as to approach the  $k_{\text{cat}}$  of NAD<sup>+</sup>/isopropanol, where  $k_{\text{cat}}$  equals  $k_{\text{H}}$ .

It is known that  $k_{\text{H}} \approx 100.k_{\text{cat}}$  in the reaction of NAD<sup>+</sup> and ethanol<sup>[21]</sup>. As the  $k_{\text{cat}}$  of the formyl analogue is five times lower than the  $k_{\text{cat}}$  of NAD<sup>+</sup>, a factor of 500 has to be explained. In view of the results with isopropanol (where a factor of 7 was involved, Table 6.2), the turning around of the carbonyl group of the coenzyme (Table 6.3) is unable to cover this large factor of 500. An additional phenomenon is apparently required to explain the discrepancy. There are some indications that this may be found in the proton relay system (cf. Chapter 5, paragraph 5.5.7), but the data concerned are considered not to be significantly reliable to warrant further discussion.

Up to now the changes of  $k_{\text{cat}}$  have been discussed in those cases where  $k_{\text{cat}}$  equals  $k_{\text{H}}$ . It is also possible to say something regarding the  $k_{\text{cat}}$  values when the rate of dissociation of the coenzyme from the enzyme is limiting, which occurs mainly when ethanol is substrate. It is generally accepted that the actual dissociation from HLADH is preceded by a conformational change of the enzyme that widens the coenzyme cleft sufficiently to allow the coenzyme to pass outside<sup>[5,22]</sup>. As the conformational change is a relatively slow process,

the overall dissociation rate of the coenzyme, 1.14 to 7.36 s<sup>-1</sup> in the present cases (Table 6.1), is considerably lower than the association/dissociation rates of ligands and enzymes in general (10<sup>4</sup> s<sup>-1</sup> using similar concentrations, reference 23). By this mechanism the various dissociation rates can be understood in terms of the interaction energies between enzyme and coenzyme (Table 6.6). In the first row the total energies are given. In order to have solely the interaction energies of enzyme and coenzyme, the interaction energies between coenzyme and substrate (second row) are subtracted, yielding the third row. It is evident that in both the EtO<sup>-</sup> and the iPrO<sup>-</sup> complexes the interaction energies of the acetyl- and formyl analogues are consistently lower than those of NAD<sup>+</sup>, and so is the energy of sNAD<sup>+</sup> in the iPrO<sup>-</sup> complex. The energy in the sNAD<sup>+</sup>/EtO<sup>-</sup> complex happens not to quite fit the general trend. On the other hand both PEG-NAD<sup>+</sup> complexes exhibit a higher interaction energy. In the bottom row of Table 6.6 the corresponding relative  $k_{cat}$  values are given again (from Table 6.2). In spite of the discrepancy regarding the sNAD<sup>+</sup>/EtO<sup>-</sup> complex, the trend is obvious enough; a high interaction energy is related to a low rate of dissociation, whereas a low one relates to an increased rate. Because a higher interaction energy will keep the walls of the cleft somewhat more tight than does a lower energy, retarding or enhancing respectively the rate of conformational change and therefore lower or increase the rates of dissociation, i.e. the  $k_{cat}$  values. This explains the kinetic results discussed (Table 6.2).

One more conclusion may be drawn from the data in Table 6.5. In the EtO<sup>-</sup>/fPdAD<sup>+</sup>

**Table 6.6** The total interaction energies ( $E_{INTER}$  in kcal.mol<sup>-1</sup>) for the NAD<sup>+</sup> (analogues) derived from their corresponding MM calculations, and relative  $k_{cat}$  values of coenzyme/substrate combinations when enzyme-coenzyme dissociation is rate limiting (from Table 6.2 and 5.2).

	EtO <sup>-</sup> complexes						iPrO <sup>-</sup> complexes				
	NAD	sNAD	acPdAD	fPdAD	fPdAD <sup>a</sup>	PEG	NAD	sNAD	acPdAD	fPdAD	PEG
E <sub>INTER</sub> tot. <sup>b</sup>	-318	-322	-311	-298	-294	-377	-319	-312	-312	-293	-378
E <sub>INTER</sub> alc. <sup>c</sup>	-12	-13	-12	-14	-14	-12	-12	-12	-13	-13	-12
E <sub>INTER</sub> enz. <sup>d</sup>	-306	-309	-299	-284	-280	-365	-307	-300	-299	-280	-366
relative $k_{cat}$	1	2.4	6.5			0.32					

<sup>a</sup> No extra water molecule present near the formyl side-chain of the coenzyme.

<sup>b</sup> Total interaction energy of the coenzyme.

<sup>c</sup> E<sub>INTER</sub> between the coenzyme and the alkoxide.

<sup>d</sup> E<sub>INTER</sub> between the coenzyme and enzyme.

complex the interaction energy is low; the rate of dissociation is therefore expected to be high, say  $10 \text{ s}^{-1}$ . If  $k_{\text{H}}$  is sufficiently low, this will now become rate-limiting, resulting in  $k_{\text{cat}} = k_{\text{H}}$ . This confirms the proposal made in paragraph 6.4.1 and the beginning of 6.5 concerning the interpretation of the kinetic results of the reaction of ethanol and the formyl analogue (Table 6.1).

By now most of the  $k_{\text{cat}}$  values presented in Table 6.1 and of the PEG-NAD<sup>+</sup>/EtO<sup>-</sup> complex of Chapter 5 can be qualitatively explained by MM and MD calculations. Two issues however are not covered:  $k_{\text{H}}(\text{NAD}^+/\text{EtO}^-) \gg k_{\text{cat}}(\text{NAD}^+/\text{iPrO}^-)$ , and the fact that the rotation of the carbonyl group of the formyl analogue in the complex of this analogue and ethanol only partly explains its low  $k_{\text{cat}}$  value. The second issue most likely being a consequence of the former.

Furthermore, there are a few smaller discrepancies, in that the MD-averaged value of  $\theta$  of NAD<sup>+</sup>/EtO<sup>-</sup> is only  $3^\circ$  instead of the expected value of around  $30^\circ$  (Table 6.3). The C1-C4 distance of the acPdAD<sup>+</sup>/EtO<sup>-</sup> complex is  $4.35 \text{ \AA}$  instead of about  $3.5 \text{ \AA}$  (Table 6.5), and the EINTER enz. of the sNAD<sup>+</sup>/EtO<sup>-</sup> complex is some  $9 \text{ kcal.mol}^{-1}$  too high (Table 6.6). These discrepancies might be resolved by repeating the MD calculations with the improved 2OHX file instead of the 6ADH file used now (see Chapter 5, section 5.5.2).

The important matter of  $k_{\text{H}}(\text{NAD}^+/\text{EtO}^-) \gg k_{\text{cat}}(\text{NAD}^+/\text{iPrO}^-)$  requires further studies after application of the improved file.

## 6.6 Conclusion

Notwithstanding the above mentioned questions, the conclusion can be maintained that the out-of-plane rotation of the carbonyl group of the coenzyme or its analogue in HLADH greatly affects the activity of the enzyme.

## References

1. P.M.T. De Kok, N.A. Beijer, H.M. Buck, L.A.Æ. Sluyterman and E.M. Meijer, *Recl. Trav. Chim. Pays-Bas* **107**, 355-361 (1988).
2. P.M.T. De Kok, N.A. Beijer, H.M. Buck, L.A.Æ. Sluyterman and E.M. Meijer, *Eur. J. Biochem.* **175**, 581-585 (1988).
3. N.A. Beijer, H.M. Buck, L.A.Æ. Sluyterman and E.M. Meijer, *Biochim. Biophys. Acta* **1039**, 227-233 (1990)
4. N.A. Beijer, H.M. Buck, L.A.Æ. Sluyterman and E.M. Meijer, *Ann. N. Y. Ac. Sc.* **613**, 494-500 (1990).

5. H. Eklund, J.-P. Samama and T.A. Jones, *Biochemistry* **23**, 5982-5996 (1984).
6. W.F. van Gunsteren and H.J.C. Berendsen, *Mol. Phys.* **34**, 1311 (1977).
7. QUANTA/CHARMM 3.3.2, Molecular Simulations Inc., Waltham, Massachusetts, USA.
8. D.A. Pearlman, D.A. Case, J.C. Caldwell, C.L. Seibel, U.C. Singh, P. Weiner and P.A. Kollman, AMBER 4.0, University of California San Francisco, California, USA (1991).
9. "Coenzymes and Cofactors, Pyridine Nucleotide coenzymes" (D. Dolphin, O. Avramovic and R. Poulson, eds.) John Wiley and Sons, New York, 2A, 536 (1987).
10. J.D. Shore and H. Theorell, *Eur. J. Biochem.* **2**, 32-36 (1967).
11. B.M. Anderson, C.D. Anderson, J.K. Lee and A.M. Stein, *Biochemistry* **2**, 1017-1022 (1963).
12. R.J. Kazlauskas, *J. Org. Chem.* **53**, 4633-4635 (1988).
13. W.W. Cleland, *Methods Enzymol.* **63**, 103-138 (1979).
14. G. Blankenhorn and E.G. Moore, *J. Am. Chem. Soc.* **102**, 1092-1098 (1980).
15. M. Scharschmidt, M.A. Fisher and W.W. Cleland, *Biochemistry* **23**, 5471-5478 (1984).
16. C. Woenckhaus and R. Jeck in "Coenzymes and Cofactors, Pyridine Nucleotide Coenzymes", (D. Dolphin, O. Avramovic and R. Poulson, eds.), John Wiley and Sons, New York, 2A, 449-568 (1987).
17. M.E. Brewster, M.-J. Huang, J.J. Kaminski, E. Pop and N. Bodor, *J. Comput. Chem.* **12**, 1278-1282 (1991).
18. IUPAC-IUB Nomenclature, *Eur. J. Biochem.* **131**, 9-15 (1983).
19. S. Ramaswamy, H. Eklund and B.V. Plapp, *Biochemistry* **33**, 5230-5237 (1994).
20. H. Eklund, J.-P. Samama and L. Wallén, *Biochemistry* **21**, 4858-4855 (1982).
21. V.C. Sekhar and B.V. Plapp, *Biochemistry* **29**, 4289-4295 (1990).
22. H. Eklund, J.-P. Samama, L. Wallén, C.-I. Brändén, Å. Åkeson and T.A. Jones, *J. Mol. Biol.* **146**, 561-587 (1981).
23. T.E. Creighton in "Proteins, Structures and molecular principles", W.H. Freeman and Company, New York, p. 339-340 (1984).

---

*This chapter is based on:*

S.A.M. Vanhommerig, L.A.Æ. Sluyterman and E.M. Meijer, *Biochim. Biophys. Acta*, in preparation.





## 7

## The synthetic NADH model N,N,1,2,4-pentamethyl- 1,4-dihydro-nicotinamide

### 7.1 Introduction

In the past many efforts have been made to design synthetic model compounds, based on the concept of the working mechanism of dehydrogenases. In the enzymatic cavity, one of the diastereotopic C4 hydrogens of NADH is shielded and the other hydrogen is transferred to the substrate. The development of an efficient NADH model, mimicking the activity and stereoselectivity of the NAD-dependent enzymes, has resulted in a variety of 1,4-dihydropyridines<sup>[1-3]</sup>. Numerous asymmetric reductions by such model compounds have already been reported<sup>[4-6]</sup>. In our laboratory, efficient enantioselective hydride-transfer has been achieved with N,N,1,2,4-pentamethyl-1,4-dihyronicotinamide (**1**, see Figure 7.1)<sup>[7]</sup>. The introduction of a methyl substituent at C4 of this compound provides a stereocenter at the reaction center. It was shown that this NADH-model combines excellent stereoselectivity with high reactivity. The stable axial chirality in the oxidized form **2** (see Figure 7.1) provides information about the mechanism of hydride-transfer. Only a transition in which the migrating hydrogen of C4 and the amide carbonyl dipole feature a *syn*-out-of-plane orientation, may account for the observed stereochemistry.

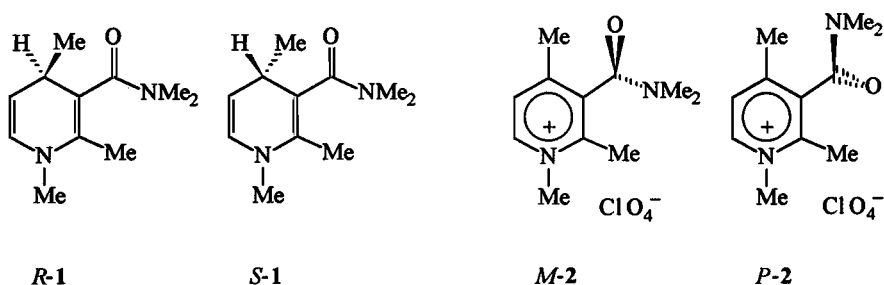


Figure 7.1 The reduced (left) and oxidized forms (right) of the NADH model.

The successful stereoselective reduction of several prochiral carbonyl substrates, e.g. methyl benzoylformate<sup>[7]</sup> and benzoin<sup>[8]</sup>, with high optical yields, encouraged us to extend our investigations to new prochiral substrates. The reactivity of several carbonyl compounds towards NADH model 1 and the efficiency of the chirality transfer were investigated.

## 7.2 Experimental

NMR spectra were recorded on a Bruker AC400 spectrometer (<sup>1</sup>H-NMR at 400.1 MHz, <sup>13</sup>C-NMR at 100.6 MHz, using TMS as internal standard and <sup>31</sup>P-NMR at 162.0 MHz). All reactions involving dihydronicotinamide 1 were performed under an argon atmosphere.

*N,N,1,2,4-Pentamethyl-1,4-dihydronicotinamide* (1) was synthesized in three steps from *N,N*-dimethylacetacetamide as outlined previously<sup>[7]</sup>. Enantiomeric separation of racemic 1 (35 mg, dissolved in *n*-hexane/*i*PrOH (4:1, 120  $\mu$ L)) was accomplished with HPLC (cellulose triacetate column, Merck 16362, 15-25  $\mu$ m, 30 g, 300 mm  $\times$  16 mm, 12 bar, 4 mL min<sup>-1</sup>). Elution with *n*-hexane/*i*PrOH (7:3) afforded pure (*R*)-1 (10 mg, ee > 95%) and (*S*)-1 (15 mg, ee > 90%).

*Reduction of keto compounds with racemic NADH model 1; General procedure.* To a stirred and cooled (0°C) solution of Mg(ClO<sub>4</sub>)<sub>2</sub> (45 mg, 0.2 mmol) in CD<sub>3</sub>CN (0.4 mL) were consecutively added a solution of the keto compound (0.2 mmol) in CD<sub>3</sub>CN (0.3 mL) and a solution of racemic dihydropyridine 1 (40 mg, 0.2 mmol) in CD<sub>3</sub>CN (0.3 mL). A <sup>1</sup>H-NMR spectrum taken after 15 min showed that the reaction was complete (disappearance of vinylic proton signals of 1 (4.4 and 5.7 ppm); appearance of aromatic proton signals of 2 (7.7 and 8.5 ppm). Aqueous NH<sub>4</sub>Cl (0.1 M, 4 mL) was added and the CD<sub>3</sub>CN was evaporated. The residue was extracted with CH<sub>2</sub>Cl<sub>2</sub> (2  $\times$  8 mL). The organic layer was washed with H<sub>2</sub>O (2  $\times$  1 mL), dried over MgSO<sub>4</sub> and concentrated. The products were identified by <sup>1</sup>H-NMR. Successful reductions were repeated with optically active 1.

*Reduction reactions with optically active 1.* To a stirred and cooled (-25°C) solution of Mg(ClO<sub>4</sub>)<sub>2</sub> (45 mg, 0.2 mmol) in CD<sub>3</sub>CN (0.2 mL) were consecutively added a solution of the keto substrate (0.2 mmol) in CD<sub>3</sub>CN (0.4 mL) and a solution of optically active 1 (40 mg, 0.2 mmol) in CD<sub>3</sub>CN (0.4 mL). The stirred mixture was allowed to attain room temperature within 1 hour. Aqueous NH<sub>4</sub>Cl (0.1 M, 2 mL) was added and the CD<sub>3</sub>CN evaporated below 30°C. The residue was partitioned between CH<sub>2</sub>Cl<sub>2</sub> (8 mL) and H<sub>2</sub>O (4 mL). The organic layer was dried (MgSO<sub>4</sub>), concentrated and purified by column chromatography on silica gel. The combined aqueous layers were concentrated in vacuo

below 30°C. The residue was suspended in CH<sub>3</sub>CN, filtered and the filtrate concentrated to give pyridinium perchlorate **2**. <sup>1</sup>H-NMR (CD<sub>3</sub>CN): δ 2.48 (s, 3H, C-4 Me); 2.60 (s, 3H, C-2 Me); 2.90 (2, 3H, *anti* N-Me); 3.20 (s, 3H, *syn* N-Me); 4.17 (s, 3H, N-1 Me); 7.65 (d, 1H, H-5); 8.55 (d, 1H, H-6). To a solution of **2** (20 mg) in CD<sub>3</sub>CN (0.4 mL) was added (+)-Eu(hfc)<sub>3</sub> (100 mg) and the ee was calculated using the glinfit method (Glinfit program, copyright Bruker Spectrospin AG, Switzerland) (RMS < 4%) from the resolved *syn* N-Me <sup>1</sup>H-NMR signals: δ 5.10 (*M-2*), 5.24 (*P-2*).

*Ee determination of pantolactone, 4f.* To a solution of **3f** (22.4 mg, 0.17 mmol) in C<sub>6</sub>D<sub>6</sub> (0.4 mL) was added (+)-Eu(hfc)<sub>3</sub> (12.8 mg, 0.01 mmol) and the ee was calculated from the resolved <sup>1</sup>H-NMR signals: *R-4f*: δ 1.01 (s, 3H, *anti* C-4 Me); 1.42 (s, 3H, *syn* C-4 Me); 3.62 (d, 1H, *anti* H-5); 3.73 (d, 1H, *syn* H-5); 4.69 (s, 1H, H-1). *S-4f*: 0.98 (s, 3H, *anti* C-4 Me); 1.30 (s, 3H, *syn* C-4 Me); 3.57 (d, 1H, *anti* H-5); 3.68 (d, 1H, *syn* H-5), 4.64 (s, 1H, H-1).

*Ee determination of ethyl 2-hydroxy-3-methylbutyrate, 4g*<sup>[9]</sup>. To a solution of **3g** (14.6 mg, 0.1 mmol) in C<sub>6</sub>D<sub>6</sub> (0.5 mL) were added Et<sub>3</sub>N (19 μL, 0.15 mmol), 4-dimethylamino-pyridine (2 mg, 0.01 mmol) and 2-chloro-(4*R*,5*R*)-dimethyl-2-oxo-1,3,2,-dioxaphospholane (13 μL, 0.1 mmol). The resultant suspension was filtered into an NMR tube and the ee calculated from the <sup>31</sup>P-NMR signals of the diastereomeric phosphates: *R*-butyrate: δ 14.86; *S*-butyrate: 14.80.

### 7.3 Reactivity of C=O compounds towards NADH model 1

The synthetic utility of hydride-transfer from the NADH model **1** to the C=O bond was screened with several carbonyl compounds, listed in Figure 7.2. Methyl benzoylformate (**3a**) and benzoin (**3b**) were tested before, and both react quantitatively with **1** [7,8]. Earlier work showed that acetone (**3e**) does not react with **1** to an appreciable extent, but benzaldehyde (**3d**) does for ~60% [7,8].

Since the NADH model **1** exhibits autoxidoreductive disproportionation in the presence of Mg(ClO<sub>4</sub>)<sub>2</sub>, a competitive conflict arises between the autoxidoreduction on the one hand and the hydride-transfer to the carbonyl substrate on the other. Depending on how fast or slow the reaction between substrate and NADH model **1** occurs, the autoxidoreduction is relatively faster and wins the battle. This explains the fact that many substrates are only partially or not at all reduced by **1**.

The α-keto esters **3f** (4,5-dihydro-4,4-dimethyl-2,3-furanedione) and **3g** (ethyl 3-methyl-2-oxo-butylate) were reduced selectively with **1** in 100% and 56% yield, respectively. The dione (**3c**) 1-phenyl-1,2-propanedione afforded a mixture of 2-hydroxy-1-phenyl-1-

propanone and 1-hydroxy-1-phenyl-2-propanone. The cyclic diketones **3h** and **3i** were not reduced at all. Thus electronic features play an important role in the reactivity of the substrate.

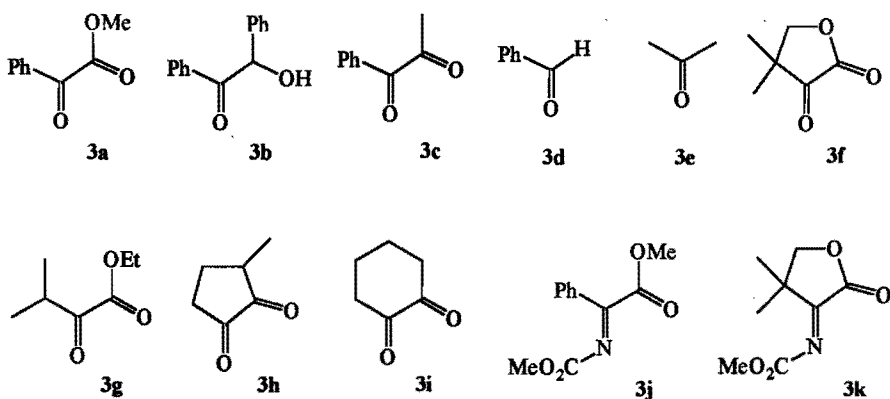


Figure 7.2 All carbonyl compounds tested with NADH model 1.

The rapid formation of a reactive ternary complex consisting of the substrate, the NADH model 1 and  $Mg^{2+}$  seems essential for an effective hydride-transfer. Apparently, the presence of an  $\alpha$ -carboalkoxy and to a smaller extent an  $\alpha$ -hydroxyalkyl or an  $\alpha$ -phenyl group in the carbonyl substrate facilitates the construction of a ternary complex, while steric crowding of bulky groups adjacent to the carbonyl bond strongly hampers its formation. In contrast to the  $\alpha$ -keto ester **3g**, the rigid cisoid structure of lactone **3f** overcomes the steric constraints imposed by the  $\alpha$ -methyl substituent, rendering the activity of **3f** comparable to that of methyl benzoylformate (**3a**). In conclusion, only carbonyl compounds with electron withdrawing substituents and carbonyl compounds carrying a polar  $\alpha$ -substituent, easily fitting in a ternary complex, are efficiently reduced by 1.

Also the reactivity of several C=N compounds with NADH model 1 was investigated. Only two imino substrates (methyl 2-methoxycarbonylimino-phenylacetate (**3j**) and 4,5-dihydro-4,4-dimethyl-3-methoxycarbonylimino-2-(3H)-furanone (**3k**)) were quantitatively reduced to their corresponding  $\alpha$ -amino acid derivatives. Other imino substrates, containing  $\alpha$ -halo substituents as protecting groups for  $\alpha$ -protons were also reduced by 1, but elimination of HX followed the reduction step immediately, leading to the stable enamine derivatives<sup>[10]</sup>.

Table 7.1 Chirality transfer from optically active 1 to reactive carbonyl substrates.

NADH model 1		substrate	product			NAD <sup>+</sup> model 2			
conf	ee <sup>a</sup> %		conf	ee %	o.y. <sup>b</sup> %	conf	ee %	o.y. <sup>b</sup> %	
<i>R</i> <sup>c</sup>	96			<i>R</i>	92	95	<i>P</i>	93	97
<i>S</i>	90			<i>S</i>	88	98	<i>M</i>	84	93
<i>R</i>	95			<i>R</i>	59	62	<i>P</i>	91	96
<i>S</i>	90			<i>S</i>	68	76	<i>M</i>	87	97
<i>R</i>	95			<i>R</i>	67	70	<i>P</i>	85	89
<i>S</i>	90			<i>M</i>			<i>M</i>	82	91
<i>R</i> <sup>d</sup>	96			<i>meso</i>	ND	95	<i>P</i>	97	ND

<sup>a</sup> Enantiomeric excess determined by HPLC. <sup>b</sup> Optical yield corrected for ee of 1. <sup>c</sup> From reference 7. <sup>d</sup> From reference 8.

### 7.4 Stereoselectivity and mechanism of the hydride-transfer

Table 7.1 lists the results of the reaction of NADH model **1** with the reactive carbonyl compounds. Reaction of optically pure **1** with C=O compounds **3a**, **3d**, **3f** and **3g** afforded axially chiral NAD<sup>+</sup> model **2** in optical yields  $\geq 82\%$ . In all cases except benzoin, the *R* configuration in NADH model **1** corresponds to the *R* configuration in the reduction products and to the *P* conformation in NAD<sup>+</sup> model **2**. Similarly, *S*-**1** yields the *S* reduction products and *M*-**2**. The observed asymmetric induction can only be explained by the intervention of a short lived, strictly organized ternary complex (**5a**) as was postulated previously.<sup>[7]</sup> In this complex Mg<sup>2+</sup> plays a crucial role in inducing both high stereoselectivity and high reactivity. The magnesium ion coordinates with the carboxamide oxygen of the NADH model, thus enhancing the hydride donor ability of **1** by the out-of-plane rotation of the amide carbonyl dipole. It also coordinates the substrate in the ternary complex by chelation and activates the C=O substrate via Lewis acid complexation. The amide carbonyl and the migrating C4 hydrogen feature a *syn*-out-of-plane orientation in this transition state.

Assuming a hexavalent arrangement of the magnesium ion in the ternary complex, coordination of Mg<sup>2+</sup> with the lone pairs of three hetero atoms allows the formation of only two chelated complexes (see Figure 7.3).

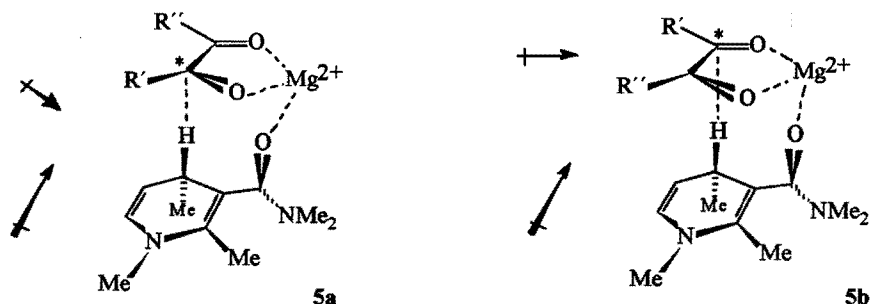


**Figure 7.3** Schematic representation of the proposed ternary complex involved in the  $Mg(ClO_4)_2$ -mediated hydride-transfer from *S*-**1** to a carbonyl substrate (**5a**) and another possible ternary complex **5b**. Arrows indicate dipoles.

The complex as drawn on the left has the C<sup>\*</sup>=O dipole of the substrate lying over the dihydropyridine ring and is oriented towards C3 (**5a**, more or less *anti*-parallel orientation of C=O and dihydropyridine dipoles). The second complex has the C<sup>\*</sup>=O dipole pointed away from the pyridine ring (**5b**, more or less parallel dipoles). Apparently, complex **5a**,

leading to the formation of the *S*-reduction product from *S*-1, is energetically favoured over complex **5b**. With semiempirical MINDO/3 calculations on a ternary complex consisting of NADH model 1,  $\text{Mg}^{2+}$  and 2-oxo-3-butynoic acid it was also found that there was a preference for an orientation of the  $\text{C}^*=\text{O}$  dipole in the direction of C3 (difference in  $\Delta\text{H}$ : 3 kcal.mol<sup>-1</sup>)<sup>[11]</sup>.

The importance of the formation of a chelated ternary complex during the hydride-transfer is clearly demonstrated in the reaction of *S*-benzoin with racemic **1**<sup>[8]</sup>. In this case kinetic resolution has been observed affording exclusively meso-1,2-diphenyl-1,2-ethanediol, in agreement with the preferred mode of addition expected for substrates obeying Cram's rule<sup>[12]</sup>. Whereas *R*-1 and *S*-benzoin easily fit in a chelated ternary complex with  $\text{Mg}^{2+}$ , thus enabling a fast hydride-transfer reaction, *S*-1 is unable to form a productive ternary complex with *S*-benzoin (one phenyl group interferes with the pyridine ring), and hence no hydride-transfer takes place.

## 7.5 Concluding remarks

It can be concluded that the proposed ternary complex is capable of explaining the present experimental data. Efficient chirality transfer (up to 95%) has been observed to both the pyridinium ( $\text{NAD}^+$  model) and the reduced substrate<sup>[7]</sup>. In contradiction to native NADH, the source of chirality in the NADH model is induced by the methyl substituent on C4 and the reaction with this NADH model is an irreversible one. Hence, one has to keep in mind that the mechanisms of the enzymatic reaction and the reaction with this synthetic NADH-model are very different.

## References

1. A. Ohno, M. Ikeguchi, T. Kimura and S. Oka, *J. Am. Chem. Soc.* **101**, 7036-7040 (1979).
2. A. Ohno, M. Kashiwagi, Y. Ishihara, S. Ushida and S. Oka, *Tetrahedron*, **42**, 961-973 (1986).
3. A.I. Meyers and T.J. Oppenlaender, *J. Am. Chem. Soc.* **108**, 1989-1996 (1986).
4. Y. Inouye, J. Oda and N. Baba in "*Asymmetric Synthesis*", (J.D. Morrison ed.), Academic Press, New York, Vol. 2, 91-124 (1983).
5. A. Ohno and S. Ushida in "*Mechanistic Models of Asymmetric Reductions*", Springer Verlag, Berlin (1986).
6. V.A. Burgess, S.G. Davies and R.T. Skerlj, *Tetrahedron: Asymmetry*, **2**, 299-328 (1991).
7. P.M.T. de Kok, L.A.M. Bastiaansen, P.M. van Lier, J.A.J.M. Vekemans and H.M. Buck, *J. Org. Chem.* **54**, 1313-1320 (1989).



8. N.A. Beijer, J.A.J.M. Vekemans and H.M. Buck, *Recl. Trav. Chim. Pays Bas*, **109**, 434-436 (1990).
9. D.C.H. Bigg and P. Lesimple, *Synthesis*, 277-278 (1992).
10. J.P.G. Versleijen, M.S.T.H. Sanders-Hovens, S.A.M. Vanhommerig, J.A.J.M. Vekemans and E.M. Meijer, *Tetrahedron*, **49**, 7793-7802 (1993).
11. R.C.J. Schiepers, unpublished results, T.U.Eindhoven (1986).
12. P. Sykes in *"A guidebook to mechanism in organic chemistry"*, 5th edition, Longman, London, 230-232 (1981).

---

*This chapter is based on:*

J.P.G. Versleijen, M.S.T.H. Sanders-Hovens, S.A.M. Vanhommerig, J.A.J.M. Vekemans and E.M. Meijer, *Tetrahedron*, **49**, 7793-7802 (1993).

## 8

## The out-of-plane concept

*discussion*

In the preceding chapters the experimental and modelling studies (force field and semiempirical studies) on horse liver alcohol dehydrogenase and its coenzymes have been reported. The work on  $\text{NAD}^+$  was started one decade ago to investigate the correlation between the stereochemical course of the hydride-transfer and the amide out-of-plane orientation (see Figure 8.1), as postulated by Donkersloot and Buck in 1981<sup>[1]</sup>. Quantum chemical calculations indicate that the activation enthalpy of the hydride-transfer is minimal when the carboxamide is rotated out of the pyridinium plane and when the carbonyl moiety is directed toward the substrate. The authors claimed that the stereospecificity and the rate of hydride-transfer with  $\text{NAD}^+/\text{NADH}$  are determined by an out-of-plane rotation of the carboxamide side-chain in the kinetic step. This so-called out-of-plane concept seems to be supported by crystallographic data of a ternary complex of NADH and DMSO with the A-specific enzyme HLADH<sup>[2]</sup> and of a binary complex of  $\text{NAD}^+$  and the B-specific enzyme GAPDH<sup>[3]</sup>, the pyridinium ring and the amide group being inclined at an angle of  $23^\circ$  on the A-side and  $22^\circ$  on the B-side, respectively. Cummins and Gready<sup>[4]</sup> also found a *syn* orientation of the amide carbonyl in dihydrofolate reductase using semiempirical AM1 calculations, which they explained by the formation of a H-bond between  $\text{C}=\text{O}$  and the protonated substrate. Semiempirical calculations of transition states of active site models, of HLADH with  $\text{NAD}^+$  as coenzyme as presented in this thesis, all pointed to a preferential out-of-plane rotation of the pyridinium side-chain towards the A-side (see Chapter 2).

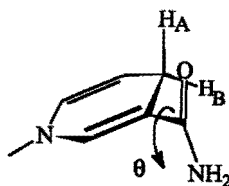


Figure 8.1: *syn*-out-of-plane orientation of the  $\text{C}=\text{O}$  and  $\text{C}-\text{H}_A$ .

Besides this *syn*-out-of-plane concept, several other hypotheses regarding the rate and stereospecificity of hydride-transfer have been put forward. Benner et al.<sup>[5,6]</sup> proposed a correlation between the stereospecificity of dehydrogenases and the value of the equilibrium constant for the catalyzed reactions. However, some exceptions to Benner's hypothesis have been reported<sup>[7]</sup>. Benner and co-workers<sup>[6]</sup> also assumed that the 1,4-dihydropyridine ring adopts a *quasi*-boat conformation (as depicted in Figure 8.2) in which the hydrogen to be transferred from C4, occupies a pseudoaxial position. The *pro-R* hydrogen ( $H_A$ ) would be transferred when the coenzyme is bound in the active site in an *anti* conformation; the *pro-S* hydrogen ( $H_B$ ) would be transferred from a *syn* conformer (see Figure 8.2). From the calculations reported by Bruice and co-workers<sup>[8]</sup> on other dehydrogenases using QUANTA/CHARMm, no stereoelectronic preference for the *syn* or *anti* conformation could be found to explain A/B-side preference for hydride-transfer. However, they suggest that ring deformation (to a *quasi*-boat form), placing the hydrogen to be transferred in a pseudoaxial position, is an essential feature of the mechanism of hydrogen-transfer.

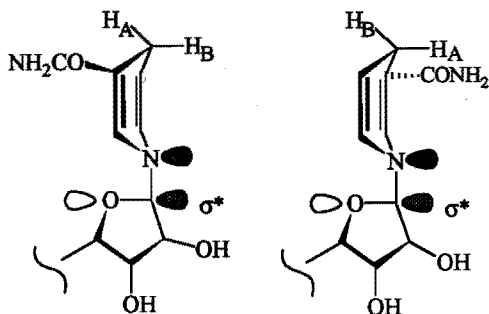


Figure 8.2: *syn* (left) and *anti* (right) conformation

Inspired by the work of Donkersloot and Buck<sup>[11]</sup>, several groups<sup>[9-13]</sup> performed quantum chemical calculations to study the geometry of  $NAD^+$  and  $NADH$  derivatives. Verhoeven et al.<sup>[14]</sup> performed calculations on various  $NAD^+$ / $NADH$  models in order to get better insight in the mechanism and exact nature of transition state during hydride-transfer. Their calculations indicated that the hydride-transfer should be a concerted process, with a linear transition state geometry between C--H--C. The angle  $\theta$  is not discussed, since no side-chain was included in the calculations.

In the present work experimental verification of the carbonyl out-of-plane orientation *in vitro* was tested using *N,N*,1,2,4-pentamethyl-1,4-dihydronicotinamide as  $NADH$  model

compound (see Chapter 7). In the oxidized form the carboxamide group is rotated permanently out of the pyridinium plane and hence the  $\text{NAD}^+$  model is axially chiral. The observed stereochemistry of the reaction of this NADH model with several substrates can only be rationalized if a transition state is adopted in which the migrating hydrogen and the amide carbonyl dipole feature a *syn*-out-of-plane orientation. As opposed to native NADH, the chirality in the above mentioned NADH model is induced by the methyl substituent on C4, which limits the number of stereochemical possibilities. Hence, one has to keep in mind that the mechanisms and selectivities of the enzymatic reaction and the reaction with this synthetic NADH-model may be very different.

The carbonyl out-of-plane concept was also believed to explain the differences in activity between  $\text{NAD}^+$  and its structural analogues with HLADH (isopropanol as substrate). Meijer and co-workers<sup>[15-18]</sup> performed MM calculations on the ternary complex of HLADH using a flexible core of amino acids (within 6 Å of the coenzyme). Their results show a good correlation between the calculated out-of-plane orientation of the carbonyl dipole and the enzymatic activity of several  $\text{NAD}^+$  analogues. It seemed worthwhile, however, to reconsider their results, utilizing recent X-ray data that show up more water molecules. With these extensive MM and MD calculations the whole enzyme is included, using a belly of free amino acids within 15 Å of the coenzyme. The MD calculations with the  $\text{NAD}^+$  analogues described in Chapter 6, again support the relevancy of the *syn*-out-of-plane rotation of the carbonyl group with respect to the rate of hydride-transfer. According to the present results, however, the values of the out-of-plane rotation diverge to a larger extent than could be calculated previously.

With regard to the original "out-of-plane" hypothesis of Donkersloot and Buck<sup>[1]</sup>, we conclude that the results presented in this thesis add further evidence as far as it concerns the hydride-transfer rate. Their "stereospecificity claim" should, however, be abandoned as far as enzymatic reactions are concerned, since the stereochemical course of hydride-transfer in an enzyme is dictated by shielding caused by its protein structure (see Chapter 1).

## References

1. M.C.A. Donkersloot and H.M. Buck, *J. Am. Chem. Soc.* **103**, 6554-6558 (1981).
2. H. Eklund, J.-P. Samama and T.A. Jones, *Biochemistry* **23**, 5982-5996 (1984).
3. T. Skarzynski, P.C.E. Moody and A.J. Wonacott, *J. Mol. Biol.* **193**, 171-187 (1987).
4. P.L. Cummins and J.E. Gready, *J. Comput. Chem.* **11**, 791-804 (1990).
5. S.A. Benner, *Experientia* **38**, 633-637 (1982).

6. K.P. Nambiar, D.M. Stauffer, P.A. Kolodziej and S.A. Benner, *J. Am. Chem. Soc.* **105**, 5886-5890 (1983).
7. N.J. Oppenheimer, *J. Am. Chem. Soc.* **106**, 3032-3033 (1984).
8. Ö. Almarsson and T.C. Bruice, *J. Am. Chem. Soc.* **115**, 2125-2138 (1993).
9. P.L. Cummins and J.E. Gready, *J. Mol. Struct. (Theochem)* **183**, 161-174 (1989).
10. Y.-D. Wu and K.N. Houk, *J. Am. Chem. Soc.* **113**, 2353-2358 (1991).
11. H. Li and B.M. Goldstein, *J. Med. Chem.* **35**, 3560-3567 (1992).
12. Y.-D. Wu and K.N. Houk, *J. Org. Chem.* **58**, 2043-2045 (1993).
13. N. Bodor, M.E. Brewster and J.J. Kaminski, *Tetrahedron* **44**, 7601-7610 (1988).
14. J.W. Verhoeven, W. van Gerresheim, F.M. Martens and S.M. van der Kerk, *Tetrahedron* **42**, 975-992 (1986).
15. P.M.T. de Kok, N.A. Beijer, H.M. Buck, L.A.Æ. Sluyterman and E.M. Meijer, *Recl. Trav. Chim. Pays-Bas* **107**, 355-361 (1988).
16. P.M.T. de Kok, N.A. Beijer, H.M. Buck, L.A.Æ. Sluyterman and E.M. Meijer, *Eur. J. Biochem.* **175**, 581-585 (1988).
17. N.A. Beijer, H.M. Buck, L.A.Æ. Sluyterman and E.M. Meijer, *Biochim. Biophys. Acta* **1039**, 227-233 (1990).
18. N.A. Beijer, H.M. Buck, L.A.Æ. Sluyterman and E.M. Meijer, *Ann. N. Y. Acad. Sc.* **613**, 494-500 (1990).

### Appendix 1 : Kinetic equations

**The initial-rate equation for HLADH:**

$$\frac{1}{V} = \frac{e}{k_{\text{cat}}} \left[ 1 + \frac{K_{\text{mA}}}{[\text{A}]} + \frac{K_{\text{mB}}}{[\text{B}]} + \frac{K_{\text{c}}}{[\text{A}] \cdot [\text{B}]} \right] \quad (1)$$

In eq. (1),  $e$  is the concentration of enzyme active centres (twice the molar concentration); A and B represent coenzyme and substrate, respectively;  $K_{\text{mA}}$ ,  $K_{\text{mB}}$  and  $K_{\text{c}}$  denote the kinetic coefficients. If the coenzyme is used at saturating conditions, eq. (1) can be simplified:

$$\frac{1}{V} = \frac{e}{k_{\text{cat}}} \left[ 1 + \frac{K_{\text{mA}}}{[\text{A}]} \right] \quad (2)$$

Of course, at saturating substrate conditions, a similar equation can be used as eq. (2). A plot of  $1/V$  versus  $1/[\text{A}]$ , called a *Lineweaver-Burk plot*, yields a straight line with an intercept of  $e/k_{\text{cat}}$  and a slope of  $K_{\text{mA}}/k_{\text{cat}}$ .

### Competition between two coenzymes $C_1$ and $C_2$ at fixed substrate concentration.

**System I: normal competition**

Conservation equation:

$$e = E + EC_1 + EC_2 \quad (3)$$

Again,  $e$  denotes the total concentration of subunits. The dissociation constants  $K'$  of the coenzymes at the chosen substrate concentration are:

$$K_1' = \frac{E \cdot C_1}{EC_1} \quad \text{and} \quad K_2' = \frac{E \cdot C_2}{EC_2} \quad (4a, 4b)$$

Insertion of (4a) and (4b) into eq. (3) yields:

$$e = E \left[ 1 + \frac{C_1}{K_1'} + \frac{C_2}{K_2'} \right] = E \cdot A \quad (5)$$

The reaction rate is given by:

$$v = k_1' \cdot EC_1 + k_2' \cdot EC_2 \quad (6)$$

in which  $k_1'$  and  $k_2'$  denote the reaction rates with the chosen substrate concentration at infinite coenzyme concentration. Insertion of eqs. (4) and (5) into eq. (6) yields:

$$v = \frac{e}{A} \left[ k_1' \frac{C_1}{K_1'} + k_2' \frac{C_2}{K_2'} \right] \quad (7)$$

### System II: semi competition

If  $C_1$  is the coenzyme that is capable of binding to only one of the two subunits, it means that only half of the subunits can bind both  $C_1$  and  $C_2$ , according to eq. (7), and the other half only  $C_2$ . This yields:

$$v = \frac{0.5 \cdot e}{A} \left[ k_1' \frac{C_1}{K_1'} + k_2' \frac{C_2}{K_2'} \right] + \frac{0.5 \cdot e \cdot k_2'}{1 + \frac{K_2'}{C_2}} \quad (8)$$

As the experiments were carried out with 10 mM ethanol as substrate, the values  $K_1' = 62.0 \mu\text{M}$  and  $K_2' = 16.3 \mu\text{M}$  could be taken directly from Table 5.1, whereas  $k_1'$  and  $k_2'$  were calculated from their corresponding values of  $k_{\text{cat}}$  and  $K_m$ , providing the ratio  $k_1'/k_2' = 0.30$ . If system II is operative, the observed  $k_{\text{cat}}$  of PEG-NAD<sup>+</sup> is due to only one of the two subunits and the actual  $k_{\text{cat}}$  would be double the one observed. For the calculation of system II the ratio  $k_1'/k_2' = 0.60$  is therefore to be used.

## Appendix 2 : AMBER force field parameters

The atomic charges for all non-standard AMBER residues: ethoxide, isopropoxide, DMSO, negatively charged cysteine, PEG-tail, NADH ring, NAD<sup>+</sup> ring, sNAD<sup>+</sup>, acPdAD<sup>+</sup> ring and fPdAD<sup>+</sup> ring; The residues included in the belly and the newly added AMBER parameters.

### Ethoxide

Atom	AMBER type	Charge
C1	CT	0.2188
O1	OH	-0.8977
H1'	HC	-0.0536
H1*	HC	-0.535
C2	CT	-0.4524
H2	HC	0.0452
H2'	HC	0.0952
H2*	HC	0.0968

### DMSO

Atom	AMBER type	Charge
S	S	0.8682
O	O	-0.7916
C1	C3	-0.0383
C2	C3	-0.0383

### PEG-tail

Atom	AMBER type	Charge
C	C2	0.1570
O	OS	-0.3510
end:		
OH	OH	-0.5500
HO	HO	0.4000

### Isopropoxide

Atom	AMBER type	Charge
C2	CT	-0.4623
H2	HC	0.0986
H2'	HC	0.0559
H2*	HC	0.1043
C1	CT	0.3637
O1	OH	-0.9119
H1'	HC	-0.0452
C3	CT	-0.4625
H3	HC	0.1020
H3'	HC	0.0962
H3*	HC	0.0611

### Negatively charged cysteine

Atom	AMBER type	Charge
N	N	-0.2678
HN	H	0.1060
CA	CH	-0.0894
CB	C2	-0.1465
SG	SM	0.2380
LP1	LP	-0.5010
LP2	LP	-0.5010
C	C	0.3568
O	O	-0.3684



NADH ring (see Figure 5.8)

Atom	AMBER type	Charge
C6	CA	0.0977
HC6	HC	0.2027
C5	CA	-0.2762
HC5	HC	0.1967
C4	CT	-0.2841
HC4	HC	0.1875
HC4*	HC	0.1593
C3	CA	-0.2362
C7	C	0.7196
O7	O	0.5829
N7	N	-0.8899
HNA	H	0.3715
HNB	H	0.3642
C2	CA	0.1456
HC2	HC	0.2366
N1	N*	-0.6900

NAD<sup>+</sup> ring<sup>a</sup> (see Figure 5.8)

Atom	AMBER type	Charge
C6	CA	0.1792
HC6	HC	0.3048
C5	CA	-0.2810
HC5	HC	0.3002
C4	C#	-0.0544
HC4	HC	0.3263
C3	CA	-0.2135
C7	C	0.7463
O7	O	-0.5198
N7	N	-0.8924
HNA	H	0.4177
HNB	H	0.3823
C2	CA	0.1871
HC2	HC	0.3240
N1	N*	-0.6256

sNAD<sup>+</sup> ring (see Figure 5.8 and 6.1)

Atom	AMBER type	Charge	Atom	AMBER type	Charge
C6	CA	0.1734	S7	SD	0.7892
HC6	HC	0.3021	LP1, LP2	LP	-0.4570
C5	CA	-0.2836	N7	N	-0.8336
HC5	HC	0.2988	HNA	H	0.4044
C4	CA	-0.0556	HNB	H	0.4444
HC4	HC	0.3200	C2	CA	0.1970
C3	CA	-0.1256	HC2	HC	0.3044
C7	C	0.1919	N1	N*	-0.5959

<sup>a</sup> C# is the same atom type as CA and only used to describe the torsion of the carboxamide side-chain.

**acPdAD<sup>+</sup> ring** (see Figure 6.1)

Atom	AMBER type	Charge
C6	CA	0.1796
HC6	HC	0.3021
C5	CA	-0.2805
HC5	HC	0.2977
C4	CA	-0.0495
HC4	HC	0.3292
C3	CA	-0.2140
C7	C	0.5819
O7	O	-0.4958
C8	CT	-0.6034
H'	HC	0.2058
H#	HC	0.2059
H*	HC	0.2631
C2	CA	0.1826
HC2	HC	0.2984
N1	N*	-0.6223

**FPdAD<sup>+</sup> ring** (see Figure 6.1)

Atom	AMBER type	Charge
C6	CA	0.1788
HC6	HC	0.3050
C5	CA	-0.2811
HC5	HC	0.3010
C4	CA	-0.0495
HC4	HC	0.3262
C3	CA	-0.2041
C7	C	0.3547
O7	O	-0.4300
H8	HC	0.2086
C2	CA	0.1788
HC2	HC	0.3029
N1	N*	-0.6056

**Residues included in the belly option**

The residue numbers of the ternary complex of HLADH (6ADH) (all within a radius of 15 Å from the coenzyme) which are allowed to move freely during the MM and MD calculations are:

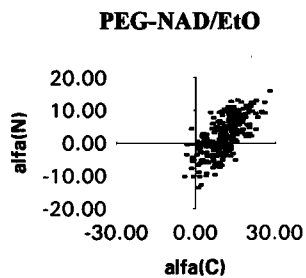
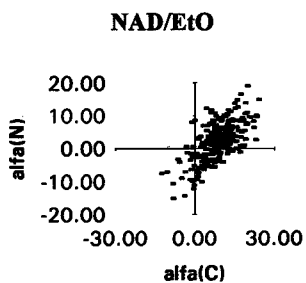
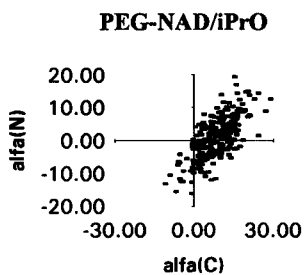
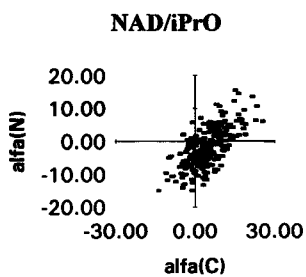
14, 17, 21, 42-59, 63, 65-70, 90-95, 102, 107-119, 140-146, 156, 158,  
165-350, 355-372, 375 (Zn), 377 (NAD), 378 (substrate), 652-665,  
680-692 and all water molecules.

## Newly added AMBER parameters

<i>nonbonded parameters for zinc</i>			Zn	$r^*=1.40 \text{ \AA}$	well depth $\epsilon=0.10 \text{ kcal.mol}^{-1}$
<i>bond bending parameters</i>			$k_\theta$	<i>bond stretching parameters</i>	
$\theta_e \text{ (kcal.mol}^{-1}\text{rad}^{-2}\text{)}$			$r_e \text{ (\AA)} \text{ (kcal.mol}^{-1}\text{\AA}^{-2}\text{)}$		
<b>for NAD<sup>+</sup></b>			<b>for NAD<sup>+</sup></b>		
CA-C-O	119.8°	80	CA-N*	1.38	448
CA-C-N	115.7°	70	<b>for fPdAD<sup>+</sup></b>		
CA-CA-N*	119.5°	70	C-HC	1.05	331
CA-N*-CA	121.2°	70	<b>for sNAD<sup>+</sup></b>		
CA-N*-CT	120.6°	70	C-SD	1.71	328
<b>for DMSO</b>			SD-LP	0.68	600
C3-S-O	107.6°	68	<i>torsional parameters</i>		
C3-S-C3	98.9°	62	$\gamma$	$V_n/2 \text{ (kcal.mol}^{-1}\text{)}$	
<b>for NADH and acPdAD<sup>+</sup></b>			<b>for NAD<sup>+</sup></b>		
CA-C-CT	120.0°	85	C#-CA-C-N/O	180°	$V_2/2=0.45$
<b>for fPdAD<sup>+</sup></b>			C#-CA-C-O	0°	$V_1/2=0.02$
CA-C-HC	120.1	35	C#-CA-C-N	180°	$V_1/2=0.02$
O-C-HC	120.1	35	<b>for acPdAD<sup>+</sup></b>		
<b>for sNAD<sup>+</sup></b>			CA-CA-C-CT/O	180°	0.39
CA-C-SD	121.2°	64	<b>for fPdAD<sup>+</sup></b>		
SD-C-N	123.7°	64	CA-CA-C-O/HC	180°	0.505
C-SD-LP	96.7°	600	<b>for sNAD<sup>+</sup></b>		
LP-SD-LP	160.0°	600	X-C-SD-X	0°	$V_3/2=1.0$
<i>constraints around catalytic zinc</i>			<b>for NADH</b>		
Zn-O	$r=2.14 \text{ \AA}$	$k_r=50$	CT-CA-C-N/O	180°	$V_2/2=0.70$
SG-Zn-SG	$\theta=132.6^\circ$	$k_\theta=50$	CA-CA-C-O/N	180°	$V_2/2=0.70$
NE-Zn-SG	$\theta=107.8^\circ$	$k_\theta=50$	CT-CA-C-N / CA-CA-C-O	0°	$V_1/2=0.40$
NE-Zn-O	$\theta=95.0^\circ$	$k_\theta=50$	CT-CA-C-O / CA-CA-C-N	180°	$V_1/2=0.40$

## Appendix 3

The variations in  $\alpha_C$  versus  $\alpha_N$  (in degrees) sampled from the period of 40-90 ps (see Chapter 5).



## Appendix 4

**Table 1** Hydrogen-bonding pattern and electrostatic interactions around the phosphate groups of the coenzyme from the time-averaged MD structures (Chapter 6) and the crystal structure 6ADH. (distances in Å).

	X-ray <sup>a</sup>	NAD	acPdAD	fPdAD	sNAD	NAD	acPdAD	fPdAD
		iPrO	iPrO	iPrO	iPrO	EtO	EtO	EtO
O1P <sub>N</sub> (NAD)-HN12 (369)	2.95	1.72	1.99	1.72	2.02	1.82	1.84	1.99
O1P <sub>N</sub> (NAD)-HN11 (369)			2.12		2.26			
O1P <sub>N</sub> (NAD)-HN (47)	3.45			2.46				
O1P <sub>N</sub> (NAD)-H (WAT)			1.88	1.76	1.77		1.91	1.74
O1P <sub>N</sub> (NAD)-HN (203)		1.99				2.02		
O2P <sub>N</sub> (NAD)-HN (202)	3.19		2.20	2.03				2.42
O2P <sub>N</sub> (NAD)-HN (203)	3.21		1.82	1.90	1.92		1.98	1.89
O2P <sub>N</sub> (NAD)-HN (204)		2.14				1.90		2.40
O1P <sub>A</sub> (NAD)-HN11 (47)	2.91	1.68	1.80	1.75	1.88	1.70	1.73	
O1P <sub>A</sub> (NAD)-H (WAT)		1.88	1.70	1.77	1.42	1.83	1.78	1.62
O1P <sub>A</sub> (NAD)-H (WAT)						1.83		2.49
O2P <sub>A</sub> (NAD)-HN (202)		2.32				2.19		
O2P <sub>A</sub> (NAD)-HO3* (NAD)								1.69
O2P <sub>A</sub> (NAD)-H (WAT)		2.11	1.78		1.96	1.75		
O2P <sub>A</sub> (NAD)-HNZ1 (228)	3.29	1.97		1.74				1.71
O2P <sub>A</sub> (NAD)-H (WAT)		2.39	1.75	2.20	2.08	1.88	1.81	1.75

<sup>a</sup> The donor-acceptor distances are taken.

**Table II** RMS deviations (in Å) of the MD-averaged structures from the crystal structure 6ADH.

	vs Crystal structure							
	NAD iPrO	acPdAD iPrO	fPdAD iPrO	sNAD iPrO	NAD EtO	acPdAD EtO	fPdAD EtO	fPdAD EtO <sup>a</sup>
All backbone atoms	1.27	1.43	1.58	1.38	1.66	1.36	1.73	1.98
<b>C<math>\alpha</math> residues near coenzyme</b>								
Cys 46	0.98	1.17	1.10	1.16	1.79	0.69	1.69	1.96
Arg 47	0.98	0.65	1.07	0.87	1.92	0.59	1.41	2.20
Ser 48	0.65	0.58	0.68	0.48	1.89	0.31	0.94	1.85
His 51	0.45	0.49	0.65	0.48	1.56	0.39	1.43	1.49
His 67	0.13	0.23	0.22	0.18	0.11	0.23	0.41	0.21
Cys 174	1.06	1.19	1.32	1.13	1.17	1.23	1.24	1.11
Thr 178	1.64	1.61	2.07	1.78	1.28	1.18	1.23	1.04
Gly 202	0.78	0.76	1.48	0.79	0.98	0.36	0.82	1.81
Val 203	0.83	0.93	1.28	0.78	0.89	0.31	0.81	1.41
Val 292	0.33	0.56	0.45	0.38	0.35	0.55	0.27	0.55
Ala 317	0.51	0.46	2.54	0.76	0.69	0.98	2.74	1.49
Phe 319	1.91	1.74	2.29	1.98	1.31	1.98	1.33	1.03
Arg 369	0.47	0.90	0.94	0.85	0.69	0.75	0.88	1.63
RMS of C $\alpha$ 's above	0.96	0.97	1.41	1.02	1.25	0.88	1.32	1.47
<b>C<math>\alpha</math> residues near enzyme surface</b>								
227	2.46	2.09	2.15	2.50	2.47	1.61	3.67	3.90
248	3.83	2.46	3.39	2.32	6.39	3.56	7.86	9.64
297	2.77	3.30	3.03	3.74	3.16	1.21	3.30	2.97

## Summary

In this thesis chemical, enzymatic and modelling studies on the important coenzyme  $\text{NAD}^+/\text{NADH}$  are discussed. In combination with the enzyme horse liver alcohol dehydrogenase (HLADH) the NAD coenzyme is involved in the reversible stereospecific dehydrogenation of many alcohols.

In order to gain better insight in the enzymatic mechanism of HLADH, semiempirical quantum mechanical calculations on active site models of this enzyme were performed. Compared to a previous study, the effect of negatively charged cysteine side-chain versus the neutral cysteines was remarkable (change in sign of  $\Delta H_{\text{reaction}}$ ). In the model with negatively charged cysteines remarkable differences in the out-of-plane value  $\theta$  was found for the calculated transition states of the acetyl and formyl  $\text{NAD}^+$  analogues, which could account partly for the observed enzymatic activity with HLADH (Chapter 2).

With semiempirical methods, only a small number of atoms can be included in the calculations. If the whole enzyme is included, one has to resort to force field methods. We checked the accuracy of the AMBER force field, starting from crystal structures of amino acids and *N*-methylacetamide determined with high resolution. The standard AMBER set using a dielectric constant ( $\epsilon$ ) of 3 gave the best results when charged groups are present. An  $\epsilon=1$  turned out to be better when simulating peptide bonds. As there are many more peptide hydrogen bonds than charged groups in a protein, the value  $\epsilon=1$  was retained in the AMBER 4.0 calculations (Chapter 3).

Most force fields, also the AMBER force field, are only optimized for proteins and nucleic acids. Therefore we added some parameters for  $\text{NAD}^+/\text{NADH}$  and adjusted the parameters describing the rotational barrier of the pyridinium side-chain of  $\text{NAD}^+$  and analogues, based on a few known experimental barriers (Chapter 4).

The enzymatic activity of the commercially attractive polyethylene glycol bound  $\text{NAD}^+$  (PEG- $\text{NAD}^+$ ) was tested with HLADH. The polymer bound  $\text{NAD}^+$  showed a 3 or 4 times lower activity with HLADH compared to the native  $\text{NAD}^+$ . Lower intrinsic reactivity, steric hindrance or interference by the PEG-tail and destabilization of the HLADH dimer could be ruled out as possible explanations. MD calculations, however, indicate that the "pulling effect" of the PEG-tail causes shifts in the positioning of the coenzyme and the surrounding peptide chains. Due to the changed interactions between the coenzyme and enzyme, the activity of PEG- $\text{NAD}^+$  might be lowered (Chapter 5).

In kinetic and modelling studies we also used analogues of  $\text{NAD}^+$ , which only differ in the C3-substituent of the pyridinium side-chain. The experimentally observed enzymatic

activities of the analogues can be qualitatively rationalized by the value of the out-of-plane angle  $\theta$  and the interaction energies between enzyme and coenzyme (Chapter 6).

Chapter 7 describes the (possible) reductions with the NADH model N,N,1,2,4-pentamethyl-1,4-dihydronicotinamide with several substrates. Efficient chirality transfer has been observed to both the oxidized ( $\text{NAD}^+$ ) model and the reduced substrate. A ternary complex is proposed which is capable of explaining the present experimental data.

In Chapter 8 a short overview is given on the history of the so-called "out-of-plane" concept, which correlates the stereospecificity and the rate of hydride-transfer in  $\text{NAD}^+/\text{NADH}$  dependent enzymatic reactions. The results as reported in this thesis indicate that there indeed is a relation between the rate of hydride-transfer and the "out-of-plane" orientation of the side-chain of the coenzyme. The stereospecificity of the reaction is, however, only determined by the enzymatic environment.



## Samenvatting

De chemische -, enzymatische - en modelleringsstudies aan het belangrijke coënzym  $\text{NAD}^+/\text{NADH}$  worden beschreven in dit proefschrift. Samen met het enzym alcoholdehydrogenase uit paardelever (HLADH) is het  $\text{NAD}$  coënzym betrokken bij de reversibele en stereospecifieke dehydrogenering van vele alcoholen.

Om een beter inzicht in het enzymatische mechanisme van HLADH te verkrijgen, werden semi-empirische berekeningen aan modellen van de actieve holte van dit enzym uitgevoerd (Hoofdstuk 2). Een opmerkelijk effect werd waargenomen indien de resultaten van berekeningen aan negatief-geladen cysteïne zijgroepen met die aan neutrale cysteïnes werden vergeleken: nl. een verandering in het teken van  $\Delta H_{\text{reactie}}$ . In het model met de negatief-geladen cysteïnes blijken er duidelijke verschillen te bestaan in de waarde van de "out-of-plane" hoek  $\theta$  van de zijketen van verschillende  $\text{NAD}^+$ -analoga, hetgeen de gemeten enzymatische activiteiten met deze analoga gedeeltelijk kan verklaren.

Indien men semi-empirische berekeningen gebruikt, kan men slechts een klein aantal atomen meenemen in een berekening. Wanneer het hele enzym erbij betrokken moet worden, zal men naar een ander soort berekeningen moeten overstappen, krachtveldberekeningen. De nauwkeurigheid van het AMBER 4.0 krachtveld werd gecontroleerd, gebruikmakende van kristalstructuren van aminozuren en *N*-methylacetamide met een hoge resolutie (Hoofdstuk 3). De standaard AMBER set en een diëlektrische constante van 3 geven de beste resultaten indien geladen groepen aanwezig zijn.  $\epsilon=1$  blijkt beter bij de simulatie van peptidebindingen. Daar er veel meer peptide H-bruggen dan elektrostatiche interacties in een eiwit aanwezig zijn, werd de waarde van  $\epsilon=1$  in de AMBER 4.0-berekeningen aangehouden.

De meeste krachtveld programma's, zoals ook AMBER 4.0, zijn alleen geoptimaliseerd voor eiwitten en nucleotidezuren. Voor de moleculen die niet tot een van deze groepen behoren zoals  $\text{NAD}^+/\text{NADH}$ , werden parameters aan de AMBER set toegevoegd. De parameters die de rotatiebarrière van de pyridinium-zijketen van  $\text{NAD}^+$  en analoga beschrijven, werden eveneens aangepast om een goede overeenkomst te krijgen met experimenteel gemeten barrières (Hoofdstuk 4).

De enzymatische activiteit van het commercieel aantrekkelijke polyethyleenglycol-gebonden- $\text{NAD}^+$  (PEG- $\text{NAD}^+$ ) werd getest met HLADH (Hoofdstuk 5). Het polymeer-gebonden- $\text{NAD}^+$  vertoont een 3 tot 4 keer lagere activiteit met HLADH, vergeleken met natuurlijk  $\text{NAD}^+$ . Mogelijke verklaringen voor de waargenomen lagere activiteit zoals de lagere intrinsieke reactiviteit van PEG- $\text{NAD}^+$  en het eventueel optreden van sterische effecten of destabilisatie van het enzym als gevolg van de aanwezige polymeerstaart, kunnen worden uitgesloten. MD-berekeningen wijzen er daarentegen op, dat de polymeerstaart

"trekt" aan het  $\text{NAD}^+$  en hierdoor een verschuiving veroorzaakt in de positionering van het coënzym en de omringende peptideketen. De interacties tussen coënzym en enzym veranderen hierdoor (hogere bindingsconstante), waardoor de lagere activiteit van PEG- $\text{NAD}^+$  kan worden verklaard.

Kinetische - en modelleringsstudies zijn ook uitgevoerd aan  $\text{NAD}^+$ -analoga, die slechts verschillen in de C3-zijgroep van de pyridiniumgroep van het coënzym (Hoofdstuk 6). Het lijkt erop dat de grootte van de "out-of-plane" hoek  $\theta$  voor de verschillende C3-gesubstitueerde analoga in de enzymatische reactie en de berekende interactie-energieën tussen enzyme en coënzym, inderdaad gerelateerd kan worden aan de activiteit van deze analoga.

Hoofdstuk 7 beschrijft de (mogelijke) reducties met het synthetische NADH-model N,N,1,2,4-pentamethyl-1,4-dihydrionicotinamide met verschillende substraten. Efficiënte chiraliteitsoverdracht werd waargenomen naar zowel het geoxideerde ( $\text{NAD}^+$ -)model en het gereduceerde substraat. Een ternair complex wordt verondersteld, dat de huidige experimentele data kan verklaren.

In hoofdstuk 8 wordt een kort overzicht gegeven van de historie van het zogenaamde "out-of-plane" concept, dat een verband legt tussen de stereospecificiteit en de snelheid van de hydride-overdracht in  $\text{NAD}^+$ / $\text{NADH}$ -afhankelijke enzymatische reacties. De resultaten beschreven in dit proefschrift wijzen er inderdaad op dat er een relatie bestaat tussen de snelheid van hydride-overdracht en de "out-of-plane" oriëntatie van de zijketen van het coënzym. De stereospecificiteit wordt echter uitsluitend bepaald door de omgeving in het enzym.

## Curriculum vitae

Sylvia Vanhommerig werd geboren op 2 juni 1967 te Heerlen. Het VWO-diploma behaalde zij in 1985 aan het Bouwens van der Boije College te Panningen. In september van datzelfde jaar begon zij met de studie Scheikundige Technologie aan de Technische Universiteit te Eindhoven. Het afstudeerwerk werd verricht bij de vakgroep Organische Chemie van prof.dr. H.M. Buck met als onderwerp "Synthese en fysisch/chemische studies aan gemodificeerde DNA-systemen" onder begeleiding van dr.ir. M.H.P. van Genderen. Het ingenieursdiploma werd op 28 maart 1990 behaald. Vanaf 1 mei 1990 was zij als Assistent in Opleiding verbonden aan dezelfde vakgroep en in september startte zij het onderzoek zoals beschreven in dit proefschrift, onder begeleiding van prof.dr. E.M. Meijer. In de periode maart-juni 1992 deed ze ervaring op met de toepassingen van het AMBER-modelleringsprogramma in de groep van prof.dr. P.A. Kollman op de UCSF te San Francisco. Een gedeelte van het onderzoek zoals beschreven in dit proefschrift werd gepresenteerd op een internationaal congres over "Molecular modelling in genetic and protein engineering" te Sopron, Hongarije.

## Geaccepteerde publicaties

- S.A.M. Vanhommerig, R.J. Meier, L.A.Æ. Sluyterman and E.M. Meijer, *J. Mol. Struct. (Theochem)* **304**, 53-59 (1994), "Rotational barriers of 1,3-substituted pyridines and benzenes as models for the NAD<sup>+</sup>/NADH coenzyme".
- J.P.G. Versleijen, M.S.T.H. Sanders-Hovens, S.A.M. Vanhommerig, J.A.J.M. Vekemans and E.M. Meijer, *Tetrahedron* **49**, 7793-7802 (1993), "Enantioselective reduction of C=O and C=N compounds with NADH model N,N,1,2,4-pentamethyl-1,4-dihydronicotinamide".
- S.A.M. Vanhommerig, M.H.P. van Genderen and H.M. Buck, *Biopolymers* **31**, 1087-1094 (1991), "A stable antiparallel cytosine-thymine base pair occurring only at the end of a duplex".
- A. Tiller, A. Gorman, R.J. Meier and S.A.M. Vanhommerig, *J. Phys. Chem.*, in press (feb. 1995), "Molecular Modelling Melamine-Formaldehyde Resins II. Vibrational spectra of methylmelamines and bridged methylolmelamines."

## Acknowledgments

I would like to thank prof.dr. Peter Kollman (UCSF, San Francisco, USA) for giving me the opportunity to work in his group and learn the tricks and ropes of the AMBER program. The useful discussions I have had with him and many people in his group helped me with how to start the modelling studies on HLADH.

The PEG-NADH was kindly supplied by prof.dr. C. Wandrey and dr. U. Kragl from the Institute of Biotechnology, Nuclear Research Centre, Jülich, Germany.

I thank Virginia Otero for carrying out many kinetic experiments.

## Dankwoord

Naast de bovengenoemde personen, wil ik ook iedereen van de vakgroep TOC bedanken die belangstelling heeft getoond en heeft meegewerkt aan de totstandkoming van dit proefschrift. In het bijzonder geldt dit voor mijn eerste promotor, prof.dr. Emmo Meijer, die mij de gelegenheid gaf mijn onderzoek zelfstandig uit te voeren en voor zijn optimisme en stimulans. Prof. Sluyterman wil ik heel hartelijk bedanken voor zijn betrokkenheid bij het onderzoek, de vele discussies en zijn kritisch meedenken bij het schrijven van dit proefschrift. Prof.dr. Bert Meijer wil ik bedanken voor het aanvaarden van het tweede promotorschap en voor de ruimte die hij mij gaf om mijn eigen onderzoek te voltooien binnen zijn vakgroep. Mijn copromotor dr. Rob Meier; bedankt voor je enthousiasme, de discussies, de nauwgezette en snelle wijze waarop je dit proefschrift en artikels hebt doorgenomen en je gastvrijheid bij DSM Research. Dr. Peter Grootenhuis dank ik voor discussies over de modelleringsberekeningen en voor de introductie bij prof.dr. Peter Kollman.

Van de medewerkers van vakgroep wil ik met name dr. Jef Vekemans, dr.ir. René Janssen, ir. Jos Versleijen, dr.ir. Noline Beijer en dr. Jana van de Goor bedanken voor hun belangrijke bijdragen en discussies. Ook ir. Mireille Sanders heeft in het kader van haar afstudeerwerk een bijdrage geleverd aan dit werk, maar daarnaast wil ik haar en mijn (ex-)kameroten ir. Marga van Zundert en ir. Jan van Hest bedanken voor hun interesse, morele steun en gezellige (wetenschappelijke) discussies.

De hulp van dr. H. Haaker (LUW) bij het uitvoeren van de stopped-flow experimenten, heb ik zeer op prijs gesteld.

Dankzij beurzen van de Nederlandse Organisatie voor Wetenschappelijk Onderzoek (N.W.O.) en het Nuffic kreeg ik de mogelijkheid om voor een stage en een internationaal congres naar het buitenland te gaan.

Tenslotte wil ik mijn familie bedanken voor hun getoonde belangstelling, in het bijzonder mijn broer(tje), ir. Mark Vanhommerig. Mijn man, John; bedankt voor alle hulp thuis en je bent een fantastische papa! Mijn ouders wil ik tot slot nog apart bedanken, voor hun steun, zorg, interesse en stimulans voor alles wat ik de afgelopen 27 jaar heb ondernomen.

## Stellingen

behorende bij het proefschrift

### Kinetic and modelling studies of the $\text{NAD}^+$ /NADH coenzyme with horse liver alcohol dehydrogenase

1. Het uitgangspunt van Ritter von Onciul en Clark dat de cysteine-fragmenten rondom het katalytische zinkatoom neutraal zijn, is onjuist, terwijl de lading juist een grote invloed heeft op het mechanisme van de waterstof-overdrachtsreactie.  
A. Ritter von Onciul en T. Clark, *J. Comput. Chem.* **14**, 392-400 (1993).  
Hoofdstuk 2 van dit proefschrift.
2. De bewering van Zeppezauer en medewerkers dat het kinetische mechanisme van de oxidatie van zowel primaire als secundaire alcoholen in HLADH een geordend bi-bi mechanisme zou zijn, is onjuist in het geval van de secundaire alcoholen.  
H.W. Adolph, P. Maurer, H. Schneider-Bernlöhner, C. Sartorius en M. Zeppezauer, *Eur. J. Biochem.* **201**, 615-615 (1991).  
K. Dalziel en F.M. Dickinson, *Biochem. J.* **100**, 34-46 (1966).
3. Gezien de populariteit van de term dendrimeren, worden veel moleculen ten onrechte als dendrimeren aangeduid.  
J.W.J. Knapen, A.W. van der Made, J.C. de Wilde, P.W.N.M. van Leeuwen, P. Wijkens, D.M. Grove en G. van Koten, *Nature* **372**, 659-663 (1994).  
D.A. Tomalia en J.R. Dewald, U.S. patent 4,507,466 (1985).
4. Het is begrijpelijk dat de resultaten van Sicsic et al. met betrekking tot het meten van de enzymatische activiteit van  $\text{NAD}^+$ -fragmenten in HLADH, niet vaak geciteerd worden.  
S. Sicsic, P. Durand, S. Langrené en F. Le Goffic, *Eur. J. Biochem.* **155**, 403-407 (1986).  
Nicoline A. Beijer, niet-gepubliceerde resultaten.
5. Bij het bedenken van aminozuur-mutaties door middel van 'genetic engineering', dient men te beseffen dat zelfs kleine verschillen in aminozuur-volume nog structurele gevolgen in het eiwit kunnen hebben, die zich verder uitstrekken dan in de directe omgeving van de mutatie.

Dit proefschrift, hoofdstukken 5 en 6.

6. Klassieke reacties kunnen tot spectaculaire resultaten leiden.  
U. Hoffmann en B. Jacobi, U.S. patent 1,992,615 (1935).  
E.M.M. de Brabander-van den Berg en E.W. Meijer, *Angew. Chem. Int. Ed. Engl.* **32**, 1308-1311 (1993).  
J.F.G.A. Jansen, E.M.M. de Brabander-van den Berg en E.W. Meijer, *Science* **266**, 1226-1229 (1994).
  
7. De veronderstelling van Fujiki dat een polymeerhelix alleen een positief of alleen een negatief Circulair Dichroïsme (CD)-effect kan geven, gaat voorbij aan het feit dat de door hem waargenomen CD-spectra ook verklaard kunnen worden met gekoppelde excitonen.  
M. Fujiki, *J. Am. Chem. Soc.* **116**, 11976-11981 (1994).  
E. Charney in *"The Molecular Basis of Optical Activity. Optical rotatory dispersion and circular dichroism"* John Wiley & Sons, Inc. New York, p. 282 (1979).
  
8. De vergelijking van toponderzoek met topsport gaat niet altijd op: een topsporter moet steeds een topprestatie leveren om nummer 1 te blijven, terwijl van een toponderzoeker, na eenmaal bekendheid te hebben verworven, te snel elke geleverde prestatie als topprestatie wordt aangemerkt.
  
9. Carrière-makers met een gezin, hebben meestal partners die de zaakjes thuis goed regelen.
  
10. Om de (bio)chemie een positiever imago te bezorgen, zou men aan het (bio)chemische vakjargon meer bekendheid moeten geven en bijvoorbeeld de liposomen in wasmiddelen gewoon liposomen moeten noemen, naast de al in gebruik zijnde term vetoplossers.
  
11. Om het gebruik van het openbaar vervoer te stimuleren, zou men bij elke benzinepomp een sticker met een doodshoofd moeten plakken, met daarbij een tekst die de mensen ervoor waarschuwt, dat ze waarschijnlijk kankerverwekkende stoffen inademen tijdens het tanken.